ELI possible experiments

ELI-NP project



ELI-NP project
Ideas

The aim of the ELI-NP project is to cover a wide variety of scientific goals together with a broad range of experimental methods and techniques.

In the following I will propose several themes that could be developed as independent research projects using the ELI-NP facilities.

Some ideas are realistic being based on former experience gained by the author or by other researchers and could be found in the literature, but other ideas arises from questions I am putting in order to understand the basic phenomena related to the physics of the high power laser beam available in this facility.

The presentation will cover the following directions:

- 1) detection and associated phenomenon
- 2) atomic phenomena involving interactions between laser beam and atoms (molecules)
- 3) optical phenomena involving high power laser beam
- 4) quantum effects induced by high power laser beam:
- 5) astrophysics; ideas on possible D – D fusion reaction
- 6) order – disorder phenomena in solids; proposed experiments
- 7) archeology and arheometry – archeological dating and other applications
- 8) learning activities and education for future students and researchers

1. Detectors

- A *very high intensity laser*, where the beams from two 10 PW lasers are coherently added to the high intensity of 10^{23} - 10^{24} W/cm^2 or electrical fields of ~ 10^{15} V/m.
- It is clear that the beam monitoring and the characteristics are difficult to obtain using conventional methods. So we propose some alternative methods of beam characterization using phenomena that could be used for this purpose.
- At least two problems are to be faced:

a) how to arrange the detector in or near the beam but not to destroy the beam profile and

b) what phenomena and devices could be involved for beam characterization.

a) In principle we consider that we can use the diffraction properties of the highly coherent beam to extract a very small amount of radiation from the beam. This can be done with the aid used in near field optics used for example in scanning optical microscopy (figure 1) [Pohl 1982]. From the geometry and the formula that gives the diffraction field intensity, proportionality could be found to monitor the power of the beam, the detector (red) being positioned as far as it is possible from the beam axis. The diffraction pattern is inherent for the propagation of a very narrow beam, at the end of the pipe.

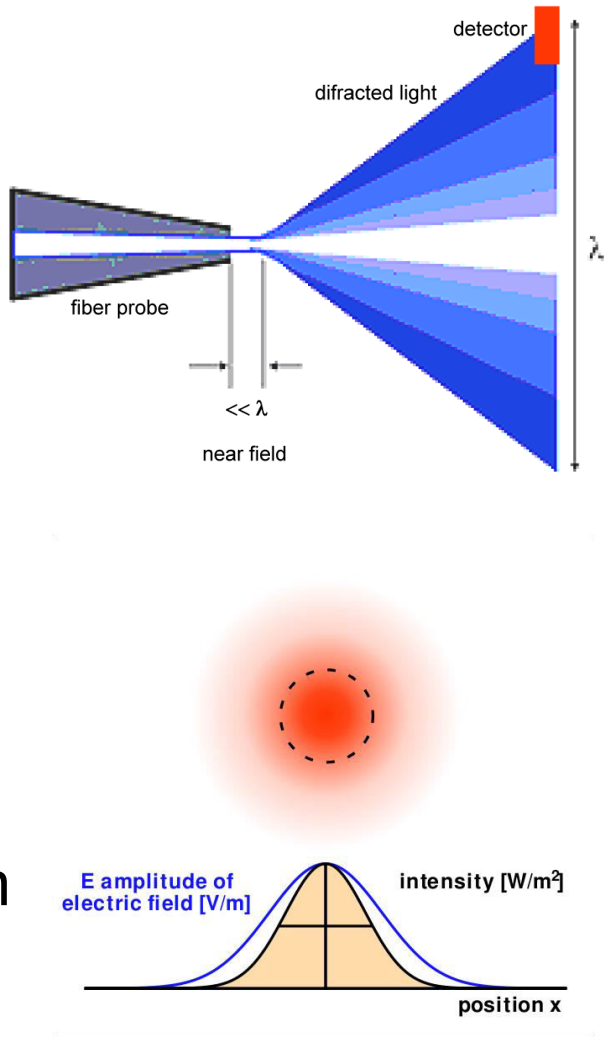


Figure 1

1.1- Laser beam power monitor – solid state detector

- Solid state detectors based on two (or more) photon excitation
- The detector principle is depicted in Figure 2 and 3. This device was first experimented by us in 1981 [Nicolau 1981] and give measurable electric current using a low power UV laser. It was a surprise because of the large band gap of the quartz (Figure 3) so no current could be established with the available photons energy. The tentative mechanism of conduction could be the following (Figure 4).
- Our explanation was based on a mechanism of two photon excitation that was first proposed by Maria Goeppert-Mayer in her doctoral dissertation in 1931 [MGMayer 1931].

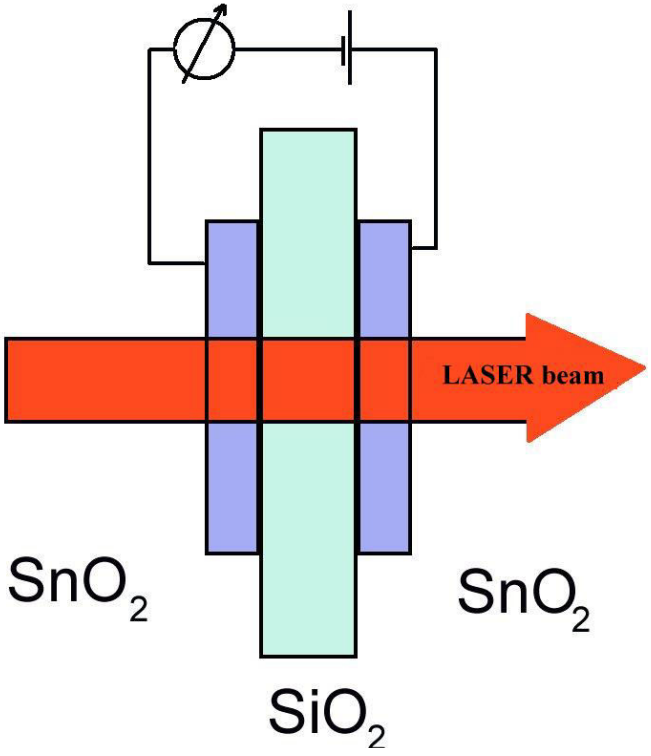


Figure 2

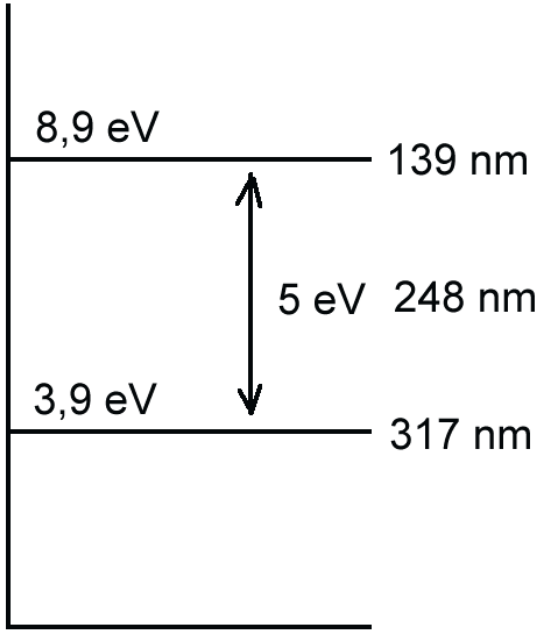


Figure 3

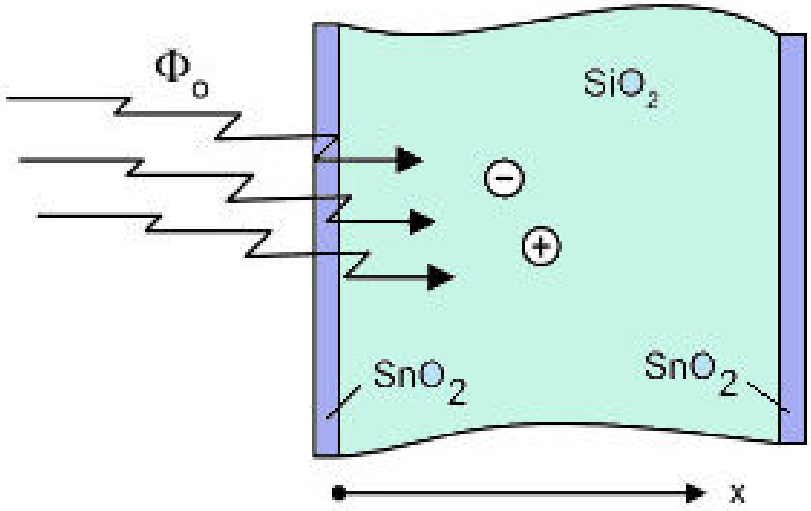


Figure 4

- The mechanism of two photon absorption was first observed in 1961 in a $CaF_2:Eu^{2+}$ crystal using laser excitation [Kaiser 1961]. I. Abella showed that in cesium vapor two-photon excitation of single atoms is possible [Abbela 1962].
- It is a nonlinear optical process and states absorption at high energies is impossible if two photons cannot bridge the band gap
- The same mechanism could be responsible for the measured current in our experiments.
- One stage – the conduction electrons for SnO2 are excited into a higher meta stable state where they stay for a short time,
- Second stage – these electrons are further excited and reach the conduction band of the SiO2 ,
- The electrons from the silica conduction band can be measured monitoring the intensity of the electric current between the to SnO2 electrodes,
- The current expected are of the order of 10^{-12} – 10^{-13} A and is proportional to their density and hence to the laser beam power.

a) SiO_2 - SnO_2

- Relative dielectric constant 3.7 - 3.9
- Dielectric strength 10^7 V/cm
- Energy band gap 8.9 eV
- DC resistivity 10^{17} Ωcm
- Thermal conductivity 3.2×10^{-3} W/(cm K)
- Melting point: 1600 ^{0}C

- 500 nm – 2,48 eV

- Crystal Structure: Rutile
- Band gap: 3.6 eV
- Optical gap: 3.9 eV
- Transparent (visible: 1.5 - 3.5 eV)
- Doped with Sb or F ions SnO_2 is a transparent conducting oxides
- (TCO): electroluminescent devices
- Melting point: 1080 ^{0}C

Photons of 500 nm have 2.48 eV , 300 nm have 4.13 eV; 100 nm have 12.4 eV

Other materials and sandwiches

- b) **Diamond** is transparent from the UV (225 nm) to the far infrared. Only minor absorption bands exist resulting from two phonon absorption between 2.5 and 6.5 µm. This makes diamond an ideal material for multispectral optical applications.
- Furthermore, its large bandgap (5.45 eV) prevents thermally generated charge carriers at elevated temperatures. Therefore diamond remains transparent even at very high temperatures and radiation intensities.

- Refraction index @500nm	2.41
- Bandgap	5.45 eV
- Absorption coefficient @10.6µm	<0.10 cm^{-1}
- Specific heat at 20° C	0.502 J/gK
- Debye temperature*	1860 K
- Bandgap	5.45 eV
- Resistivity	10^{13} - 10^{16} Ωcm

- extremely high thermal conductivity (>1800 W/mK, five times that of copper)
- Graphitization only at very high temperatures (T > 700°C in an oxygen containing and 1500°C in an inert atmosphere)

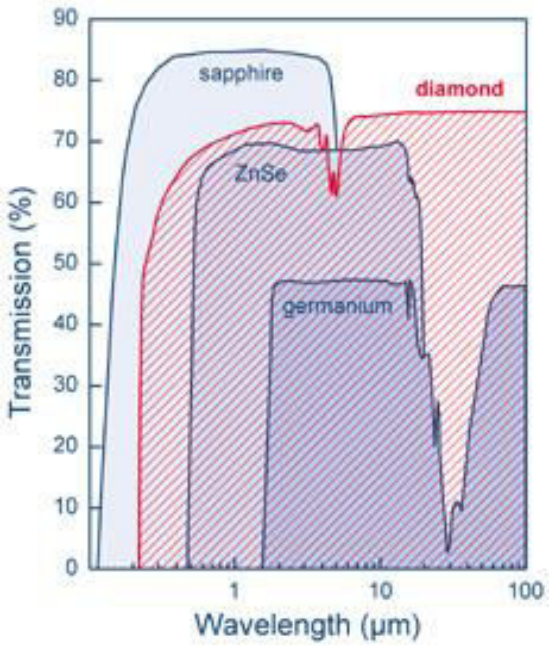


Figure 5

Other materials and sandwiches

- c) **High-quality indium–tin–oxide (ITO)** thin films (200–850 nm) have been grown by pulsed laser deposition (PLD) on glass substrates without a postdeposition annealing treatment
- d) **Polymethyl methacrylate (PMMA) layer on SnO2** nanowire (NW) field-effect transistors (FETs). As a result of the PMMA coating, the electrical properties of the SnO2 NW FETs improved.
- e) **Alkali-Halide Crystals**

  [Baldini 1968] and URL: http://link.aps.org/doi/10.1103/PhysRev.166.863;

  DOI: 10.1103/PhysRev.166.863

1.2) Optical phenomena
involving high power laser beam

- **1.2.1 Total internal reflection**

  For beam characterization and also for some experiments could be used the *total internal reflection* phenomenon.
  Total internal reflection is a phenomenon that happens when a propagating wave strikes a medium boundary at an angle larger than a particular critical angle with respect to the normal to the surface. If the refractive index is lower on the other side of the boundary and the incident angle is greater than the critical angle, the wave cannot pass through and is entirely reflected. The *critical angle* is the angle of incidence above which the total internal reflectance occurs

- An important side effect of total internal reflection is the propagation of an ***evanescent wave*** across the boundary surface. Essentially, even though the entire incident wave is reflected back into the originating medium, there is some penetration into the second medium at the boundary.
- The evanescent wave appears to travel along the boundary between the two materials. It is characterized by its propagation in the x direction and its exponential attenuation in the z direction.
- Although there is a field in the second medium, no energy flows across the boundary. The component of Poynting vector in the direction normal to the boundary is finite, but its time average vanishes. Whereas the other two components of Poynting vector and their time averaged values are in general found to be finite.

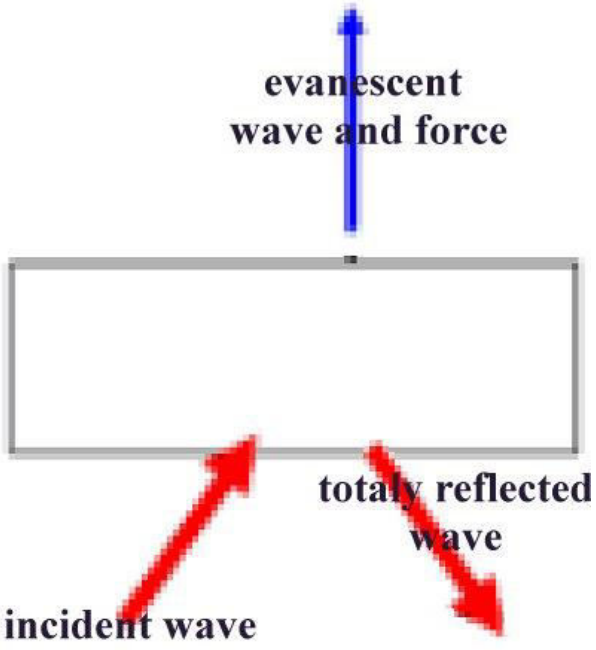


Figure 6

- Under "ordinary conditions" it is true that the creation of an *evanescent wave* does not affect the conservation of energy, i.e. the evanescent wave transmits zero net energy. However, if a third medium with a higher refractive index than the low-index second medium is placed within less than several wavelengths distance from the interface between the first medium and the second medium, the evanescent wave will be different from the one under "ordinary conditions" and it will pass energy across the second into the third medium. This process is called ***"frustrated" total internal reflection*** **(FTIR)** and is very similar to quantum tunneling. The quantum tunneling model is mathematically analogous if one thinks of the electromagnetic field as being the wave function of the photon. The low index medium can be thought of as a potential barrier through which photons can tunnel.

1.2.2 The evanescent wave

- This *evanescent wave* could be observed experimentally and could be measured using Atomic Force Microscopy (AFM). I experimented that at the Department of Applied Physics, University of Twente, Holland (1992 – 1993 with dr. Niek F. van Hulst) [Pohl 1982], [Flück 2003], [Flück 2004], [Gersen 2004], [Heilemann 2004], [Lereu 2008], [McKee 2006], [Postma 2007], [van Dijk 2005], [van Dijk 2007], [van Hulst 2001], [van Hulst 2007], [Vilfan 1998,]. The schematics are presented in Figure 9 and 10.
- The electric field of the evanescent wave act on the tip and the force will bend the cantilever, producing a measurable signal.

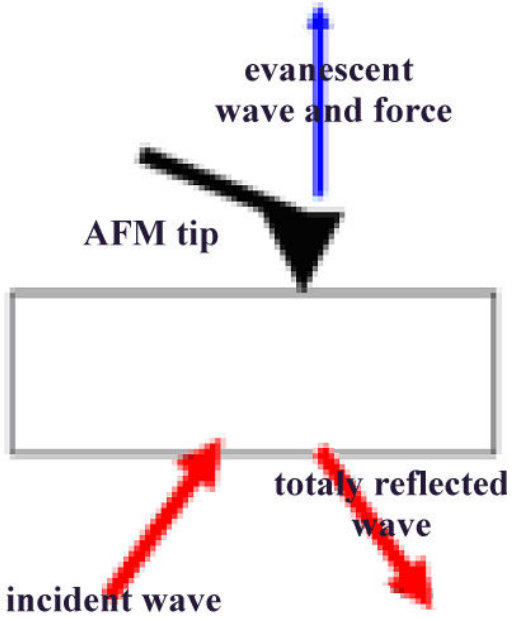


Figure 7

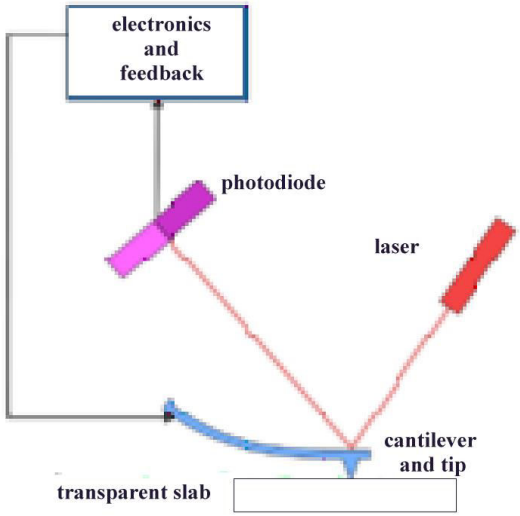


Figure 8

- A very simple and interesting application of the AFM that shows the sensitivity of the method was done by monitoring the spread of a bunch of electrons deposited on a dielectric slab.
- A dielectric sphere was attached to the AFM cantilever and placed into the evanescent light field of the Ar-laser beam illuminating a sapphire prism surface at an angle larger than the critical. A repulsive force due to the evanescent field was observed. The force decreases exponentially with the characteristic length of (45 ± 20) nm as the distance between the sphere and the total reflection surface increases. The measured magnitude of the force close to the surface is (3 ± 1.5) 10^{-10} N [Vilfan 1998], [McKee 2006].
- The idea is that a small part of the laser beam to be directed with an incidence angle above which the total internal reflectance occurs. The tip placed on the other part of the slab will be deflected corresponding to the evanescent electric field intensity. The intensity of the field could be measured and hence the beam intensity.

1.2.3- Magnetic field of the e.m. wave

- The same arrangement could be used in conjunction to a Josephson junction which is a quantum mechanical device, made of two superconducting electrodes separated by a barrier (insulating tunnel barrier, thin normal metal, etc.). On the surface of the junction a thin film of SiO_2 could be deposited that will act as a face on which the total reflection will take place. The Josephson junction will react to evanescent wave and a signal could be recorded. Exact action of the electromagnetic wave on the junction should be studied.
- I know that the standard volt is now defined in terms of a Josephson junction oscillator. The oscillation frequency of a Josephson junction is given by

$$f_{Josephson} = \frac{2e\Delta V}{h}$$

so the relationship between frequency and voltage across the junction depends only upon the fundamental constants **e** and **h**. For one microvolt applied to the junction the frequency is

$$f_{Josephson} = 483{,}6MHz$$

- The standard volt is now defined as the voltage required to produce a frequency of 483,597.9 GHz.
- The evanescent wave could produce a modification of the voltage across the junction ΔV (the junction could act also as an antenna) and that will change the frequency of oscillations.
- The frequency is today one of the most precise measurable unit so it could be extremely sensitive to the external field.

1.2.4- The SQUID device

- The electric and magnetic field in an electromagnetic field is related by the simple formula $E = c\,B$. For example a field of 75V/m has a magnetic filed of $2.5\ 10^{-7}$ T.

  If we compute the strength of the magnetic field that corresponds to an electric field of 10^{15} V/m is of order $3.3\ 10^{6}$ T, a very high value that surely will be measured with magnetic sensitive devices.

- Such a device could be a SQUID. The device may be configured as a magnetometer to detect extremely small magnetic fields - small enough to measure the magnetic fields in living organisms. SQUIDs have been used to measure the magnetic fields in mouse brains to test whether there might be enough magnetism to attribute their navigational ability to an internal compass.

- Threshold for SQUID is 10^{-14} T. I consider that using a SQUID the magnetic field component of the evanescent filed could be measured with great accuracy [Leca 2004].
- Recently were invented **SERF** atomic magnetometers (2000) which are potentially more sensitive and do not require cryogenic refrigeration but are orders of magnitude larger in size (~1cm^3) and must be operated in a near-zero magnetic field [Allred 2002].

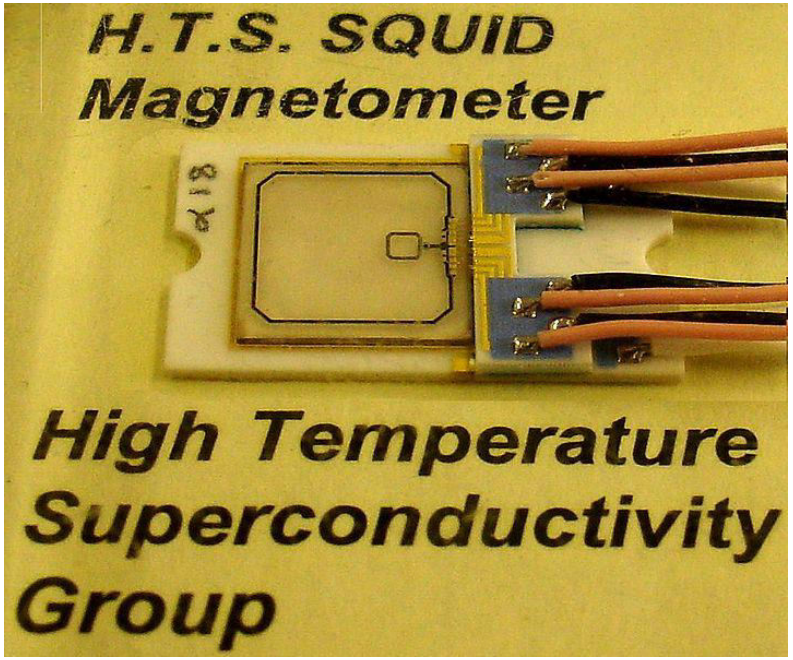


Figure 9

1.2.5- Conventional antenna

- Another attempt could be made using instead of a junction, a conventional broad band small electromagnetic antenna. Taking account that the beam has very short front of rising and decaying, a broad frequency electromagnetic wave will be generated, as a large Fourier spectra of the field variation. A broad band small antenna, like a fractal antenna could give a reasonable signal to be detected. Fractal antenna designed could give an efficiency 20% in UHF (GHz - THz), and are able to cover a large band of frequencies (non-resonant antenna, Figure 12) [Werner 2003], [Rusu 2001], [Rusu 2008].

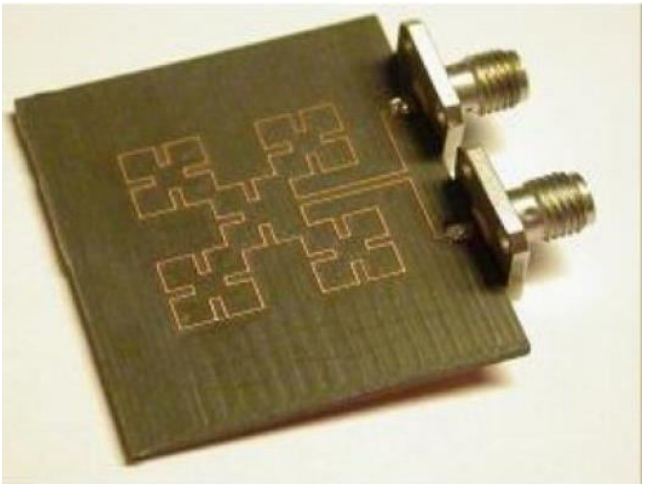


Figure 10

2) Atomic phenomena

involving high power laser beam

2.1- Two-photon absorption

- The idea of two-photon absorption was proposed by Maria Goeppert-Mayer, in her doctorate on the theory of possible two-photon absorption by atoms via virtual state (Figure 11) The first experimental verification of the TPA was obtained when two-photon-excited fluorescence was detected in a europium-doped crystal [Kaiser 1961] and observed in a cesium vapor [Abbela 1962].
- Two-photon absorption can be measured for exemple by two-*photon excited fluorescence* (TPEF) and *nonlinear transmission* (NLT). Pulsed lasers are most often used because TPA is a third-order nonlinear optical process, and therefore is most efficient at very high intensities.

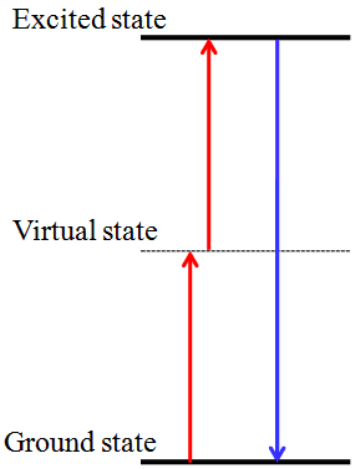


Figure 11

- If there were an intermediate state in the gap, this could happen via two separate one-photon transitions in a process described as "resonant TPA", "sequential TPA", or "1+1 absorption". In nonresonant TPA the transition occurs *without the presence of the intermediate state*. This can be viewed as being due to a "virtual" state created by the interaction of the photons with the molecule.
- The most important features of strongly TPA molecules were found to be a long conjugation system (analogous to a *large antenna*) and substitution by strong donor and acceptor groups (which can be thought of as inducing nonlinearity in the system and *increasing the potential for charge-transfer*).
- Many astrophysical processes involve multiphoton transitions:

- “Continuous emission from planetary nebulae” [Spitzer 1951],
- “Two-photon emission in planetary nebula IC 2149” [Gurzadyan 1976].

2.2- Hertzian spectroscopy

- Alfred Kastler who studied the interaction between light and atoms working on combination of optical resonance and magnetic resonance, developed the technique of "*optical pumping*" [Kastler 1950], [Kastler 1967]. Those works led to the completion of the theory of lasers and masers. He won the Nobel Prize in Physics in 1966 "*for the discovery and development of optical methods for studying Hertzian resonances in atoms*".
- These type o problems was developed at Physics Faculty from Bucharest University by professors Th. V. Ionescu, with prof V. Mihu (1954) worked on simulated emission in microwave [Ionescu 1972], [Ingram 1976]. His additional researches went on the problem of plasma resonance phenomena due to oxygen ions and hydrogen in magnetic fields. He measured magnetic resonance oscillations in hot plasmas in longitudinal magnetic fields.

- Professor Ion I. Agârbiceanu from Institute of Atomic Physics from Bucharest constructed the first Romanian laser using optical pumping in a mixture of helium and neon (1962) in his laboratory of "Optical methods in nuclear physics" [Agârbiceanu 1970].

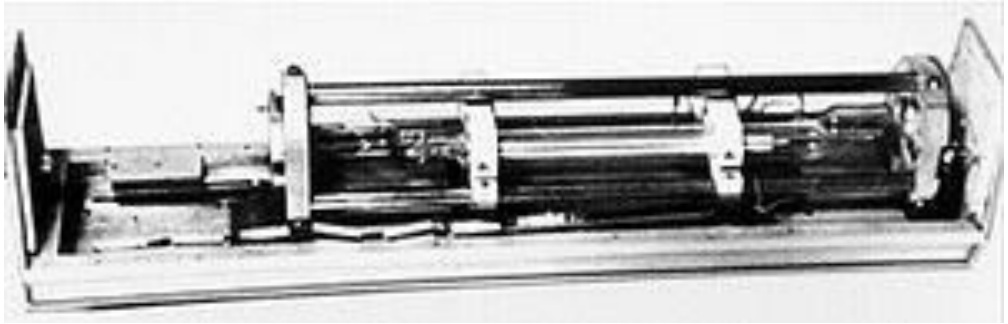


Figure 12

- His laboratory worked on finding new media for laser action and one of researcher, dr. George Victor Velculescu, studied and designed the cadmium vapor population inversion. He found that over 600 ^{0}C, it was possible to obtain laser action (unpublished results).

- So this is a field of experiments that could be imagined with the new laser facility. As examples are o long list of papers, their titles are self explaining:

- „Double irradiation en spectroscopie hertzienne gazeuse”; [Cagnac 1973], [Cagnac 1977]
- “Femtosecond Measurements of Two-Photon Absorption Coefficients at λ = 264 nm in Glasses, Crystals, and Liquids”; [Nikogosyan 1981]
- “Multiphoton high resolution spectroscopy” [Kogej 1998]
- “Mechanisms for enhancement of two-photon absorption in donor–acceptor conjugated chromophores” [Dragomir 2002]
- “Formation of free radicals in water under high-power laser UV irradiation”; [Underwood 2004]
- “Ultrafast spectroscopy of single molecules”, [van Dijk 2007]

2.3- Luminescence

- Luminescence is a collective term for different phenomena where a substance emits light without being strongly heated, i.e. the emission is not simply thermal radiation. This definition is also reflected by the term “cold light”.
- Important kinds of luminescence are:

Fluorescence is light emission caused by irradiation with light (normally visible or ultraviolet light) and typically occurring within nanoseconds to milliseconds after irradiation. It involves the excitation of electrons into states with a higher energy, from where radiative decay is possible. Typically, the emitted wavelengths are longer than the excitation wavelengths; otherwise one speaks of upconversion fluorescence.

Phosphorescence is a light emission which can occur over much longer times (sometimes hours) after irradiation. It involves storage of energy in metastable states and its release through relatively slow (often thermally activated) processes. The phenomenon was discovered early on for phosphorus.

Photoluminescence is a less specific term which embraces both fluorescence and phosphorescence.

Chemiluminescence is light emitted during (cold) chemical reactions.

Bioluminescence is chemiluminescence from living organisms.

Thermoluminescence is a type of phosphorescence which occurs at elevated temperatures. It is not to be confused with thermal radiation: the thermal excitation only triggers the release of energy from another source.

Electroluminescence is light emission triggered by electric influences. In the case of excitation by an electron beam, this is also often called *cathodoluminescence*.

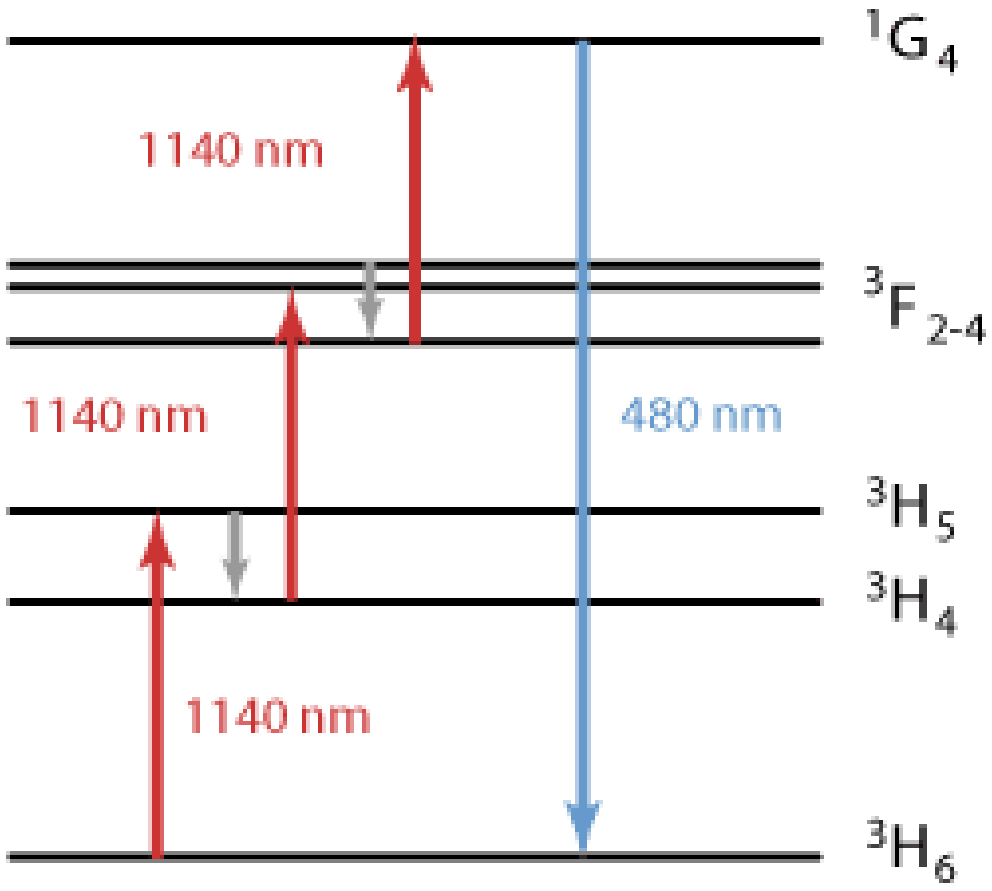
Radioluminescence is caused by excitation with nuclear radiation or X-rays.

Triboluminescence can occur when a material is mechanical treated, e.g. fractured or polished.

- http://www.rp-photonics.com/luminescence.html

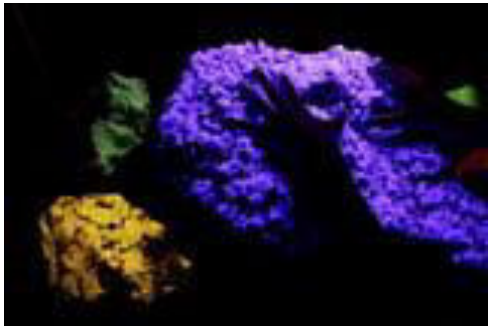
- Metastable States: excited states (particularly electronic states in laser gain media) which have a relatively long lifetime due to slow radiative and non-radiative decay.
- Solid-state gain media usually have a metastable electronic state as upper laser level, and often some additional metastable states (energy levels). Such states occur in situations where neither radiative nor non-radiative processes can lead to a rapid depopulation of a certain state. Radiative processes can be strongly reduced if all transitions to lower levels are so-called forbidden transitions (or *weakly allowed transitions*), for which efficient dipole processes are not possible.

- Strong non-radiative decay processes can arise from multi-phonon transitionsand from quenching caused by certain impurities, but such mechanisms can often be avoided. The upper-state lifetime, i.e. the lifetime of the upper laser level, can then be microseconds or even milliseconds – for example, typically around 8–10 ms for erbium-doped fiber amplifiers, or roughly 1–2 ms for ytterbium-doped gain media.
- As an example, Figure 1 shows the energy level scheme of thulium (Tm3+) ions. In fluoride fibers, having very low phonon energies, the levels 3H4, 3F4 and 1G4 are metastable, whereas e.g. 3H5 is quenched by multi-phonon processes which transfer the ions to 3H4. These circumstances make it possible to pump thulium ions efficiently into the 1G4 level, from where blue light can be emitted.



Level scheme of thulium (Tm3+) ions in ZBLAN fluoride fiber. The levels $^3H_4$, $^3F_4$ and $^1G_4$ are metastable.

- This is exploited in some upconversion fiber lasers. For thulium ions in silica fibers, 3F4 has a much shorter lifetime, since multi-phonon processes are much stronger. Therefore, silica fibers are not usable for such upconversion lasers.
- Generally, laser gain media do not have to exhibit metastable levels; a short-lived level can still be used as the upper laser level provided that the emission cross sections are large enough. (For the threshold pump power, the $\sigma - \tau$ product is the essential quantity.) However, long metastable level lifetimes are very important for Q-switched lasers, as they permit significant energy storage. They also have a strong impact on the laser dynamics, including spiking phenomena. Finally, three-level laser transitions are hardly possibly without metastable levels, since a substantial upper-state population as needed for positive net gain would be difficult to achieve.



quartz_lumen



Thermoluminescence of fluorite.

TL2000: integrated thermoluminescence unit

Our thermoluminescence laboratories are currently used in: Italian National Institute for the Physics of Matter (INFM); University of Milan-Bicocca; University of Torino; University of Lecce; University of Bari; the Research Institute Pastis CNRSM of Brindisi; the Arcadia - Technologies for Cultural Heritage, Milan; Department of Conservation and Restoration of the Museum of Xian (China); Tubitak Marmara Research Institute - CNRS, Gebze (Turkey); Department of Archeology – National Museum and Library of Myanmar.

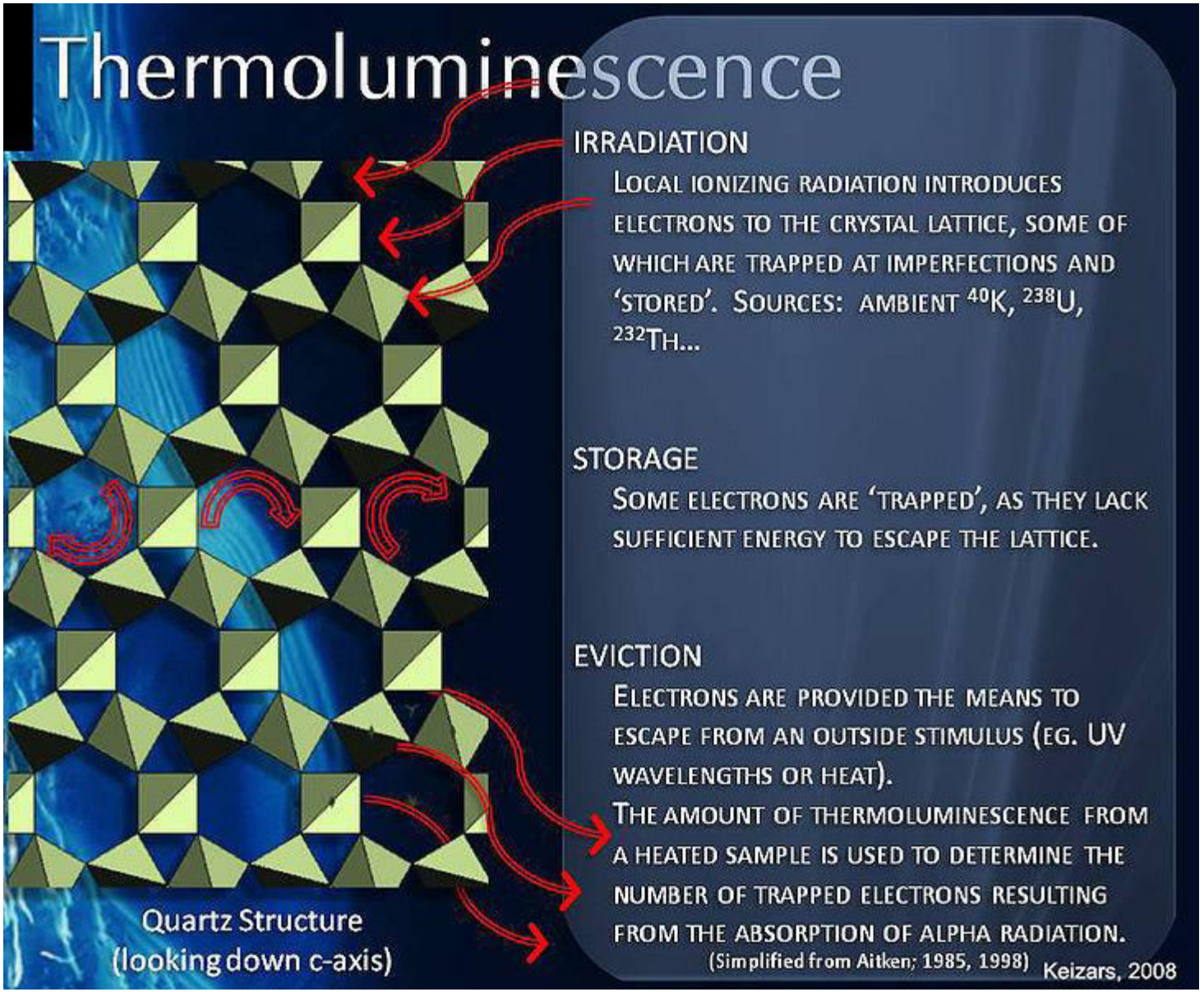
http://www.ipses.com/prod/TL/TL_Lab.php?language=en&gclid=CJSXzfvH4rwCFYjpwgodL3UA1g



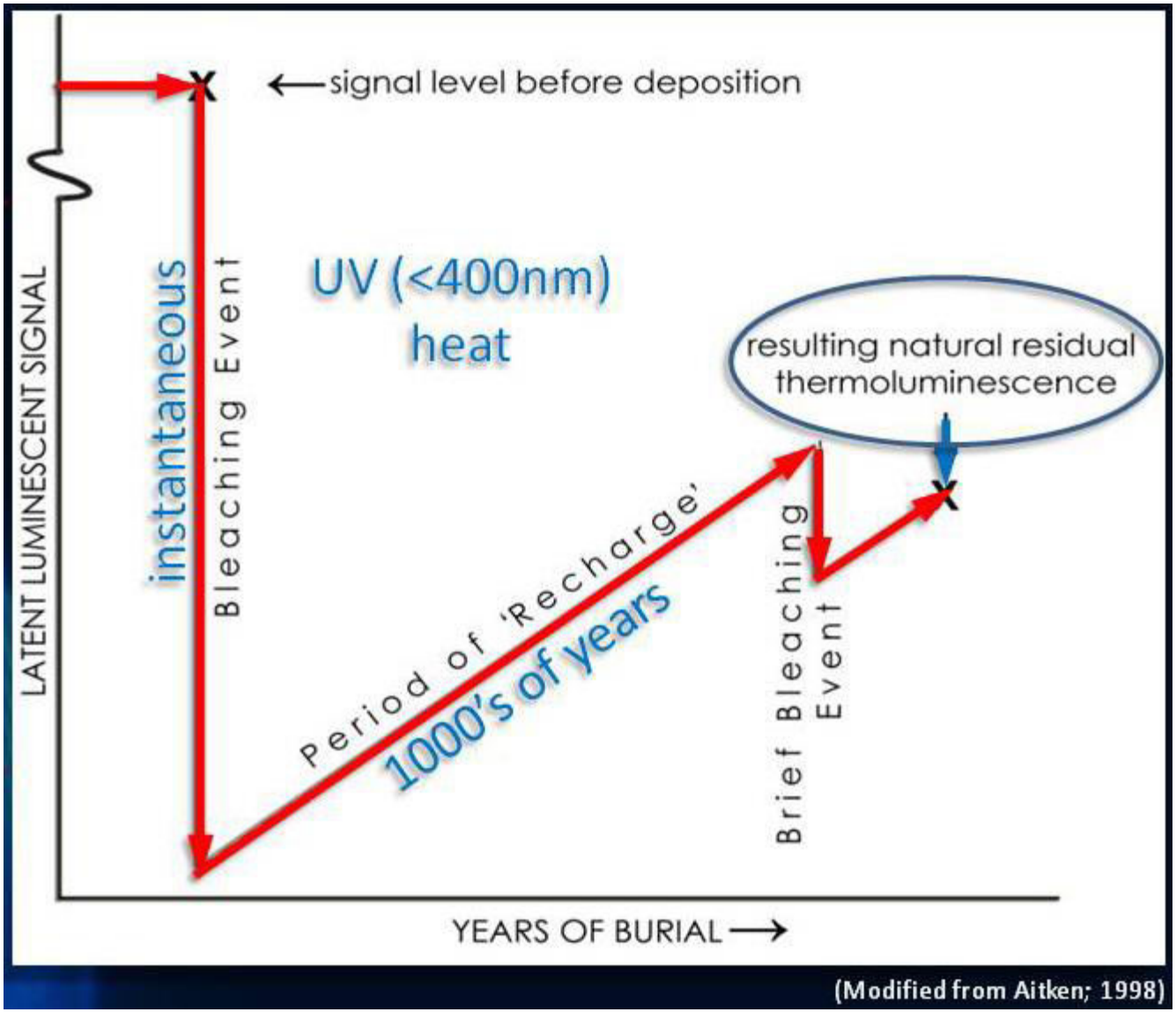
Image: C. C. WONG/Mandarin Collection**ANCIENT ARTWORK,** such as this Chinese horse, can be evaluated using thermoluminescence. The dating confirmed that the horse does indeed date back 1,000 years to the Tang dynasty, as its style suggests.

THERMOLUMINESCENCE AND ELECTRON SPIN RESONANCE

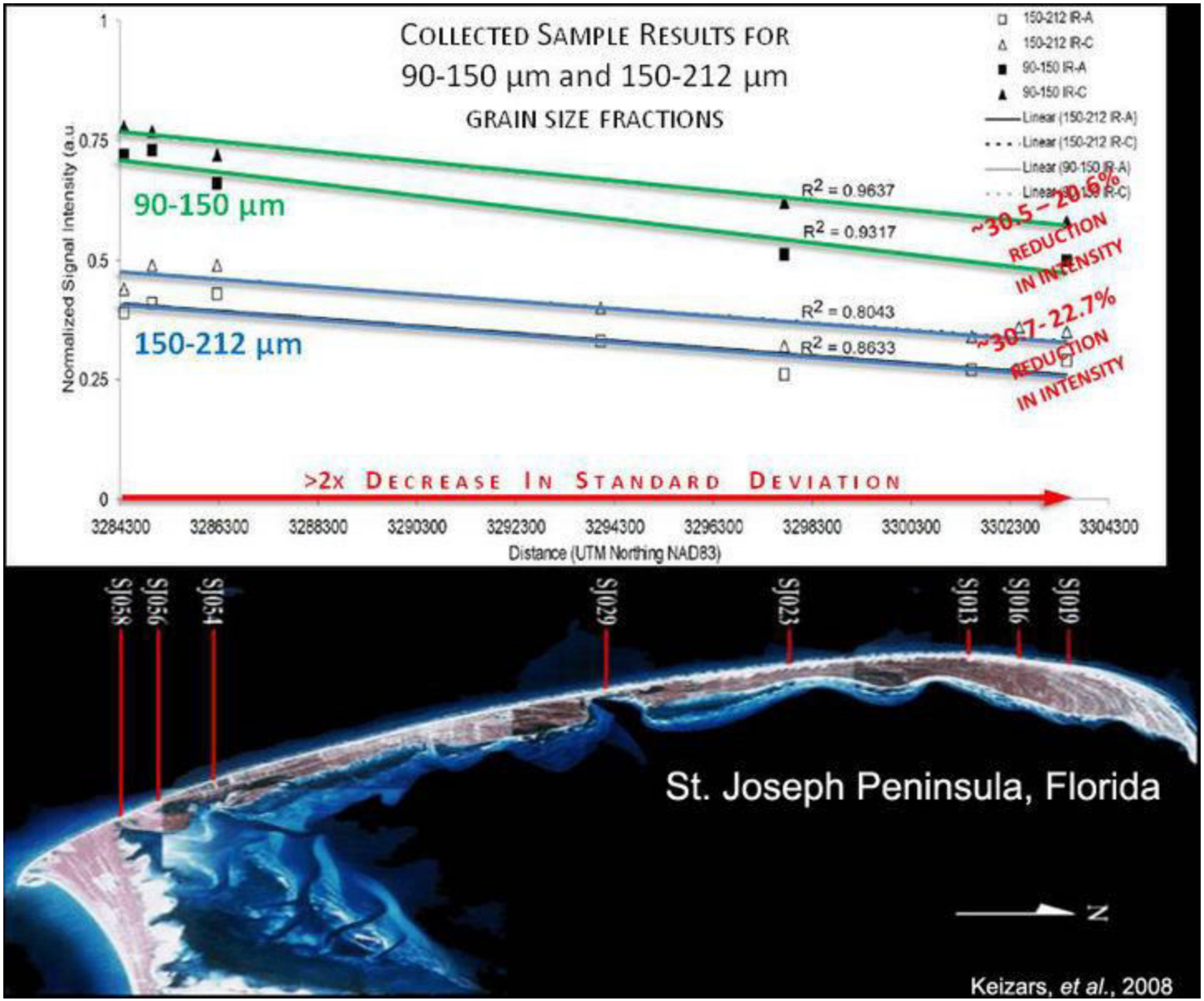
- Image: C. C. WONG/Mandarin Collection**ANCIENT ARTWORK,** such as this Chinese horse, can be evaluated using thermoluminescence. The dating confirmed that the horse does indeed date back 1,000 years to the Tang dynasty, as its style suggests.Many crystals, including diamond, quartz and feldspar, accumulate and trap electric charges at a known rate over time. Heating the crystals, it turns out, liberates these electrons, emitting a measurable amount of light. Researchers can thus determine the amount of time that has passed since the buried crystal was last exposed to heat.
- In the case of thermoluminescence, resetting the crystal clock means heating it to around 500 degrees Celsius. Because of that condition, scientists say, the technique is well suited to dating meteoritic impacts, fire-treated stones used by early humans, cooking hearths and old ceramics.
- Somewhat similar to thermoluminescence, electron spin resonance (ESR) dates crystals, too (although these are found in shells and enamel.) Unlike thermoluminescence, however, this method counts the number of "unpaired spins" of electrons trapped in the crystal, instead of freeing them.
- ESR can be used to evaluate materials up to one million years old and has become an indispensable tool for paleoanthropologists, who often use it to date the teeth of animal remains found among the precious human fossils.



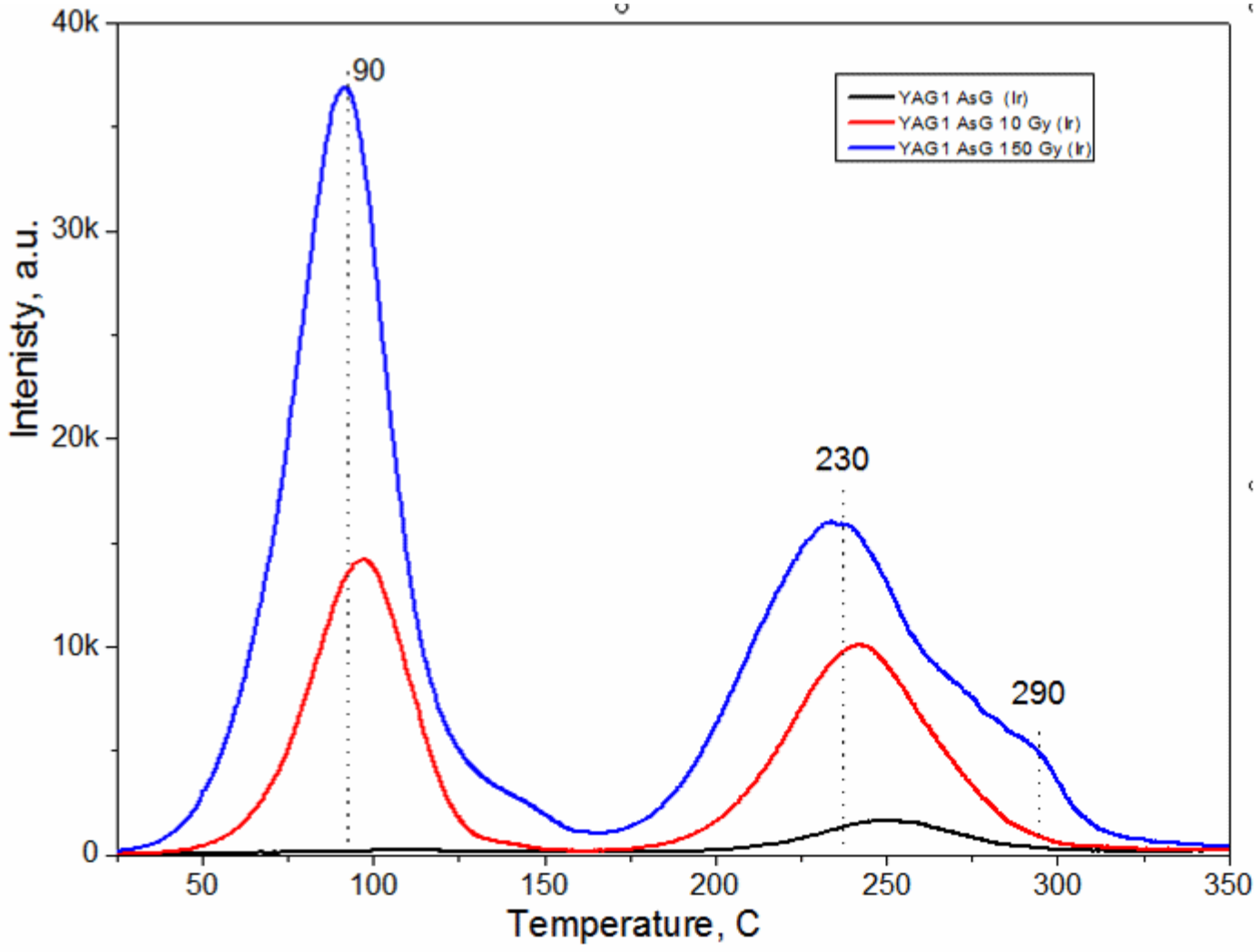
Three stages of thermoluminescence as outlined by Aitken (1985, 1998) and applied to a quartz grain (Keizars - 2008b).



The process of recharging and discharging thermoluminescent signal, as applied to beach sands. (modified from Aitken, 1998 Keizars, 2008).



Thermoluminescence signature lost during migration of two sand grain sizes (Keizars, 2008).



Graph of TSL

http://www.scientificamerican.com/article/the-dating-game/

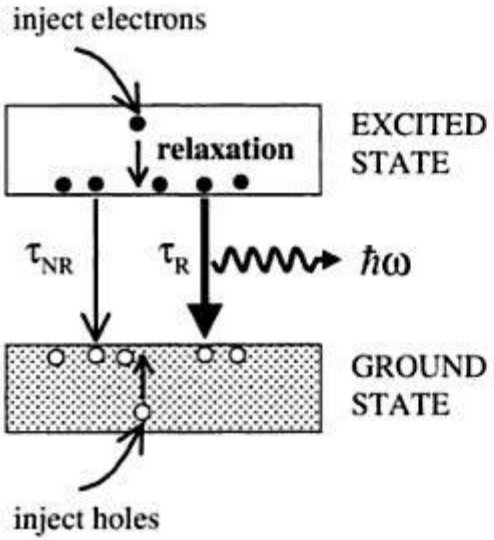


Fig. 5.1 General scheme of luminescence in a solid. Electrons are injected into the excited state band and relax to the lowest available level before dropping down to empty levels in the ground state band by emitting a photon. These empty levels are generated by the injection of holes. The radiative recombination rate is determined by the radiative lifetime τ_R. Radiative emission has to compete with non-radiative recombination, which has a time constant τ_{NR}. The luminescent efficiency is determined by the ratio of τ_R to τ_{NR}, and is given by eqn 5.5.

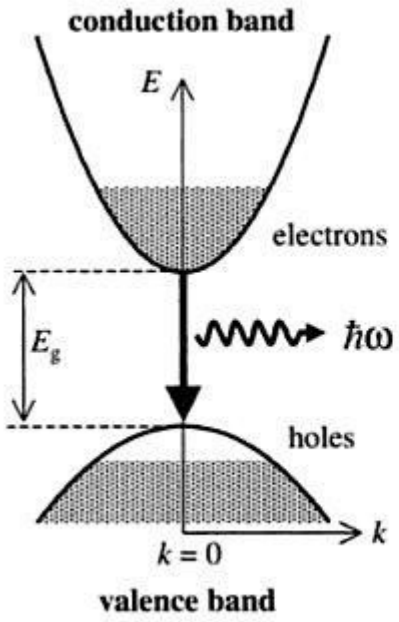


Fig. 5.2 Schematic diagram of the interband luminescence process in a direct gap semiconductor. The shading indicates that the states are occupied by electrons. The filled states at the bottom of the conduction band and the empty states at the top of the valence band are created by injecting electrons and holes into the semiconductor.

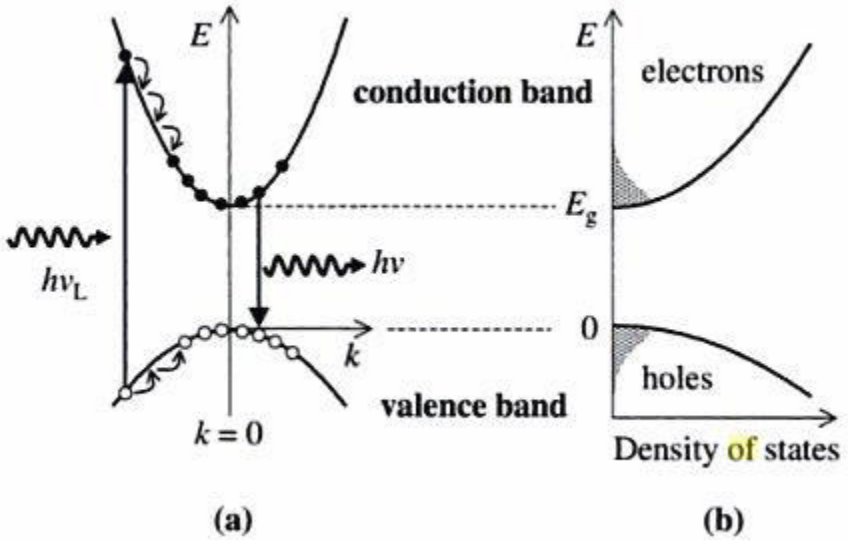


Fig. 5.5 (a) Schematic diagram of the processes occurring during photoluminescence in a direct gap semiconductor after excitation at frequency ν_L. The electrons and holes rapidly relax to the bottom of their bands by phonon emission before recombining by emitting a photon. (b) Density of states and level occupancies for the electrons and holes after optical excitation. The distribution functions shown by the shading apply to the classical limit where Boltzmann statistics are valid.

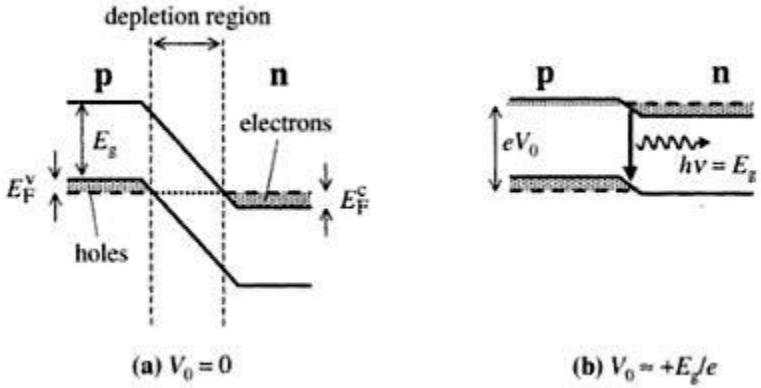


Fig. 5.12 Band diagram of a light emitting diode at (a) zero bias, and (b) forward bias $V_0 \approx E_g/e$. The diode consists of a p-n diode with heavily doped p and n regions. The dashed lines indicate the positions of the Fermi levels in the p and n regions. Light is emitted in (b) when the electrons in the n-region recombine with holes in the p-region at the junction.

Bibl TL

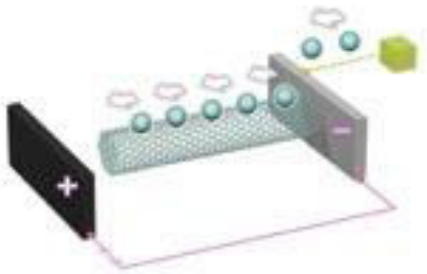
- GlobalNet.co.uk, Quaternary TL Surveys - Guide to thermoluminescence date measurement
- Aitken, M.J., *Thermoluminescence Dating*, Academic Press, London (1985) – Standard text for introduction to the field. Quite complete and rather technical, but well written and well organized. There is a second edition.
- Aitken, M.J., *Introduction to Optical Dating*, Oxford University Press (1998) – Good introduction to the field.
- Keizars, K.Z. 2003. NRTL as a method of analysis of sand transport along the coast of the St. Joseph Peninsula, Florida. GAC/MAC 2003. Presentation: Brock University, St. Catharines, Ontario, Canada.
- JCRonline.org, Keizars, Z., Forrest, B., Rink, W.J. 2008. Natural Residual Thermoluminescence as a Method of Analysis of Sand Transport along the Coast of the St. Joseph Peninsula, Florida. Journal of Coastal Research, 24: 500-507.
- Keizars, Z. 2008b. NRTL trends observed in the sands of St. Joseph Peninsula, Florida. Queen's University. Presentation: Queen's University, Kingston, Ontario, Canada.
- Liritzis, I., 2011. Surface Dating by Luminescence: An Overview. Geochronometria, 38(3): 292-302.
- Antiquity.ac.uk, Rink, W. J., Bartoll, J. 2005. Dating the geometric Nasca lines in the Peruvian desert. Antiquity, 79: 390-401.
- Sullasi, H. S., Andrade, M. B., Ayta, W. E. F., Frade, M., Sastry, M. D., & Watanabe, S. (2004). Irradiation for dating Brazilian fish fossil by thermoluminescence and EPR technique. Nuclear Instruments and Methods in Physics Research Section B: Beam Interactions with Materials and Atoms, 213, 756-760.doi:10.1016/S0168-583X(03)01698-7

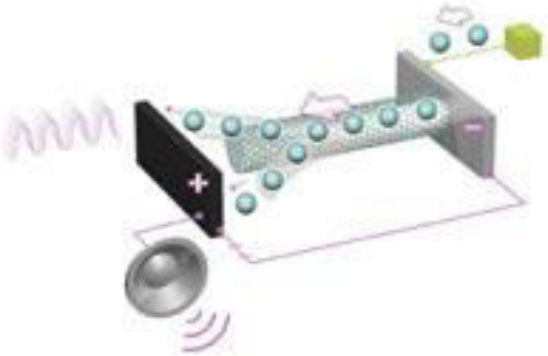
2.4- Nanotube radio receiver

- Nanotube antenna and receiver [Zettl 2008]

The physicist at the University of California, Berkeley, and his colleagues have come up with a nanoscale radio, in which the key circuitry consists of a single carbon nanotube.

Zettl's nano receiver works by translating the electromagnetic oscillations of a radio wave into the mechanical vibrations of a nanotube, which are in turn converted into a stream of electrical pulses that reproduce the original radio signal. Zettl suggests that nanoradios attached to tiny chemical sensors could be implanted in the blood vessels of patients with diabetes or other diseases.





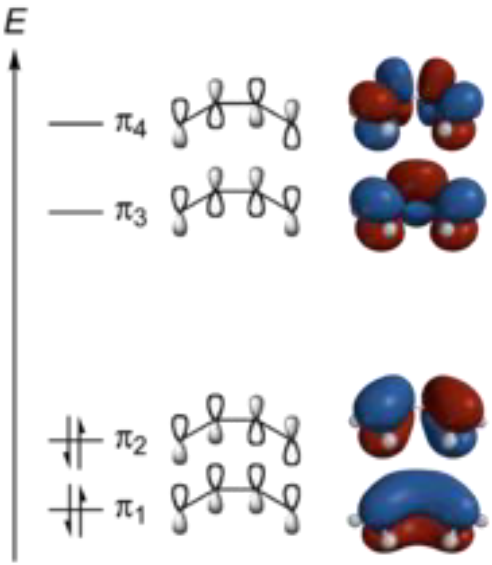
2.5- Poliatomic molecules as antennas for radiation

- Hückel and Möbius annulenes: relationships between their hückel-level orbitals and their hückel-level energies [Huckel 1931], [Langler 1999],
- Linear polyenes: models for the spectroscopy and photophysics of carotenoids, [Christensen 2004]



Molecular orbitals ethylene

$$E = \alpha + \beta$$



Butadiene molecular orbitals

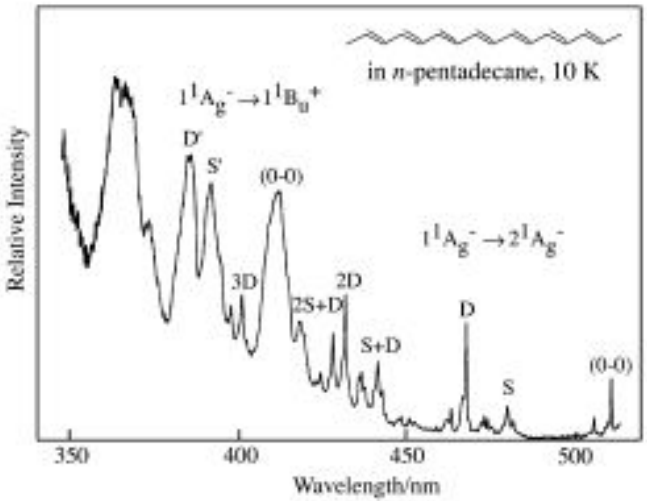


Fig. 6. Fluorescence excitation spectra ($1^1A_g^- \rightarrow 2^1A_g^-$ and $1^1A_g^- \rightarrow 1^1B_u^+$) of *all-trans*-2,4,6,8,10,12,14-hexadecaheptaene in 10 K *n*-pentadecane. Fluorescence was detected at 560 nm. The excitation spectrum is not corrected for the wavelength dependence of the excitation system. (Figure adapted by the author, RLC, from his own Fig. 3 of [28].)

3) Phenomena involving high power laser beam

- **3.1 Laser induced breakdown**,

Laser beam could ignite a kind of spark, and the medium becomes electrically conducting. The mechanism behind this effect is based on the acceleration of free electrons to high energies so that collisions with other atoms or molecules can lead to secondary free carriers. This starts an avalanche process, during which appreciable densities of free carriers can be built up within a short time. A plasma is formed, which can have a significant electrical conductivity. The plasma can be maintained by further current flow, which generates additional free carriers.

Breakdown in air and in other transparent media can be initiated by intense light (electromagnetic waves) with frequencies of hundreds of terahertz. The high optical intensities required can be reached in pulses as generated e.g. in a Q-switched laser (with nanosecond durations) or in a mode-locked laser and amplified in a regenerative amplifier (for pulse durations of picoseconds or femtoseconds). The intensity required for optical breakdown depends on the pulse duration. For example, for 1-ps pulses an optical intensity of $\approx 2 \times 10^{13}$ W/cm^2 is required.

Laser induced gas breakdown: A bibliographical review [DeMichelis 1969], *Fractal phnomena in electric discharges* [Ene 2004], *Handbook of Laser-Induced Breakdown Spectroscopy* [Cremers 2006],

4) Quantum effects induced by high power laser beam

4.1- Possible changing of the radioactive time decay of some nuclei by modifying coulomb barrier height (C.II.4)

Alfa radioactivity is completely determined by nuclear-coulomb barrier. It is dependent on the height of the barrier above the energy level from where the alpha particle is coming. So, a strong electric field that could change the barrier (in the height and length) will modify the rate of decay. Electrical fields of ~ 10^{15} V/m could be obtained in beam. The effect on barrier could be seen and measured.

So, I propose to verify changes in radioactive constant or time of radioactive decay, using short living nuclei placed in the very intense laser beam that produce a very high electric field. Possible nuclei are listed here:

- Alfa decay nuclei with short time decay could be:

90-Th-228	1.9 y	5.4 MeV
88-Ra-224	3.64 d	5.68 MeV
88-Ra-223	11.2 d	5.33 MeV
86-Rn-222	3.8 d	5.48 MeV
84-Po-218	3.05 min	6 MeV
84-Po-210	139 d	5.3 MeV

The importance of the Coulomb barrier for nuclei to decay is given by the approximate formula for coulomb potential combined with an approximate rectangular nuclear potential (Figure 13), radioactive constant:

$$\lambda = \frac{h}{mR_0^2} \exp\left(-\frac{4\pi}{h} \sqrt{2m} \int_{x=R_0}^{x=R_1} \sqrt{U-E} \cdot dx \right)$$

where R_0 and R_1 are nuclear radius and respectively the distance form the center of the nucleus to the position of particle at the coulomb barrier, at the particle energy, U being the height of the barrier above the particle energy E.

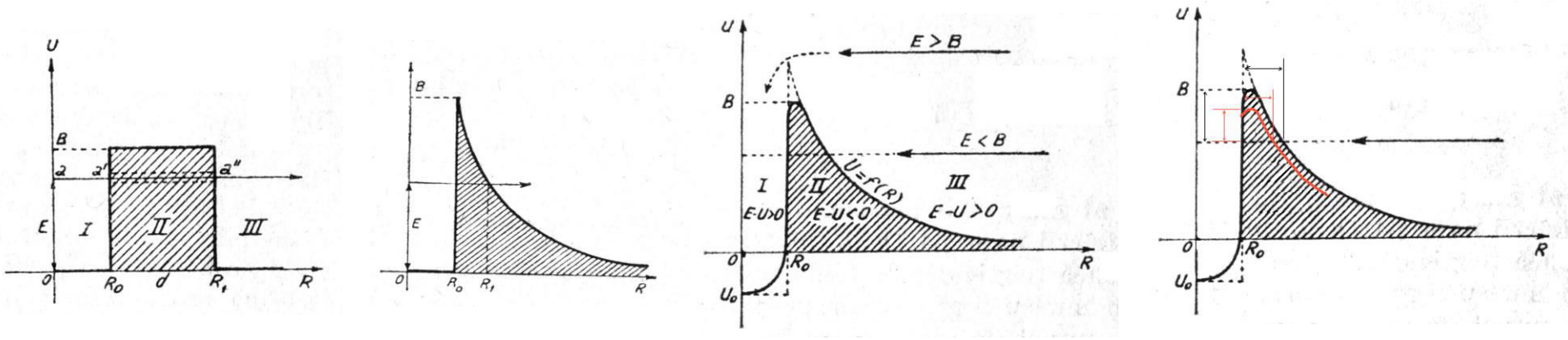


Figure 13

$$\lambda = \frac{h}{mR_0^2}\exp\left(-\frac{4\pi}{h}\sqrt{2m}\int_{x=R_0}^{x=R_1}\sqrt{U-E}\cdot dx\right)$$

To compare the validity of such a simple approximation we compute for two well known and studied nuclei the values of the λ using the above formula:

for 238 U-92 (T = 4.5 109y; λ = 7.04 10-18 1/s) exp(-90) = 8.2 10^{-40}
for 218 Po-84 (T = 3.05 min; λ = 5.46 10-3 1/s) exp(-55.7) = 6.510^{-25}

,

- For both nuclei the pre-exponential coefficient have approximate the same value, the ratio of the computed values (Po/U) is:

$$\frac{6.46 \cdot 10^{-25}}{8.2 \cdot 10^{-40}} = 7.9 \cdot 10^{14}$$

and the ratio of radioactive constants (Po/U) is:

$$\frac{5.46 \cdot 10^{-3}}{7.04 \cdot 10^{-18}} = 7.7 \cdot 10^{14}$$

- So we expect a sensible effect on the radioactive decay rate if the coulomb barrier is even slightly modified. The high electric field of the laser beam could affect both the height of the barrier (U - E) and also the length (extent) of the barrier (R1 – R0) at the energy level.

4.2- Compressing deuterium gas – changing the rate of D-D fusion reaction

- If a measurable effect is seen in the experiment 4.2, it is possible to try to act on deuterium atoms (vapor) to compress them in order to modify the rate of the fusion rate as in the case of inertial fusion experiment. One of the difficulties encountered in the laser fusion experiments was the instability of the deuterium pallet under the influence of the geometry of irradiation, i.e. asymmetry of irradiation and hence the instability of the pallet in the combined field of beams.
- Using one beam of maximum power (from ELI), this instability could be overcome if the deuterium pallets are supplied in the middle of a hollow beam (a cylindrical one) that could increase the stability of the inertial compression. At least it could be experimented because a better stability could be a good hope for fusion experiments.

4.3- Physics of diffusion of Hydrogen in some porous metals (Pd)

5) Astrophysics and possible D – D fusion reaction

5.1- Continuous emission from planetary nebulae that are usually produced by multiple photon excitations

5.2- The role of small cross sections nuclear reactions in the balance of p-p chain

5.3- Mathematical study of the possible oscillatory solutions in the system of equations for p-p chain

5.4- Simulating nucleosynthesis in stars

5.5- Modeling periodicity of Sun's activity (the 11 years cycle)

5.6- Rate generation of energy in Sun's core

- - Element synthesis in astrophysics (in Sun) and instabilities of stars
- - Fundamental problems of astrophysics
- - Modeling supernova explosion

6) Order – disorder phenomena in solids and materials of biological origins

6.1- Local order in amorphous materials

a)- Ge-a and Si-a (local order at atomic scale) and momentum distributions of electrons in solids, type of crystalline structure: disordered polyhedron ? Voronoy polyhedron? "amorfon" ?

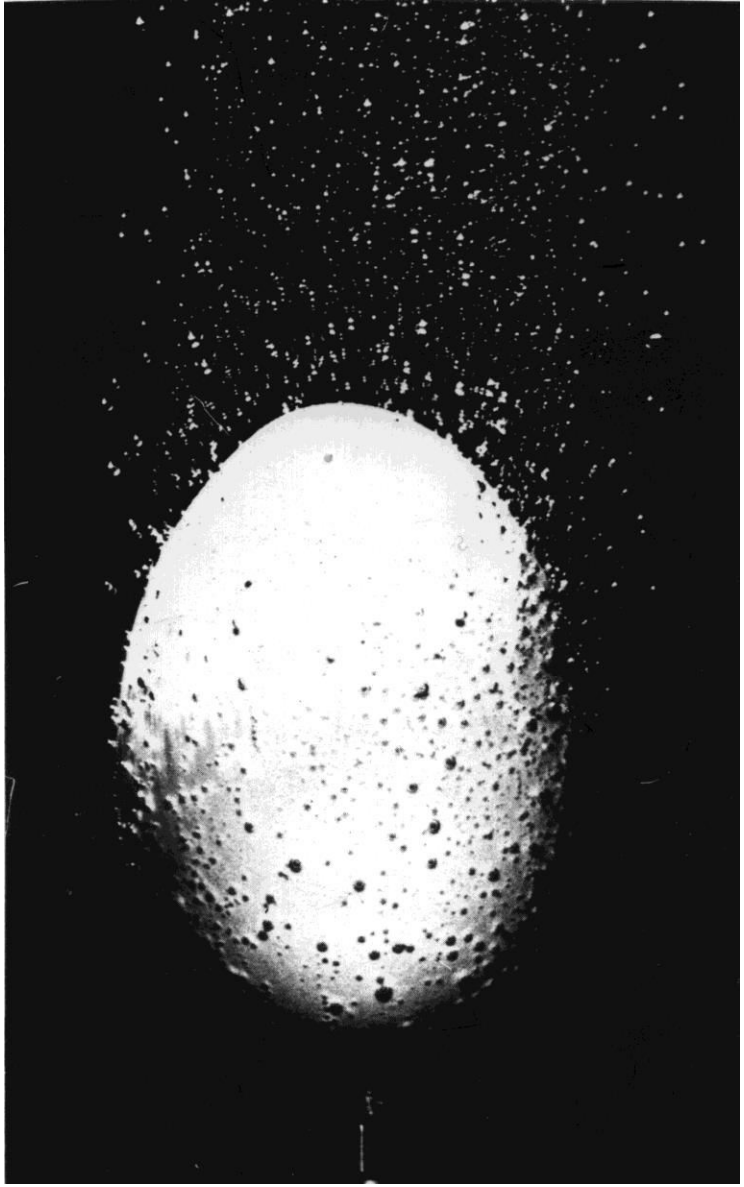
b)- Study of order – disorder transition in solids under very short pulse shock wave (high energy deposition, radiation pressure, local order, specific defects, …)

c)- study of the anomaly of calcite crystalline structure for mineral origin and for organic origin

6.1a- Mössbauer experiments with non-Mössbauer nuclei

- By Mössbauer spectroscopy it is possible to find the type of local order, which is important for disordered materials.
- An example is the whole category of amorphous materials like a-Ge or a-Si, materials of interests for microelectronics.
- For example Ge is not a Mössbauer nuclei so it could not be used for studying the order in a-Ge. But there is a possibility of obtaining Ge as Mössbauer source if we use Ge-77 in the metstable state. It has a 0.088 MeV γ transition that could be used. The idea is to investigate such interesting cases and use the facility to study difficult crystalline structures.

6.1c Study the order - disordered in materials of biological origin



Demonstration of pores:

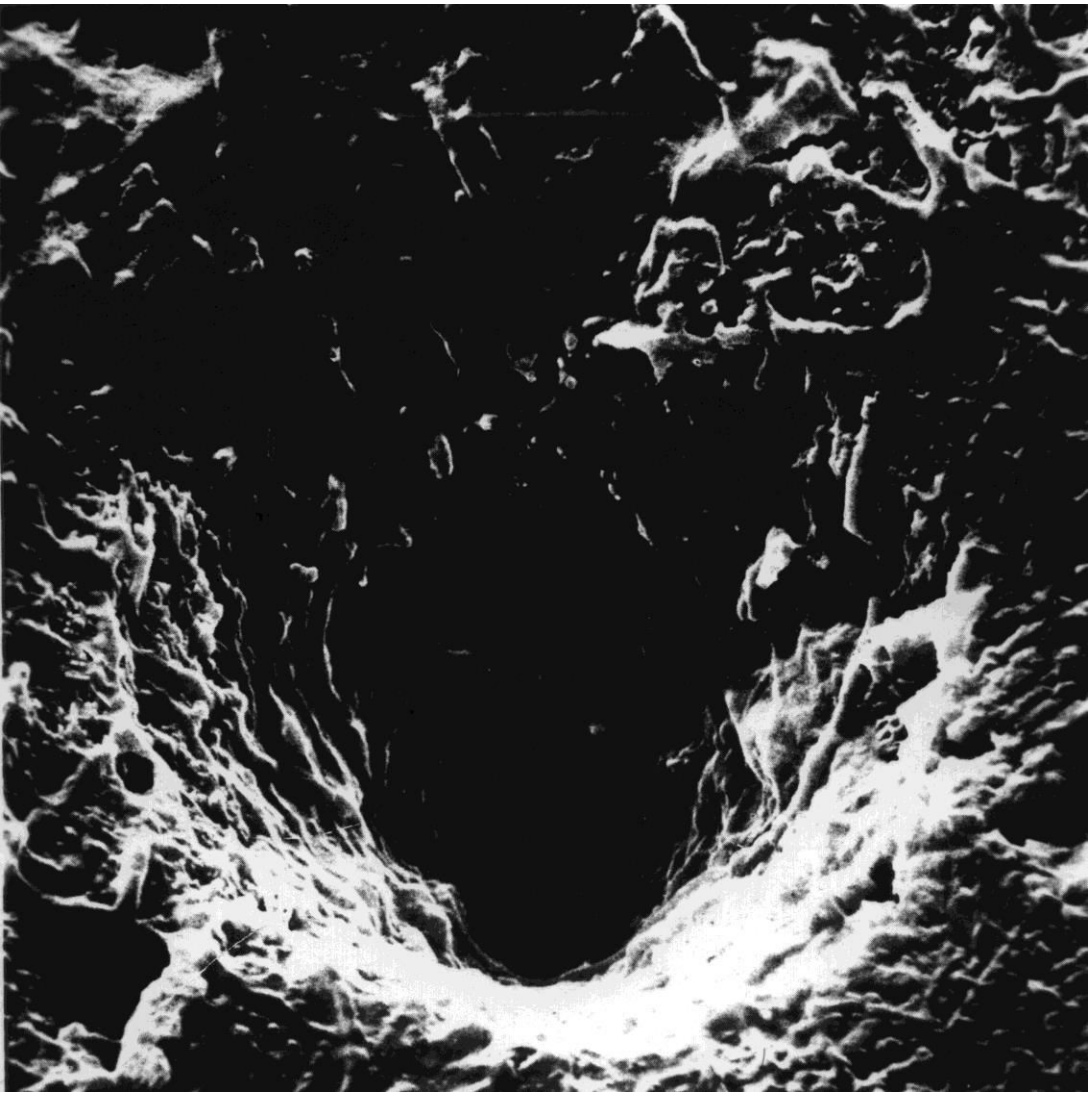
Injecting pressurized air at the blunt end of a chicken egg, bubbles emerge from the entire Surface of the egg (D.R.Atkinson, State Univ. N.Y. at Buffalo)

The egg

The concept that avian eggshells can adapt to fit eggs to different nesting environments has been considered by Board R.G. (1982- “Properties of avian eggshells and their adaptative value”, *Biol. Rev.* 57, pp.1-28)

Changes in pore number, pore area and pore length have all been observed in eggs adapted to unusual nesting regimes. The nature of such adaptations and particular the ways in which shell porosity can be regulated by the laying bird are areas of interest for the time to come (Tullet, S.G. “The Porosity of Avian Eggshells”, Comp. Biochem. Physiol. Vol- 78A. No. 1, pp. 5-13, 1984)

Pore in the eggshell of a cuckoo of Java, magnified 3,800 diameters (SEM).

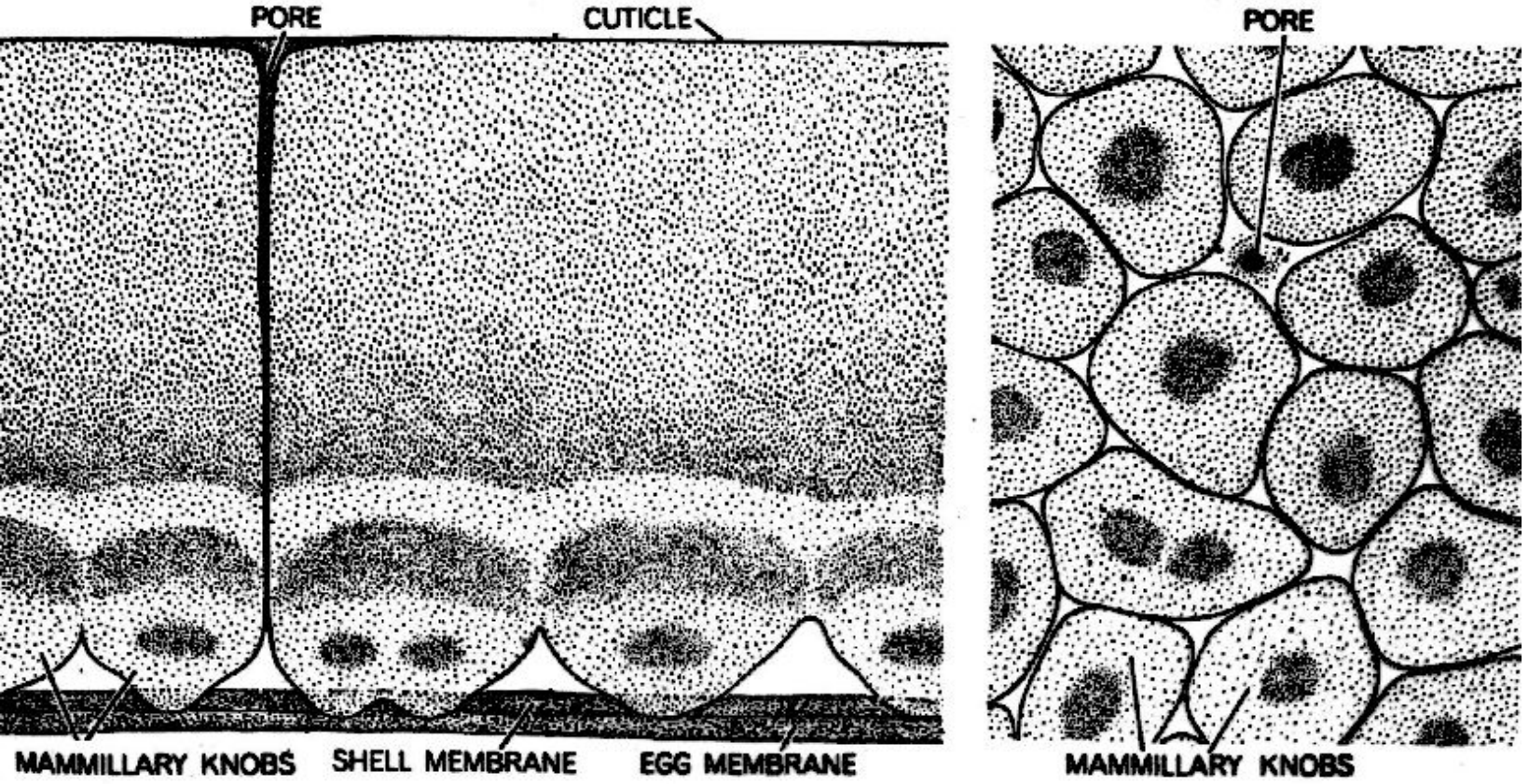


The conical pore opening narrows into a cylindrical tube of a few micrometers in diameter. Atmospheric oxygen enters the egg and metabolic CO_2 leaves it by passive diffusion through thousands of similar pores distributed over the egg surface.

(Micrograph by J.Backing)

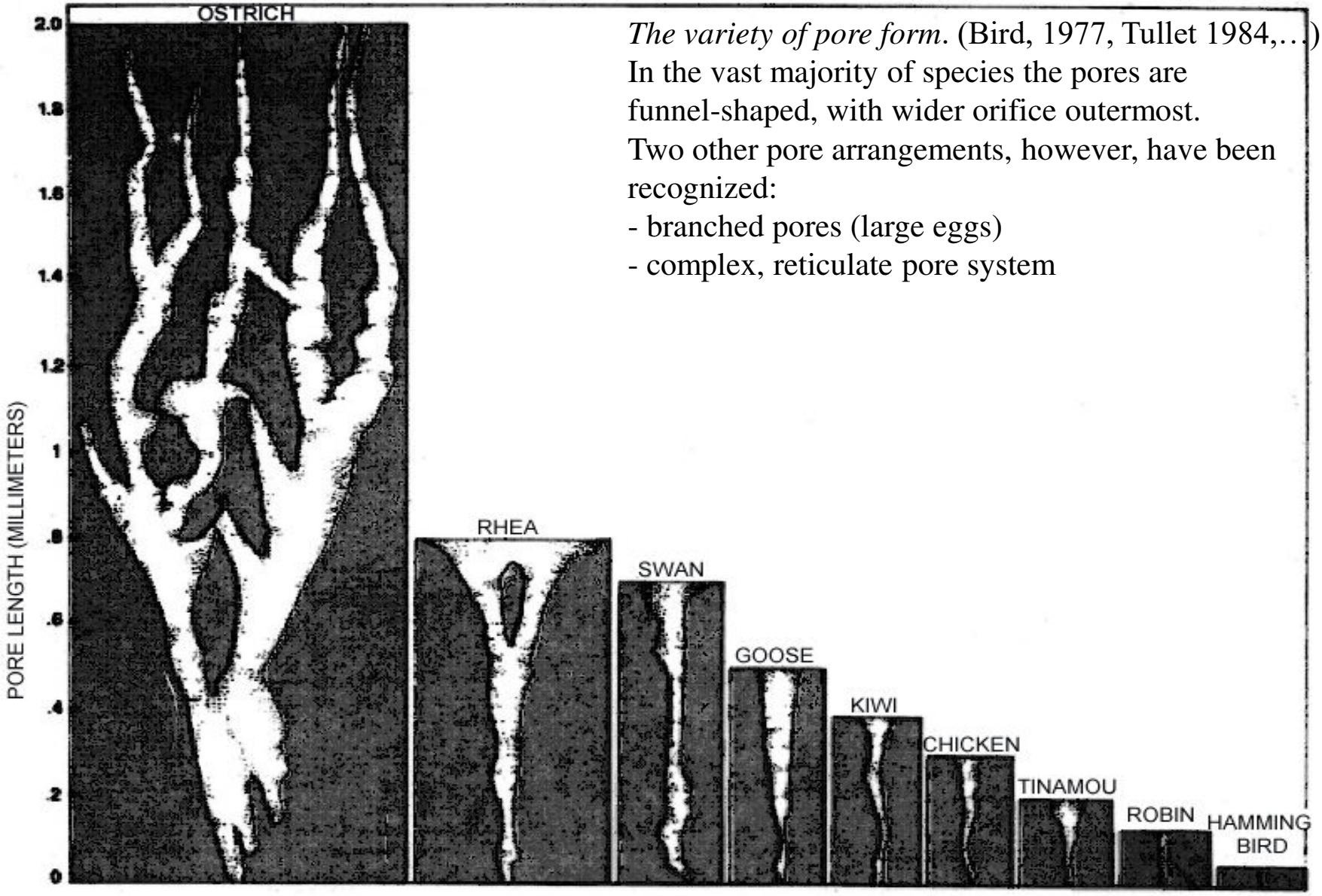
Structure of eggshell, cross section (left) and tangential section (right).

Mammillary knobs, which attach the shell to the outer membrane of the egg by fibres, have an organic core; the rest of the structure is made of oriented ions of calcium that apparently act as seeds for the shell's calcite crystals.



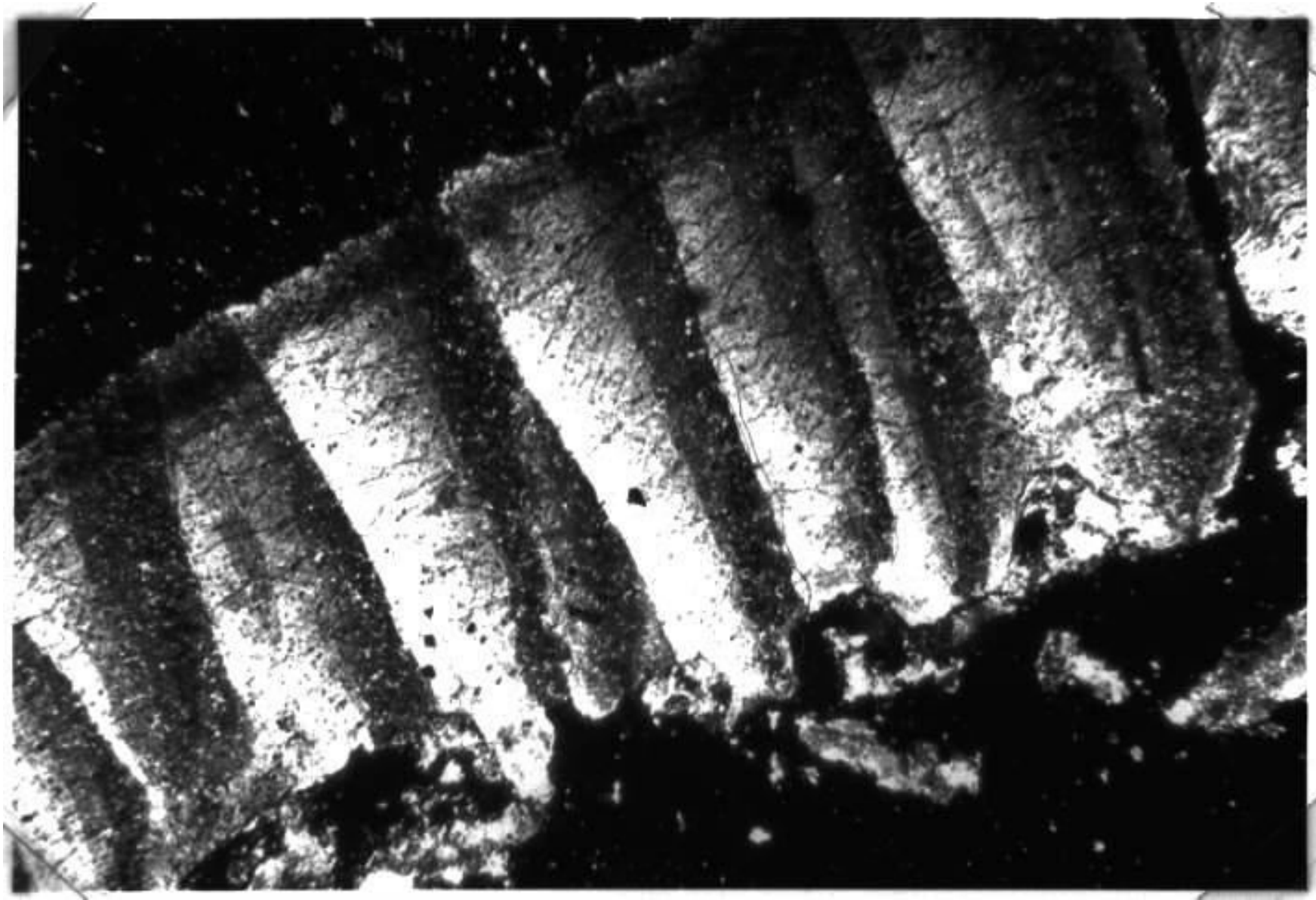
Shape of shell pores – different morphologies

(C.Tyler, K.Simkiss, Univ. of Reading)

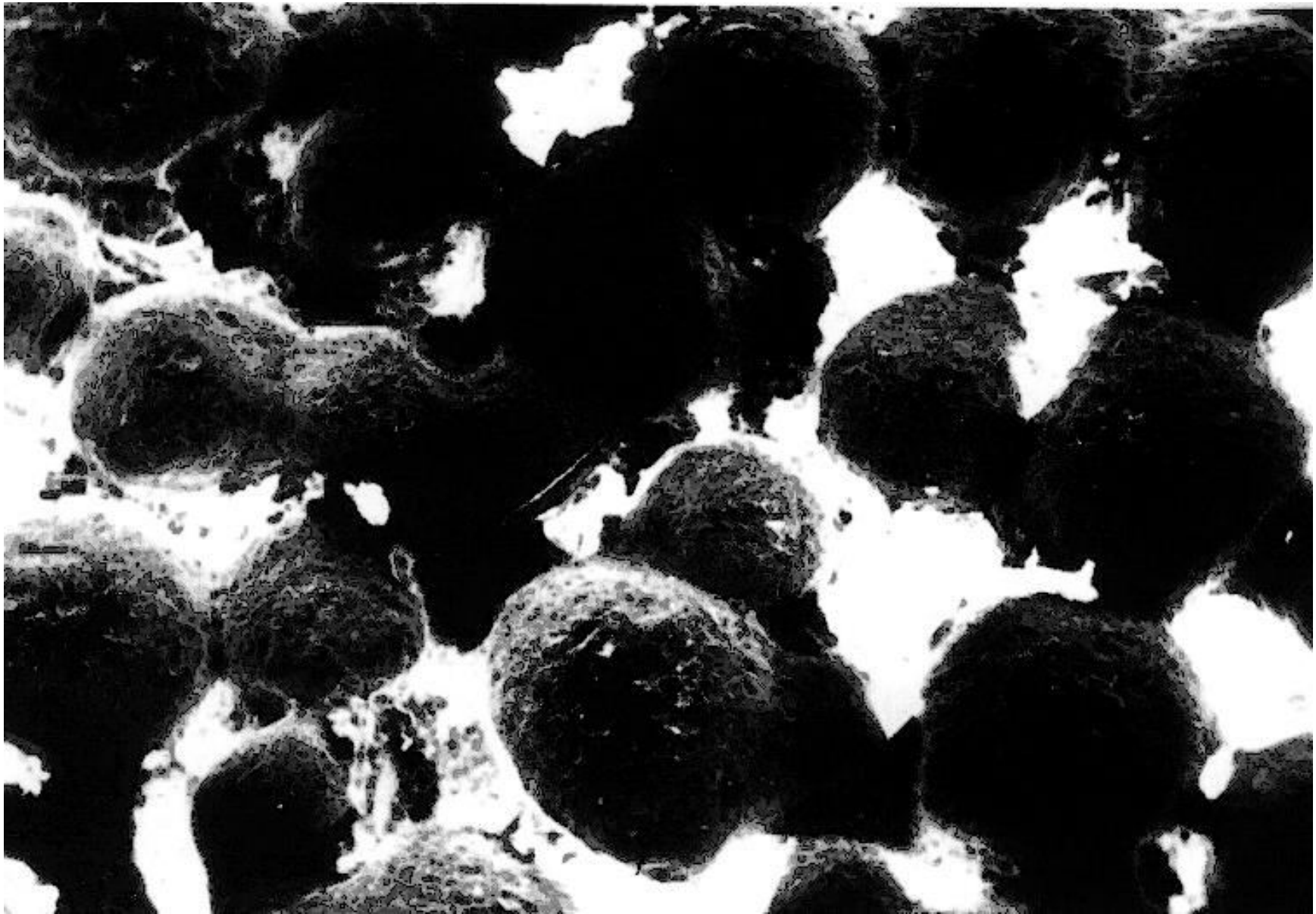


The variety of pore form. (Bird, 1977, Tullet 1984,…)
In the vast majority of species the pores are funnel-shaped, with wider orifice outermost.
Two other pore arrangements, however, have been recognized:
- branched pores (large eggs)
- complex, reticulate pore system

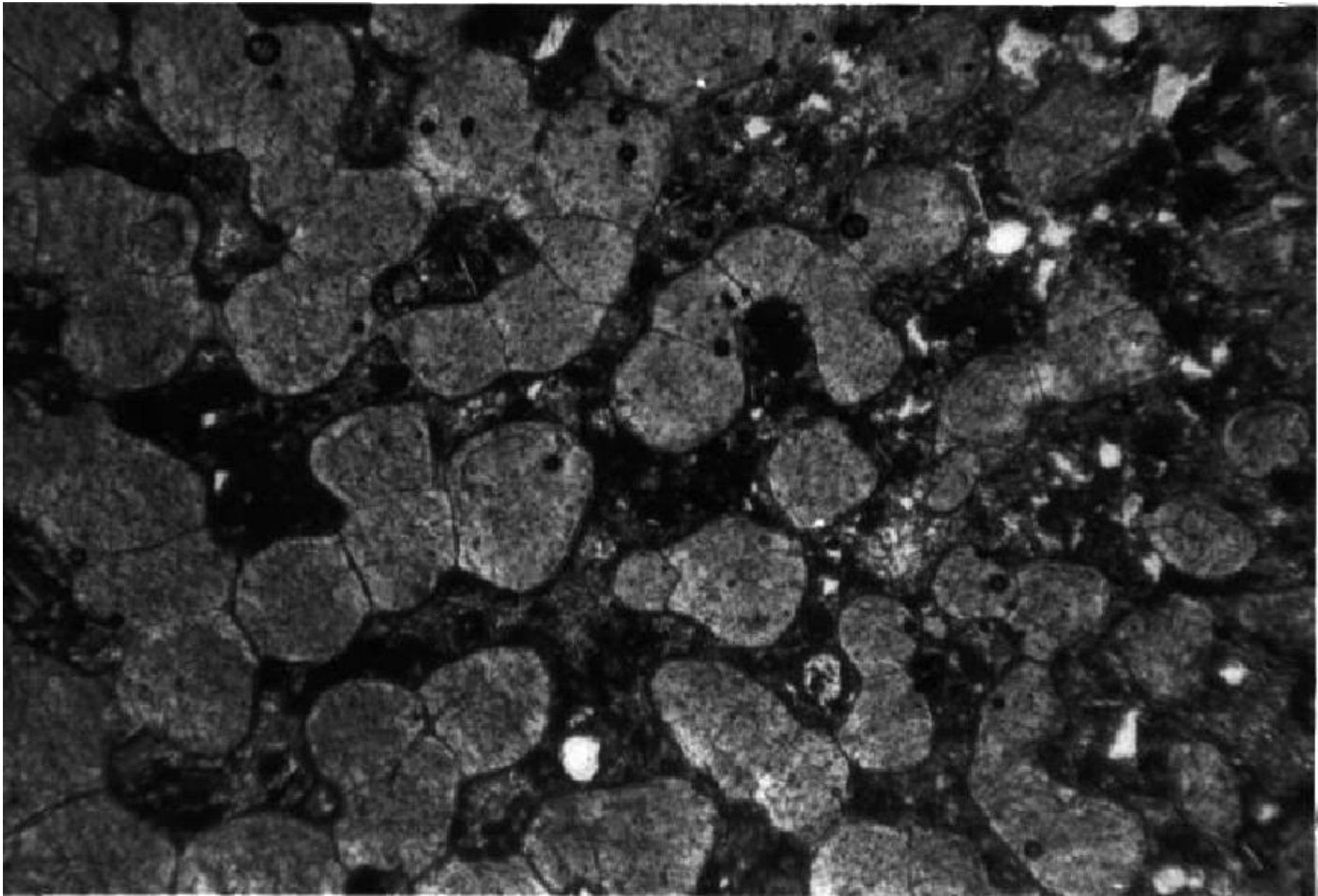
Transversal section through eggshell – optical microscopy; the eggshell is built up by packing bundles of calcite “carrots” well aligned with their axis perpendicular to eggshell surface.



SEM of external surface of a Hateg eggshell showing tuberculate surface



Longitudinal section through eggshell, first layer – optical microscopy

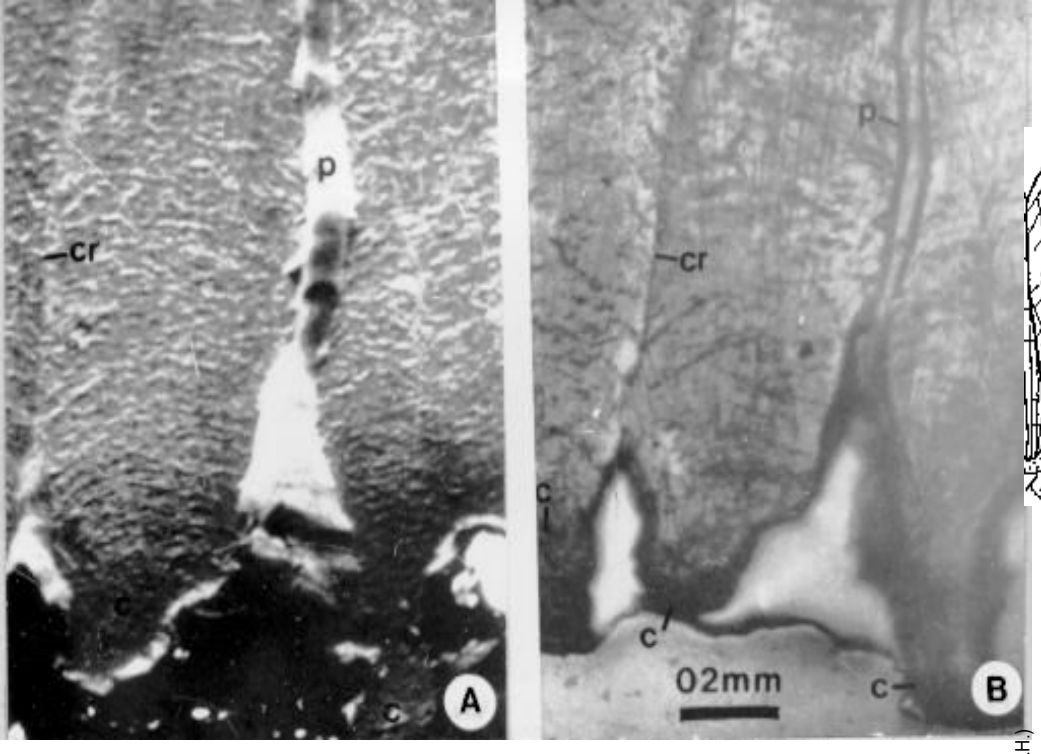


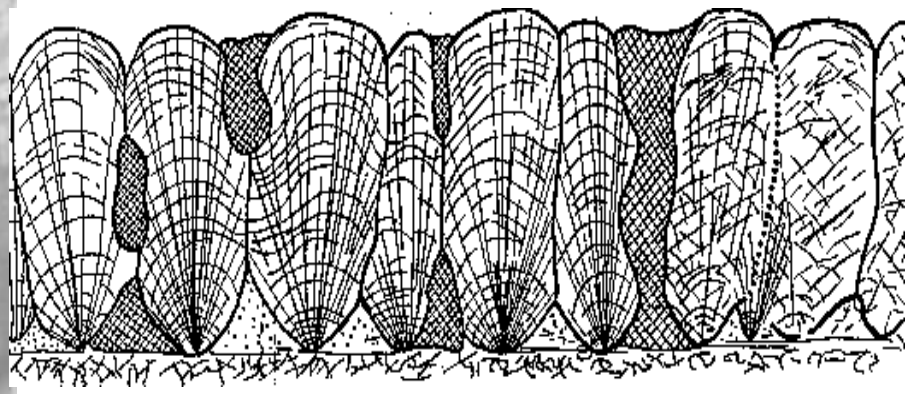
Eggshell porosity is determined by three factors.

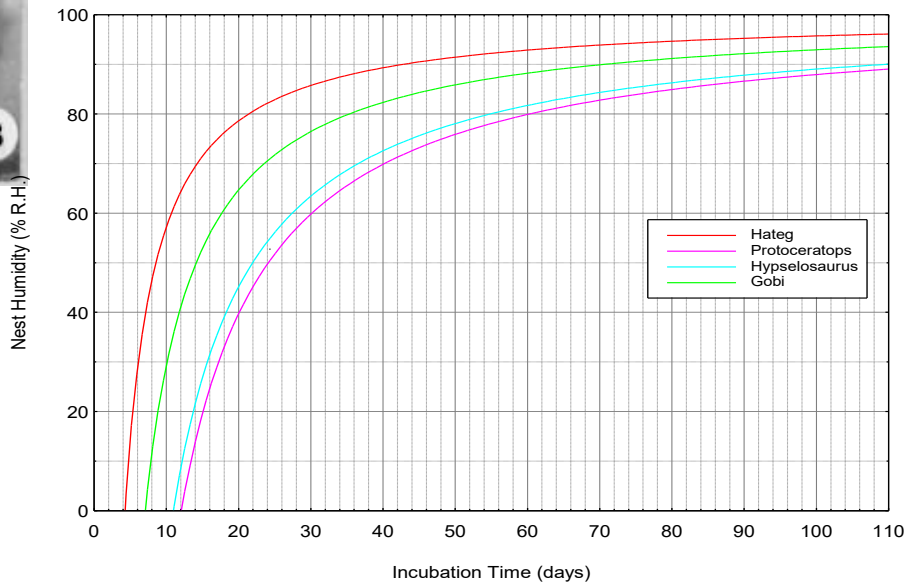
- the number of pores
- their individual cross-sectional area
- their length

- Mechanisms for the control of shell porosity may lie in the:
- a)- seeding sites upon which shell calcification is initiated. These sites determine the number of crystals columns in the shell which in turn are positively correlated with the number of pores (Tullett, 1975).
- The number of columns in a unit area is inversely proportional to shell thickness (i.e. pore length) and may also determine the individual cross-sectional area of the pores (Tullett and Board 1979).
- Thus, the distribution of the oviduct cells which secrete the initial seeding sites ultimately determine the overall porosity of the eggshell and that evolutionary pressures operate at this cellular level. Tullet (1978) suggested that the volume of “plumping fluid” moving through the shell during its formation may also play a role in determining the cross-sectional area of the pores.

Humidity using eggshell pores data







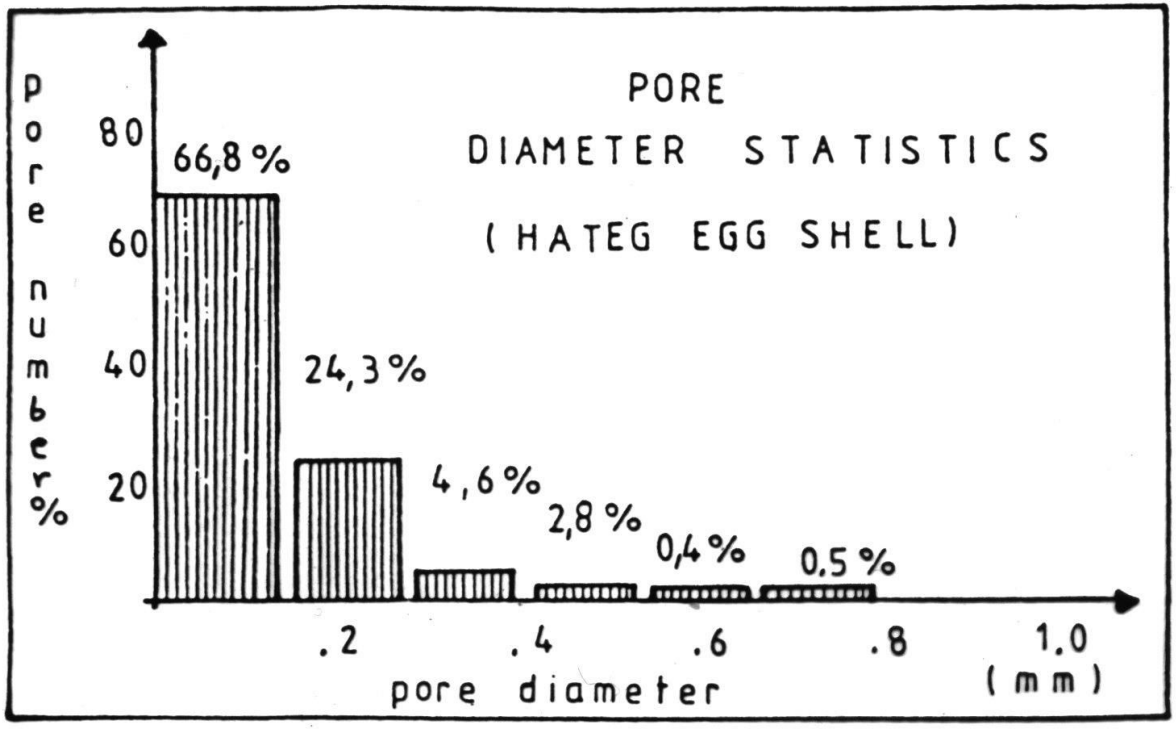
Analyzing the eggshell porosity we are able to estimate the humidity of the environment of the hatching site using the formula:

$$H_u = 100\ P_{ext}/P_{sat}$$

where P_{ext} represent the water vapor pressure from the atmosphere and the saturation pressure P_{sat} at the temperature t = 300 C considered as a real situation. Pext was estimated using the formula discussed by Seymour (1979) from the conductance computed from the experimental data (total pores area and the thickness of the shell). The graph contains his data end ours also. The values estimated are between: Hu=83%...97% for a conductance values between 2,782 et 1,391 mg/day/torr

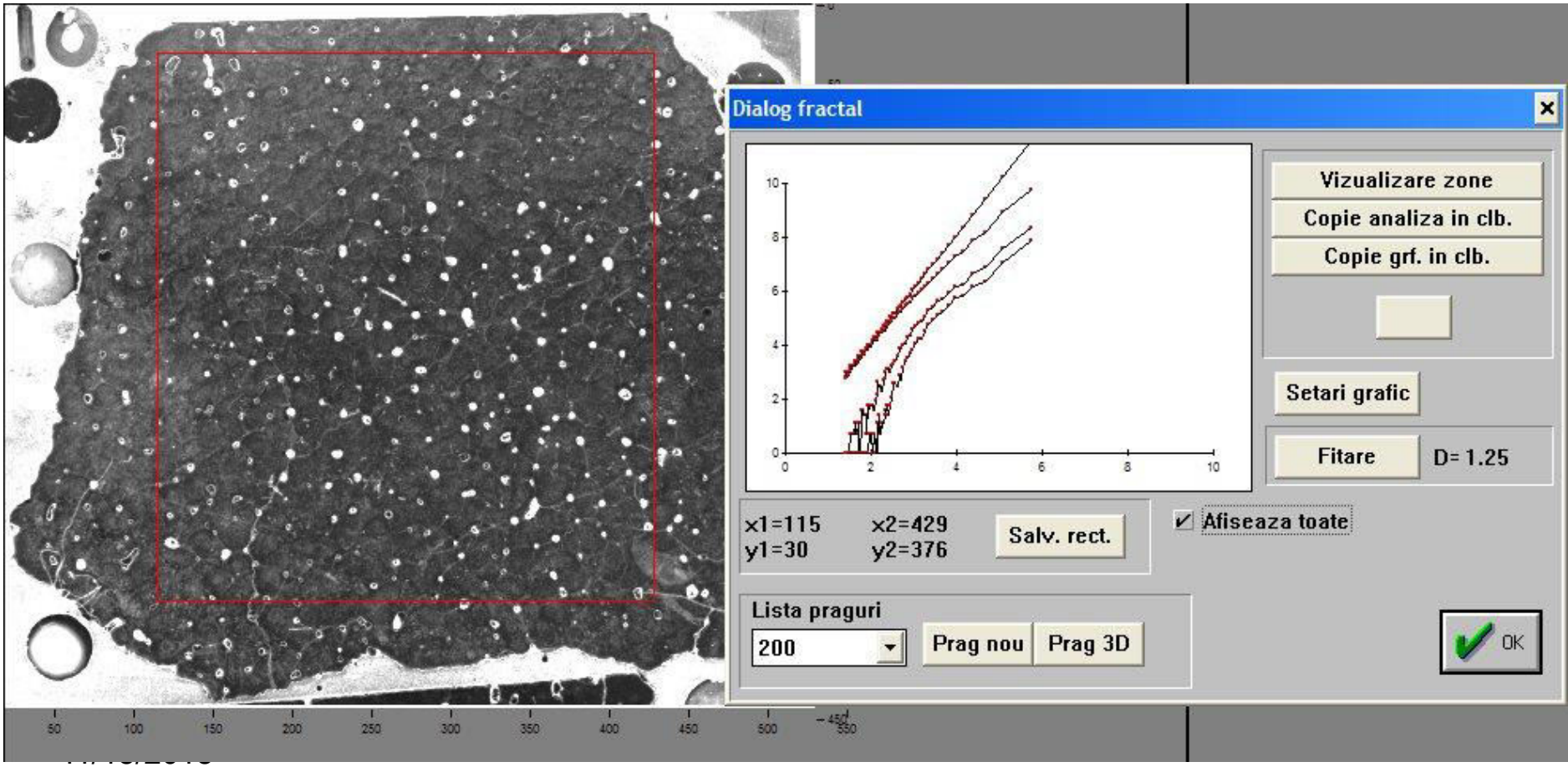
Pore measurement on serial eggshell sections

z	Investigated Area (cm^2)	Number of pores	Pore density (cm^{-2})	Mean pore diameter (cm)	Total pore area (cm^2)	Area occupied by pores (%)
3	1.07	106	98.9	0.386	0.0395	3.690
4	1.07	159	148.5	0.213	0.0180	1.685
5	1.43	244	170.7	0.173	0.0182	1.277
6	1.43	233	163	0.162	0.0153	1.069
7	1.43	221	154.6	0.137	0.0104	0.725
8	1.43	252	176.3	0.153	0.0147	1.031
9	1.43	272	190.3	0.133	0.0120	0.841
10	1.43	296	207.1	0.133	0.0131	0.915
11	1.43	312	218.3	0.167	0.0217	1.521

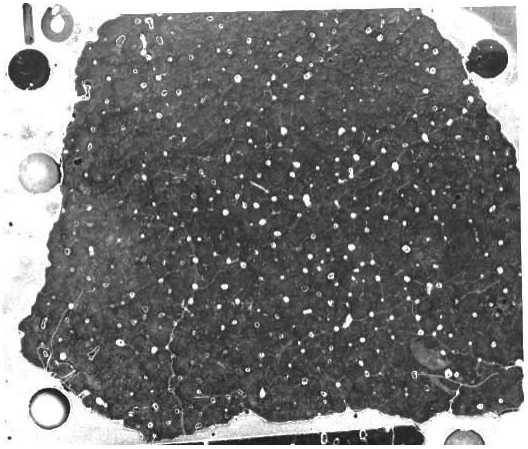


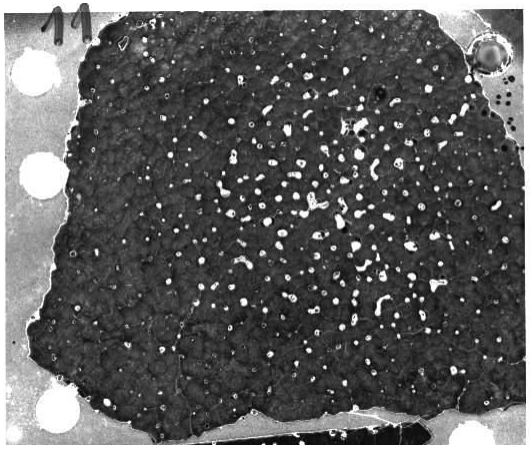
Relationship between pore frequency and diameter in Transylvanian dinosaur eggshell.

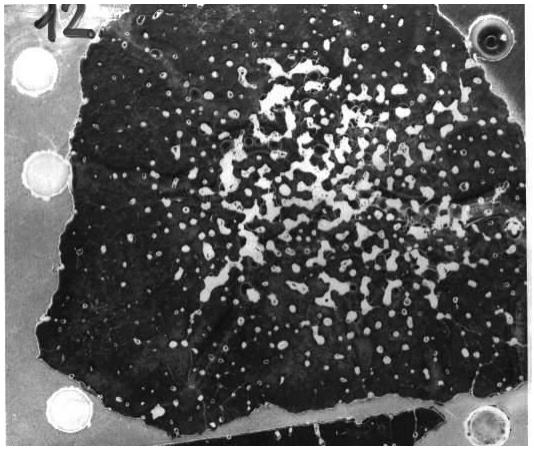
Example of fractal dimension computation using box counting method applied direct to the image

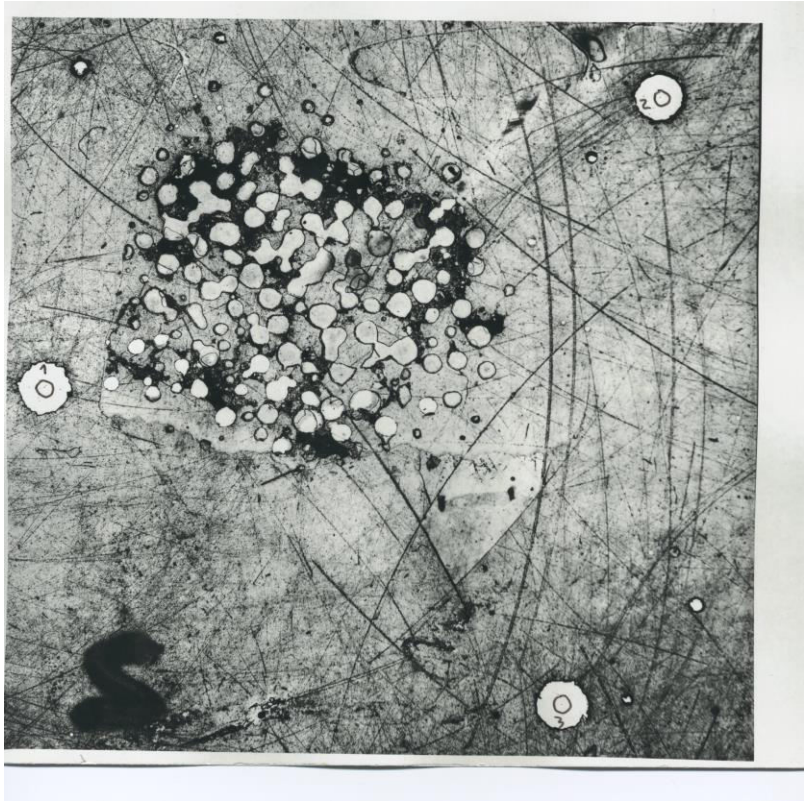


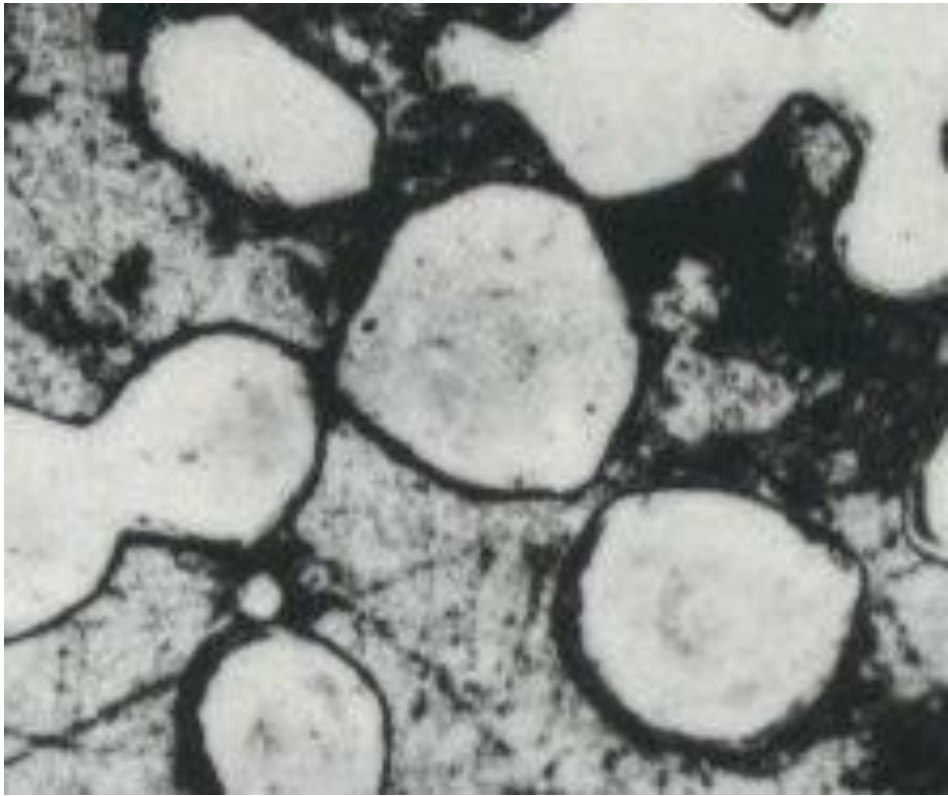
Different sections in microscopic view



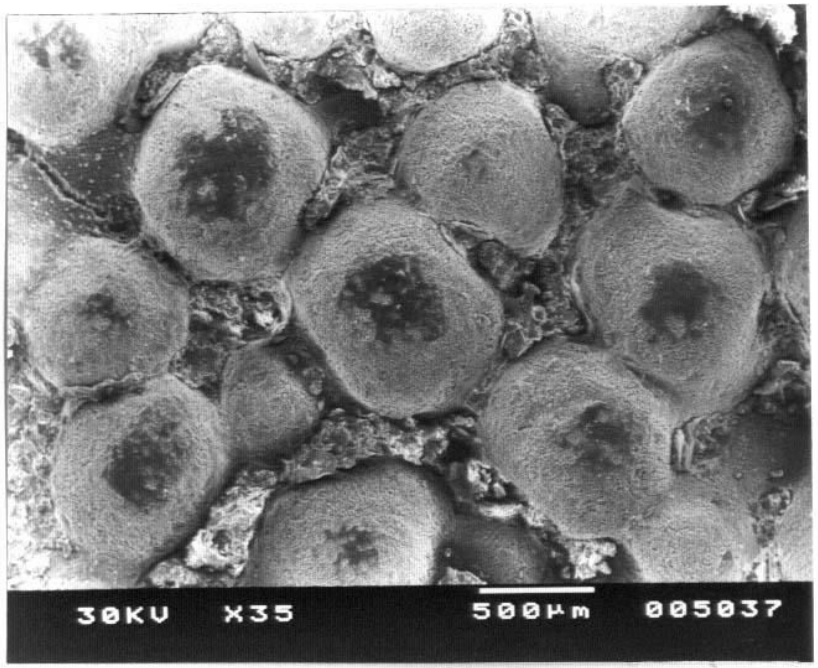


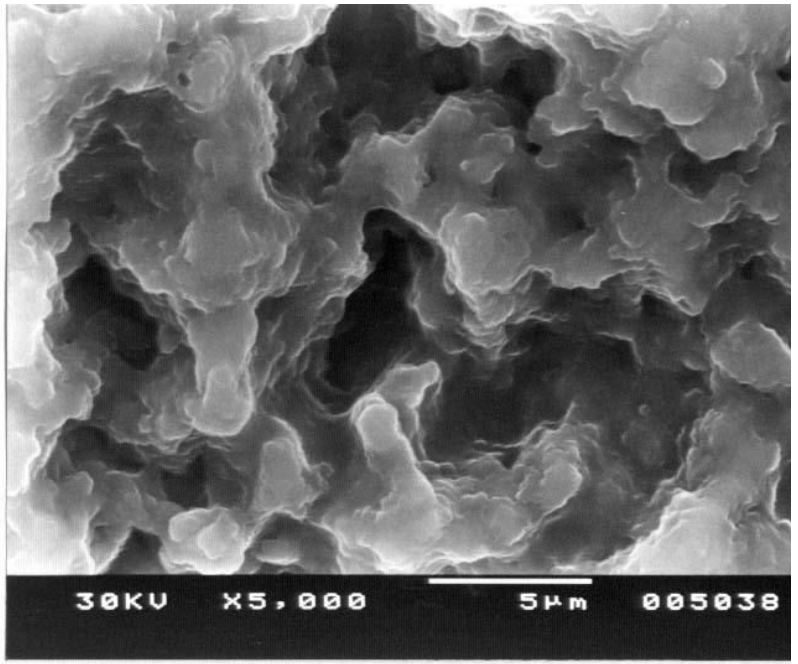


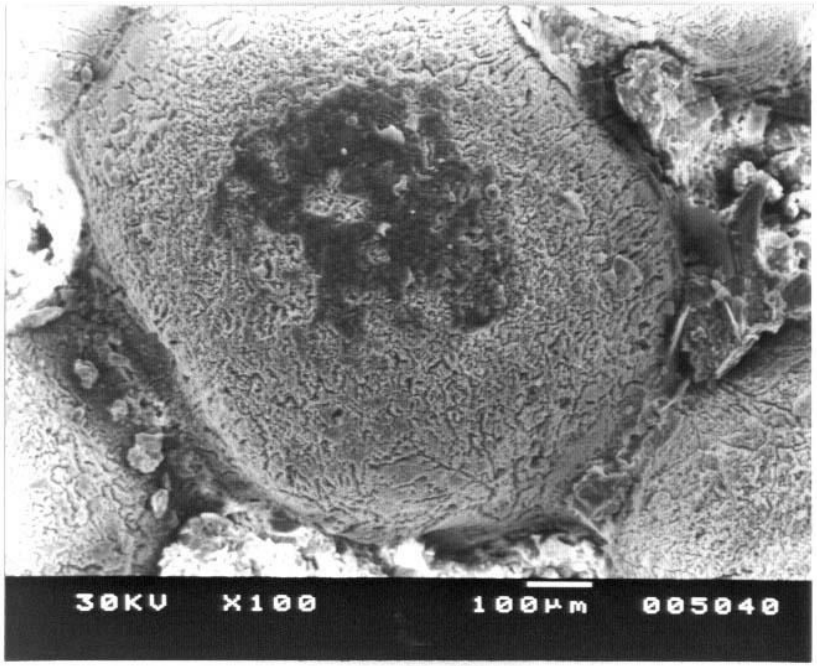


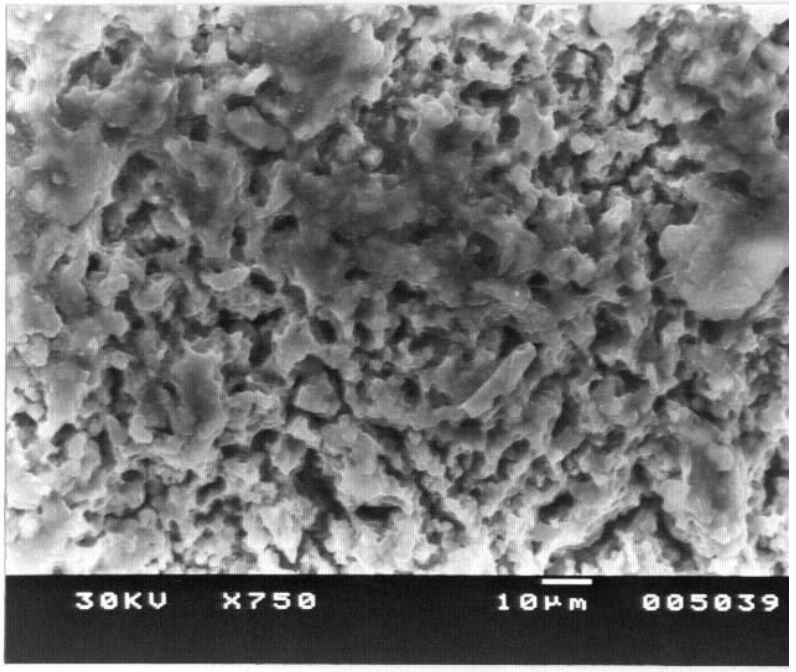


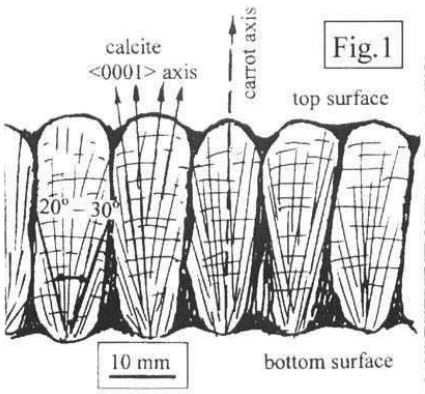
Electron microscopy and diffraction studies











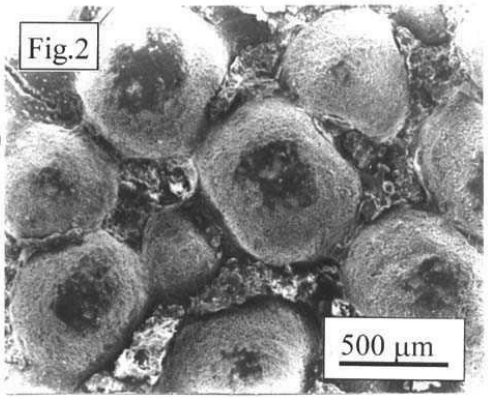


Figure1. Shematics of the cross section of the eggshell structure.
Figure 2. SEM image of the eggshell surface showing the eggshell surface.

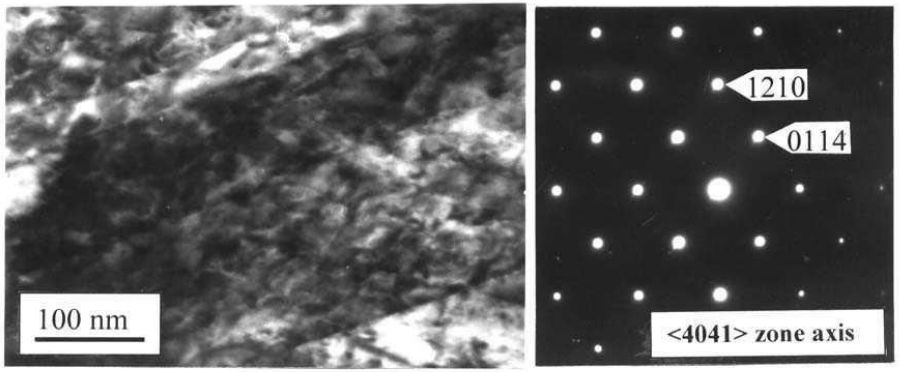
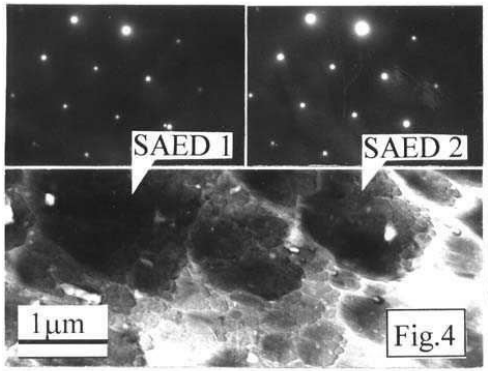


Figure 3. TEM image of a calcite micro-flake obtained from the eggshell, showing the very defected structure. However, the corresponding SAED pattern reveal a very good singlecrystal structure.



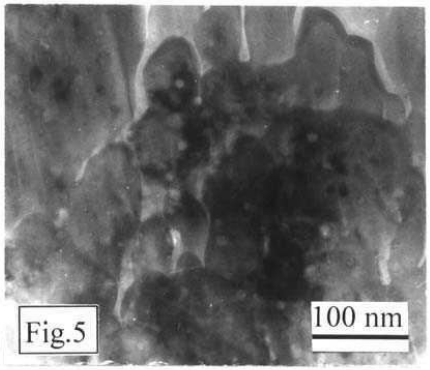
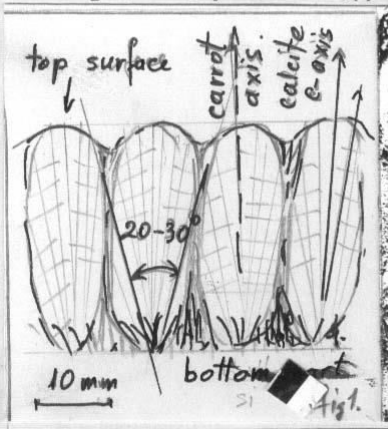
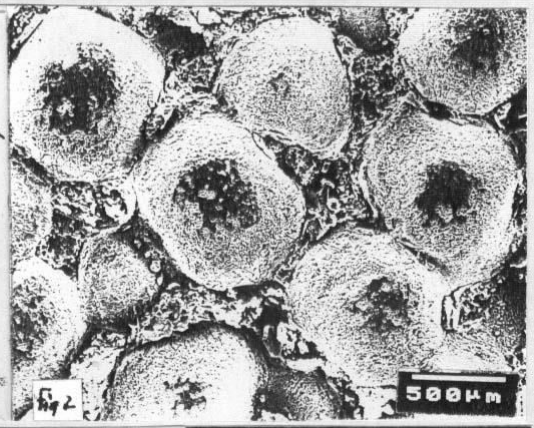
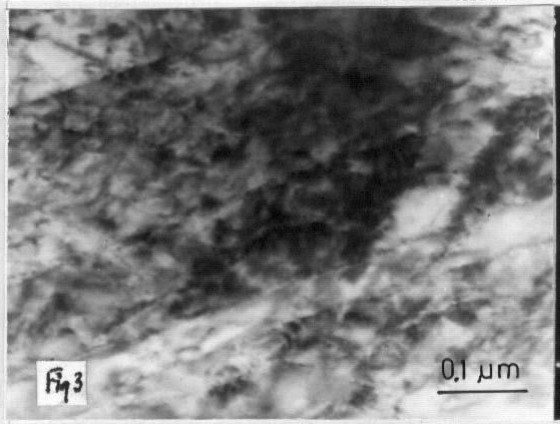


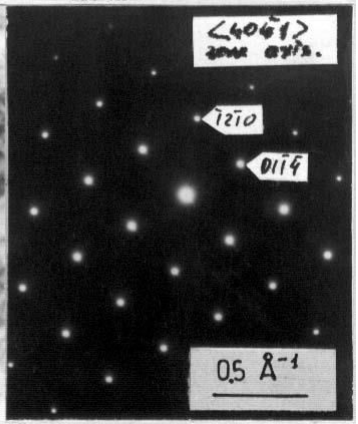
Figure 4. Low magnification TEM image of calcite singlecrystals (bricks) forming the carrots structure. SAED patterns of adjacent calcite bricks.
Figure 5. Nanopores revealed by the ion milling insight a calcite brick.

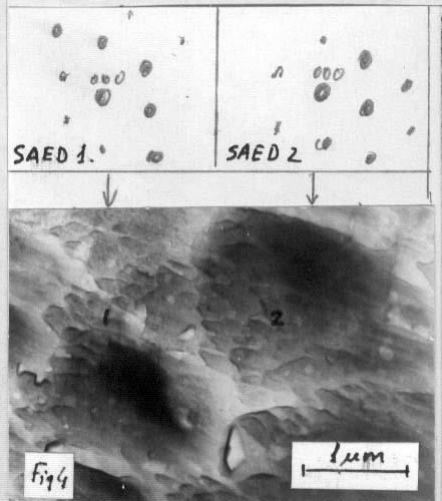
(1) D. Grigorescu, D. Weishampel, D. Norman, M.Seclamen, M.Rusu, A. Baltres, V. Teodorescu, in „ Dinosaur Eggs and Babies“ ed. K.caspenter, K.Hirsck, J. Hornes, Cambridge University Press 1994, pp 75 – 87.

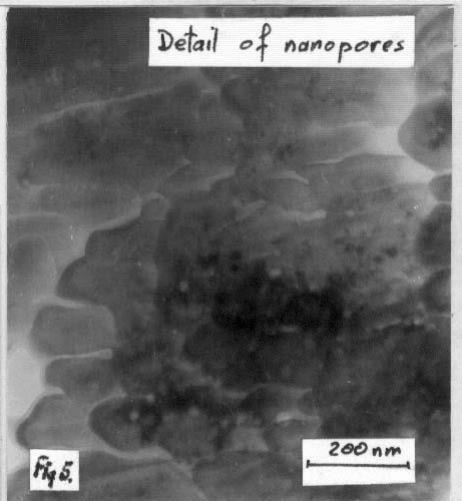




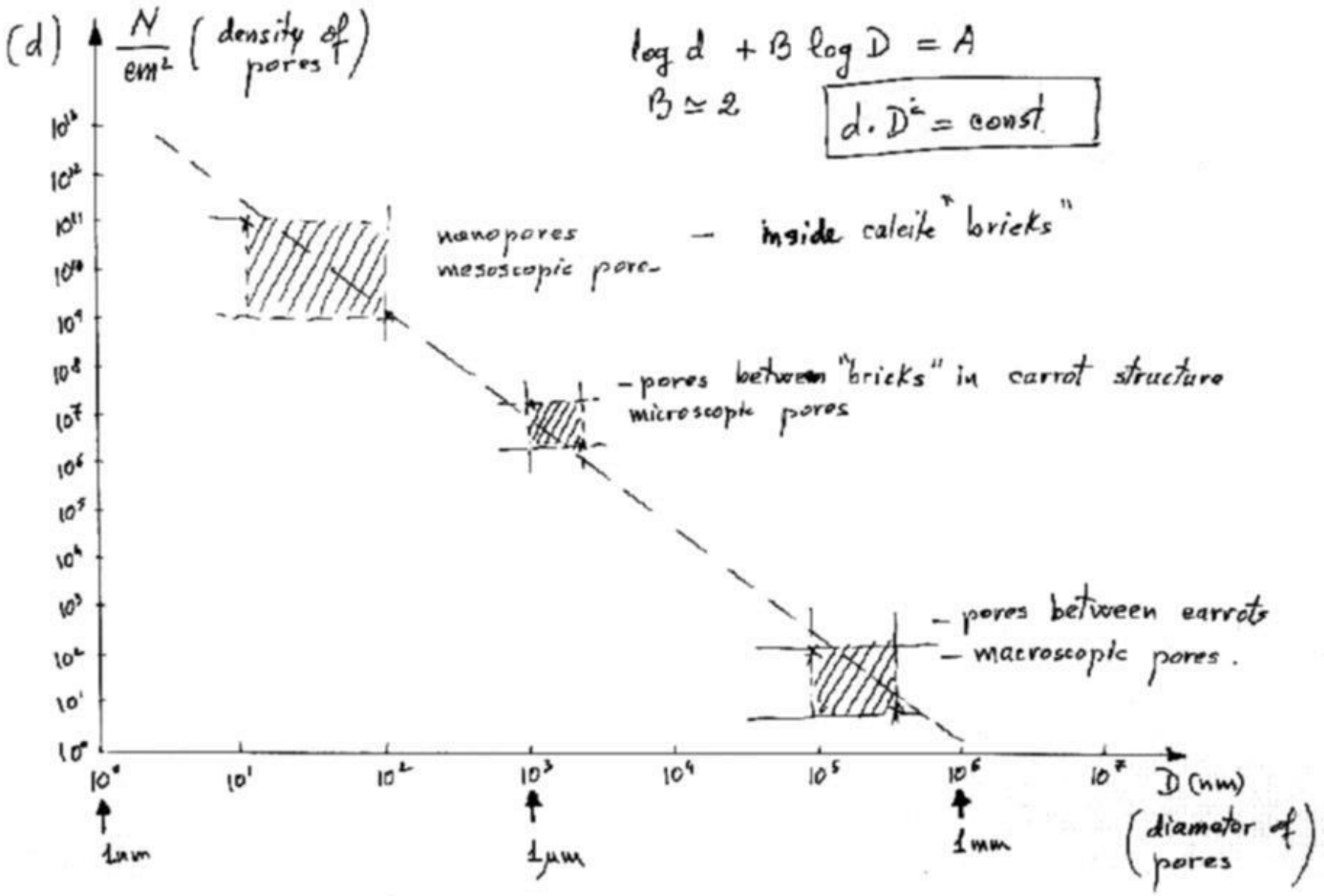








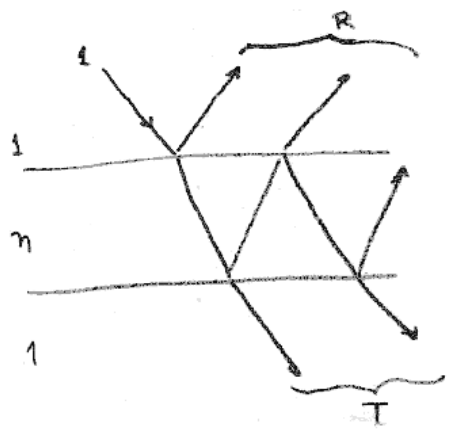
Pore density at different scales



B) Parallel dielectric plate

Normal incidence

a) without multiple reflections



b) with multiple reflections

a) $T_0 = \left(\frac{4n}{(n+1)^2}\right)^2$

$R_0 = 2\left(\frac{n-1}{n+1}\right)^2$

b) $T = \frac{(1-R_0)^2 e^{-\varkappa d}}{1-R_0^2 e^{-2\varkappa d}}$

n - index of reflection

d - thickness of the plate

T - transmittance

R - reflectance

$T_0 = \left(\frac{4n}{(n+1)^2}\right)^2 e^{-\varkappa d}$

$R_0 = 2\frac{(n-1)^2 + k^2}{(n+1)^2 + k^2}$

$T = \frac{(1-R_0)^2 e^{-\varkappa d}}{1-R_0^2 e^{-2\varkappa d}}$

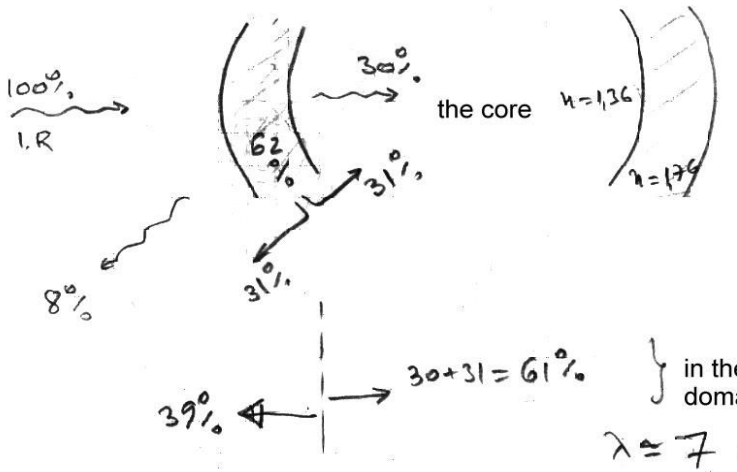
$R = \frac{R_0\left[1-(2R_0-1)e^{-\varkappa d}\right]}{1-R_0^2 e^{-2\varkappa d}}$

$\varkappa$ - linear coefficient of absorption

k - absorption coefficient

CONCLUSION:

radiation balance:

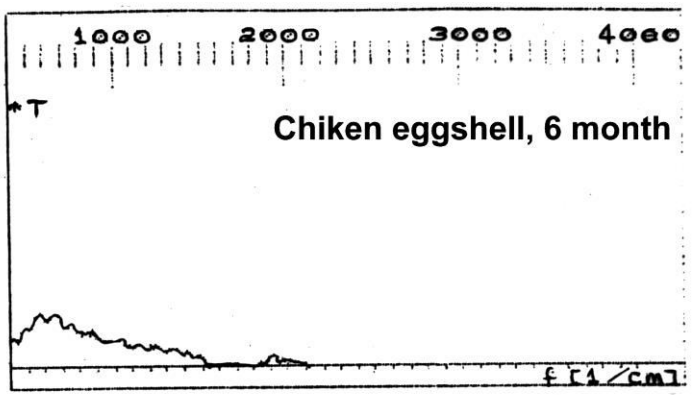


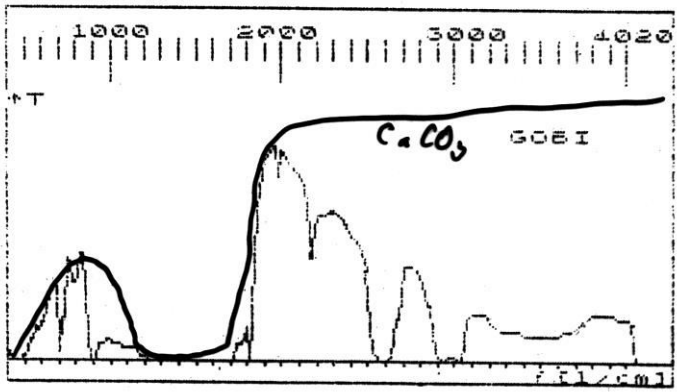
in the transparence domain

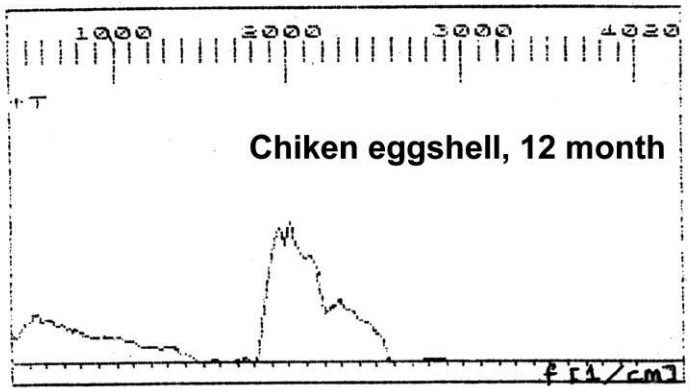
$\lambda \simeq 7 \div 13\ \mu m.$

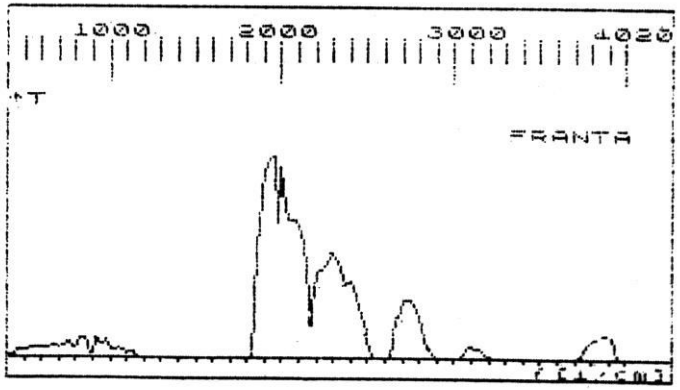
Radiation balance

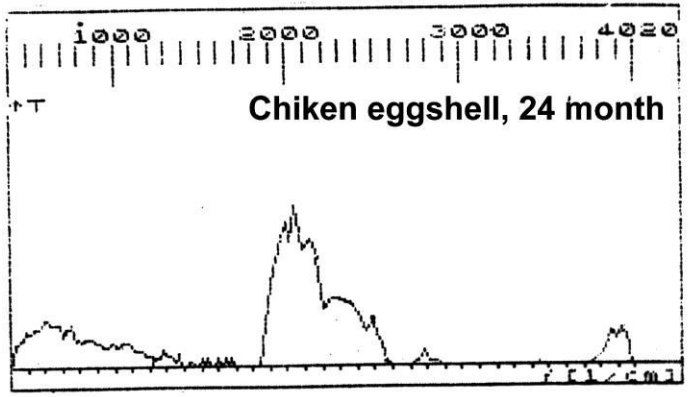
IR transmittance, chicken eggshells and dino eggshells

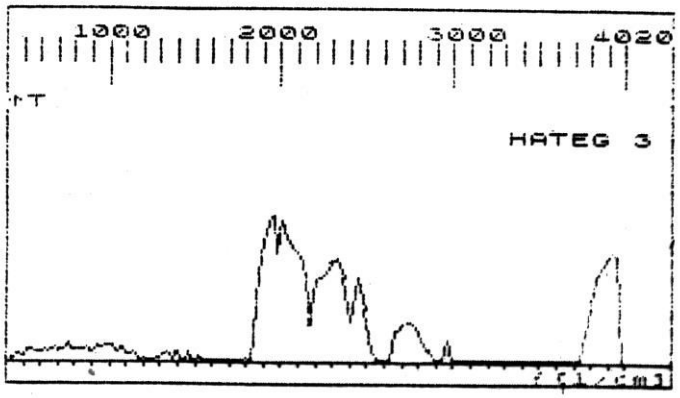










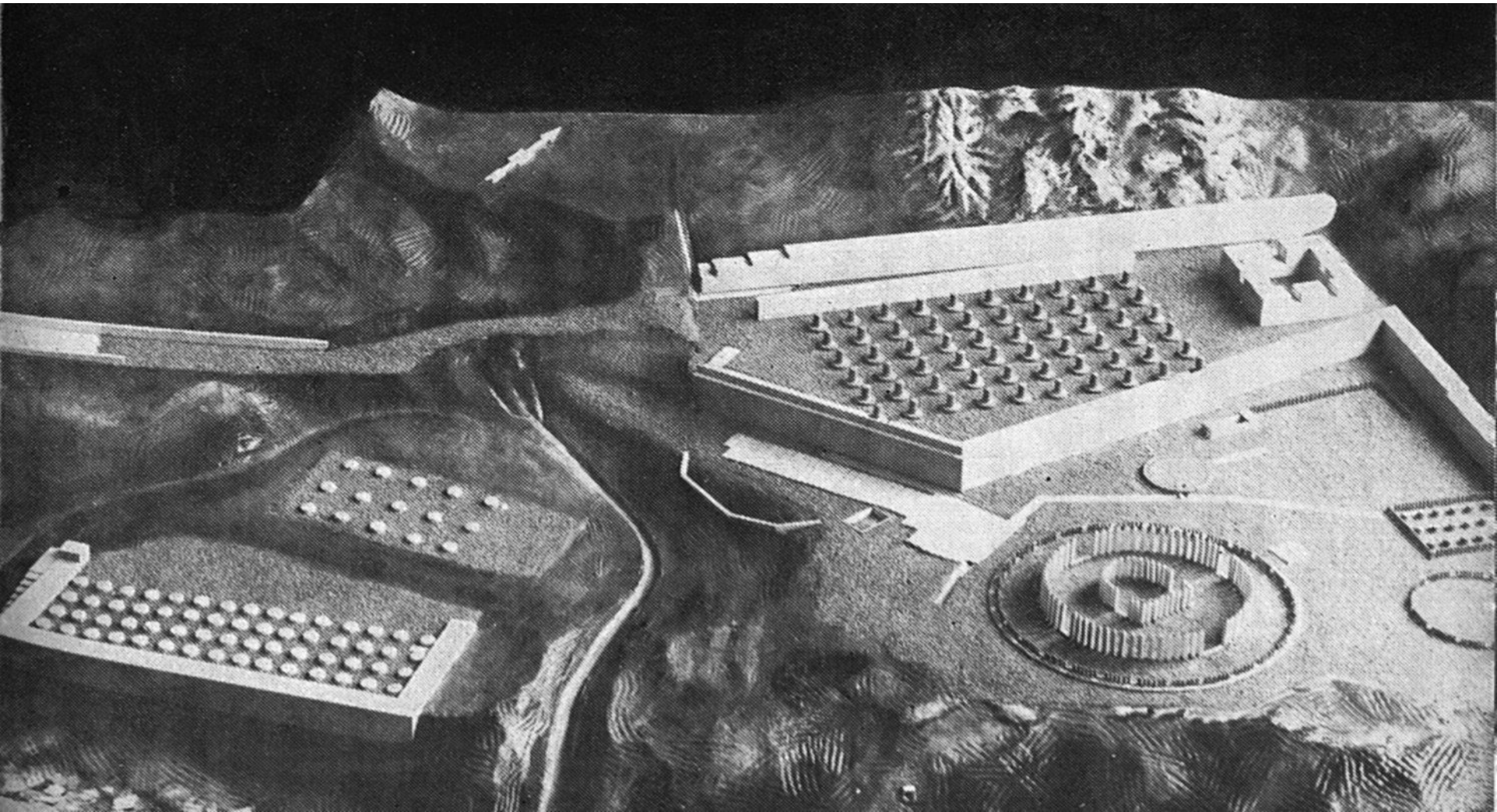


7) Archeology and arheometry

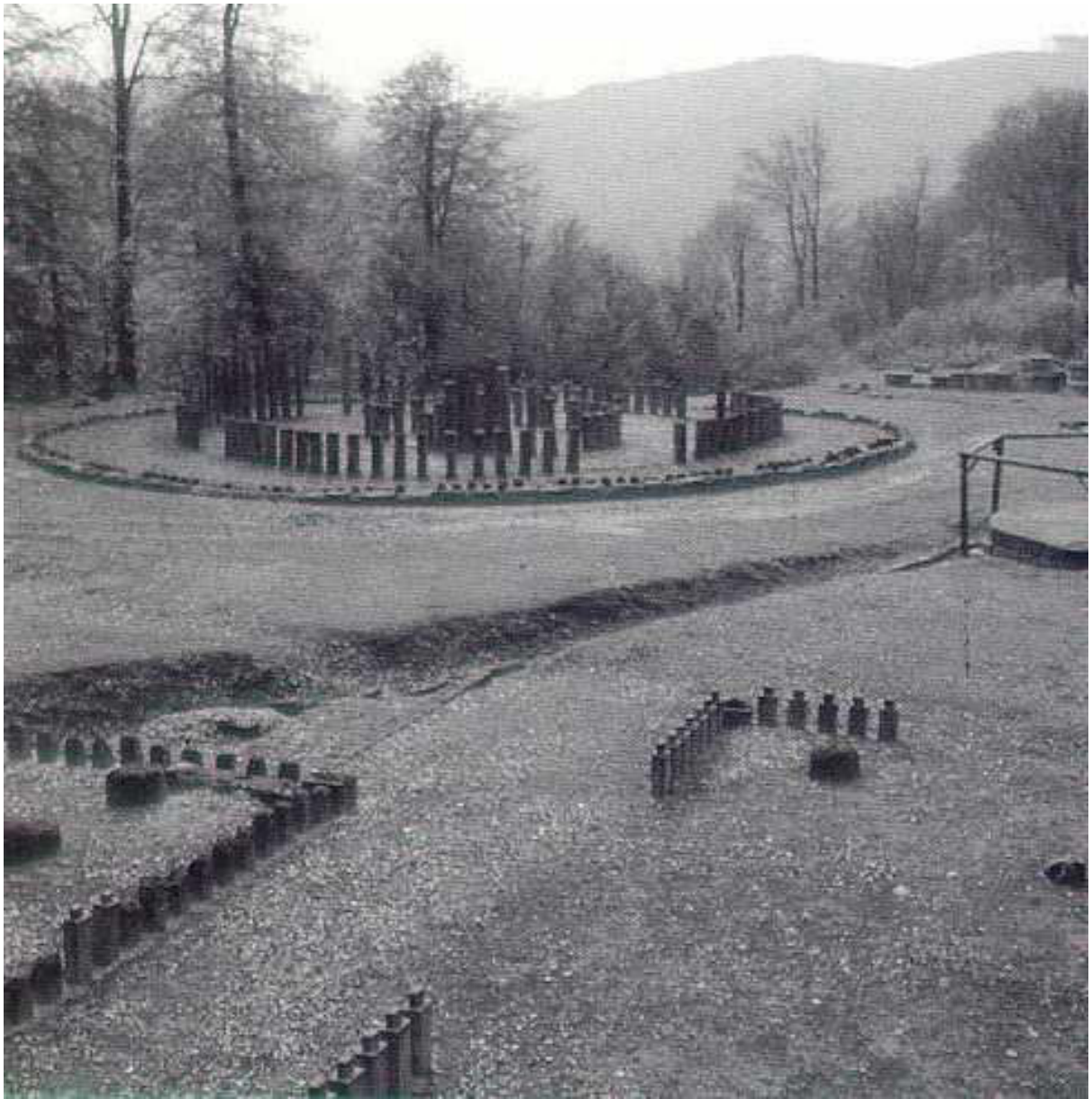
7.1- Archeological dating using power laser beam: equivalent thermoluminescence induced by laser beam

- - Formation of free radicals in water under high-power laser UV irradiation

CALENDARUL DE LA SARMIZEGETUSA REGIA



Sanctuarul - reconstituire

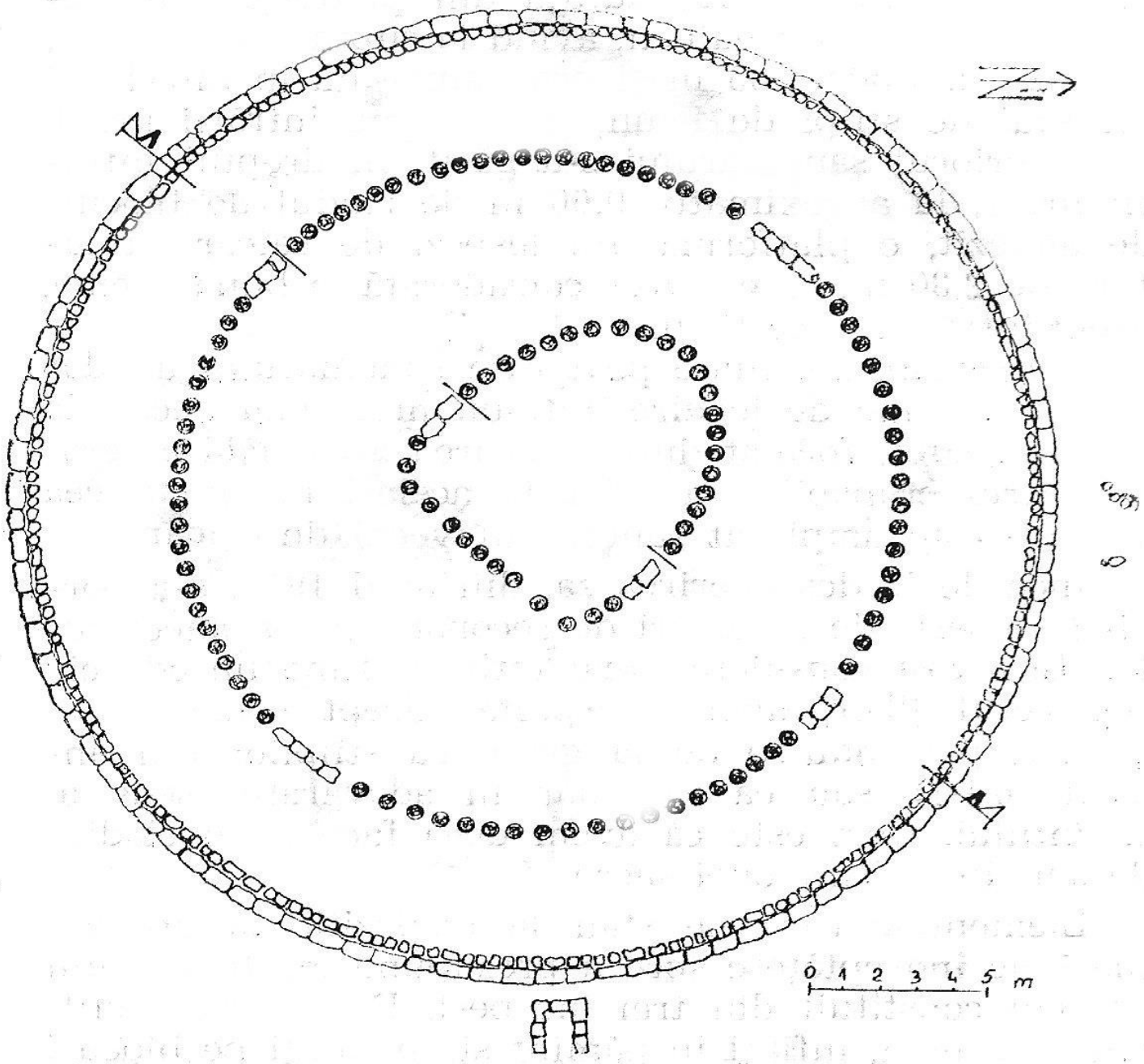


- La Sarmizegetusa Regia din Munţii Haţegului, în apropiere de Grădiştea Muncelului, s - au descoperit capitala dacică şi vestigii ale activităţilor astronomice concretizate prin calendare solare. Analizarea sistemului calendaristic dacic, constituit din formaţiuni circulare, absidale şi dreptunghiulare s – a finalizat prin ideea că era format de fapt din două calendare distincte ce se sincronizau anual, civil şi ritualic. În timp ce anul calendarului civil avea 47 săptămâni, anul calendarului ritualic avea 60 săptămâni, ambele poziţionând prima zi a unui nou an în prima zi a săptămânii respective iar zilele de corecţie ale anului, ciclului sau secolului aveau corespondentul material în structura numerică a sanctuarelor .

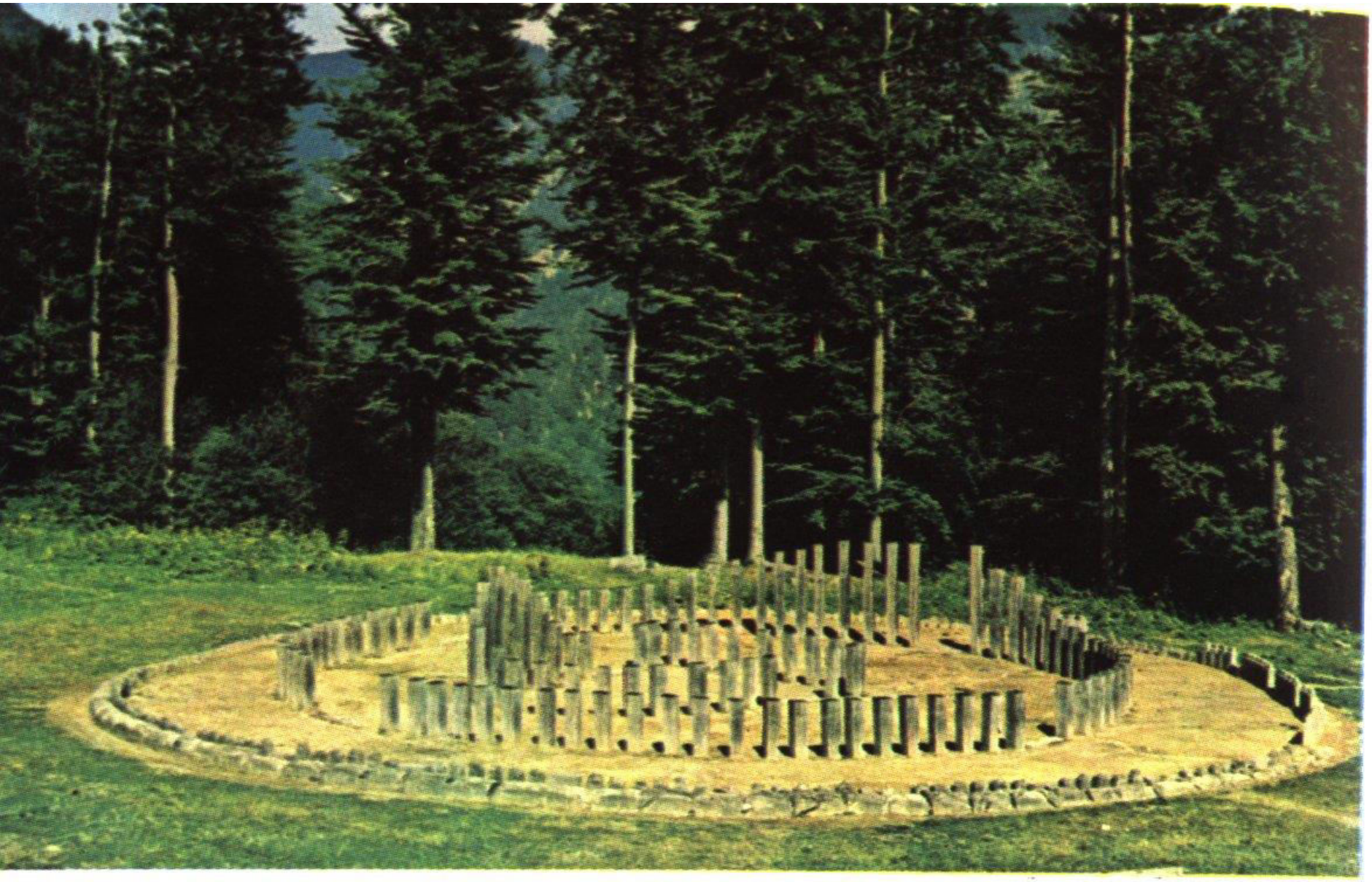
- Sistemul calendaristic dacic era structurat după un **ciclu de 13 ani** .

- Marcarea timpului se efectua pe componentele sanctuarelor în mod corespunzător unei parcurgeri continue şi ordonate, intr-un singur sens pentru sanctuarele circulare, repetabilă în mod identic şi materializată prin marcarea cu însemne specifice; această parcurgere era întreruptă numai la apariţia zilelor de corecţie.

- Simbolizarea calendarelor dacice circulare implica deci proprietăţi remarcabile: măsurarea timpului se efectua prin numărarea unui număr de lespezi şi de stâlpi sumaţi prin procedeul rotirii continue, ceea ce avea ca rezultat unităţi de timp mărite progresiv ajungânduse la **materializarea conceptului de timp infinit - trecut, prezent, viitor** - iar prin rotirea nesfârşită, la noţiunea de infinit; totodată timpul era marcat prin ciclicitatea fenomenelor naturale .


N
A
A
0 1 2 3 4 5 m

Sarmizegetusa Dacica



- Variaţia în zile a anilor - de 364, 365, 366 şi 367 zile - se efectua printr–o succesiune de trei tipuri de săptămâni, conform calendarului civil sau printr–un an cu săptămâni fixe de 6 zile după calendarul ritualic, corecţia fiind aplicată la sfârşit cu un număr fluctuant de zile - de 4, 5, 6 sau 7 - în scopul sincronizării anuale a celor două tipuri de calendare .
- **Micul sanctuar circular** este interpretat ca fiind un calendar solar cu un ciclu de 13 ani finalizat printr–o zi de corecţie şi totodată de mare sărbătoare . Divizarea se realiza în funcţie de 13 grupe (săptămâni).
- Micul sanctuar marca trecerea a 13 ani în 4747 zile.
- **Marele sanctuar circular** este interpretat ca fiind un calendar solar pentru care stâlpii mici de piatră ai cercului B marcau zilele, stâlpii mari de piatră ai cercului C marcau zilele de corecţie iar stâlpii absidei simbolizau săptămânile .
- Timpul era reprezentat prin transpunerea rotaţiei continue şi intr-un singur sens pe circumferinţa sanctuarului circular şi marcat pe diferitele piese ale structurilor.
- Absida centrală avea rolul unui sistem de evidenţă a celor 47 săptămâni ale fiecărui an dacic din micul sanctuar circular, cele două fiind sistemele de memorare şi de evidenţă ale calendarului dacic, iar unităţile de timp implicate de micul sanctuar circular au fost păstrate şi pentru cel mare, numit ritualic .
- **Sanctuarele dreptunghiulare** erau compuse din aliniamente parcurse în mod ordonat şi marcate cu însemne caracteristice pe tamburi. Însemnarea sau parcurgerea completă a tamburilor într–o structură dreptunghiulară marca momentul unei corecţii în acelaşi mod ca la parcurgerea completă a lespezilor unei circumferinţe a sanctuarelor. În zilele de corecţie se reiniţializau toate structurile numerice care au semnalat acea zi.
- Tamburii erau simbolul anilor sau al ciclurilor de 13 ani, cel mai important fiind sanctuarul de 4x13 + 7 tamburi.
- **Soarele de andezit** prezintă o structură interioară centrală circulară dinspre care pornesc 10 raze.

Sarmizegetusa Dacica



Sarmizegetusa Dacica

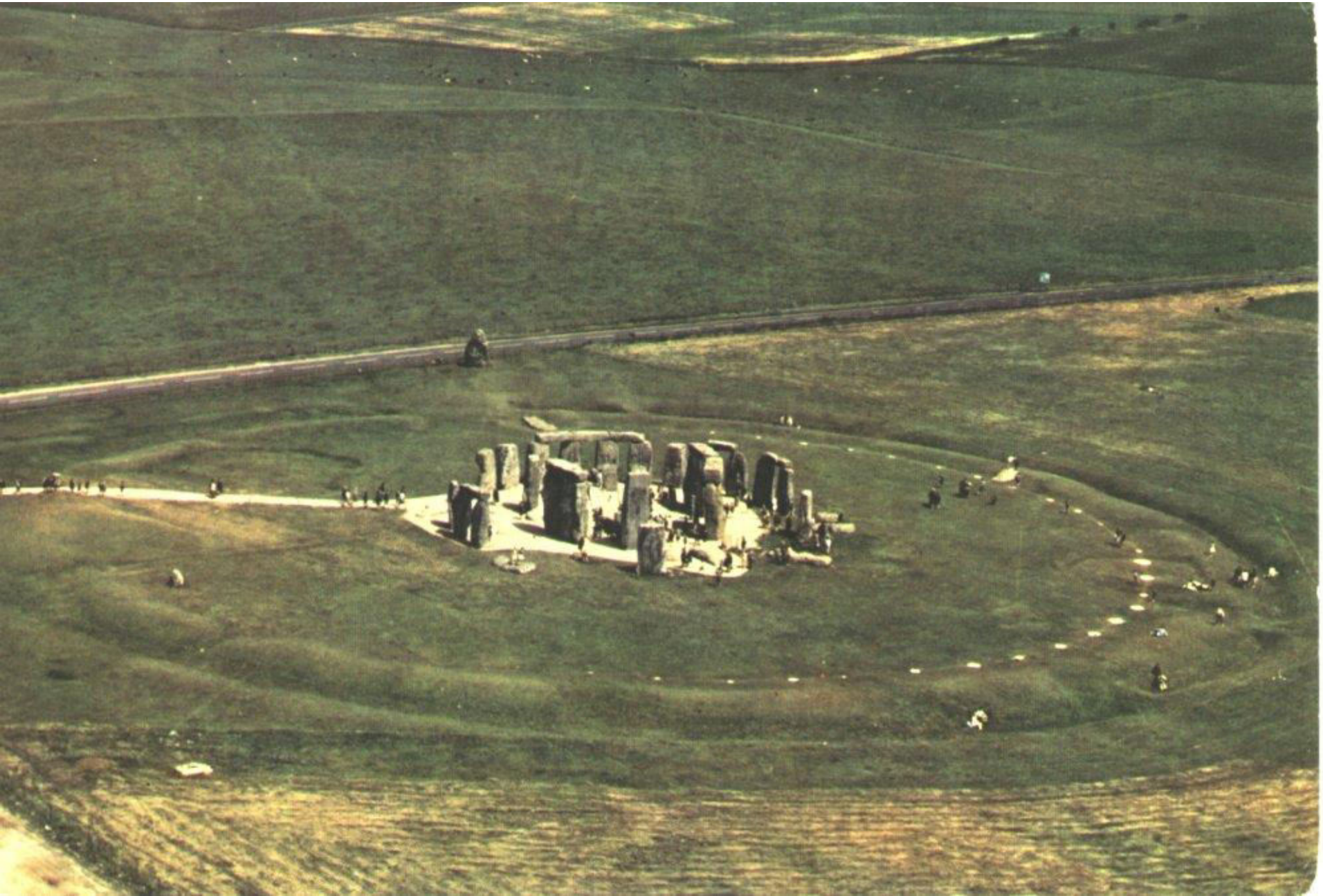


CALENDARE SOLARE ŞI LUNARE
- Stonehenge



- Ansamblul de la Stonehenge a fost ridicat în sudul Angliei, în comitatul Wiltshire, pe câmpia Salisbury, prezentând–se ca o formaţiune de forme megalitice şi inele de piatră. El a fost construit în mai multe etape între anii 3100-1600 î.e.n. Piatra – călcâi (*heel stone*) şi cele 56 orificii utilizate în scop religios datează din perioada 3100–2300 î.e.n., urmând construirea a două şiruri de pietre albastre între anii 2150–2000 î.e.n. care au fost apoi înlăturate. În perioada 2100–2000 î.e.n. au fost ridicate pietrele sarsen (*saracen* sau *sazarin* se traduce prin străin), cele mari fiind pilonii celor 5 trilitioane originale iar cele orizontale cu rolul de praguri şi dispuse în formă de potcoavă; ele erau înconjurate de un cerc de pietre sarsen care prezentau şi praguri. Mai târziu a fost ridicat un inel de pietre albastre, în interiorul inelului de pietre albastre sarsen, fiind adăugate apoi piatra altar, pietrele *station* 91 şi 93, piatra abator şi orificiile 92 şi 94.

Stonehenge - Anglia



- Cercetările contemporane au relevat faptul că digul original avea intrarea orientată în direcţia răsăritului de soare la mijlocul verii iar aliniamentele includeau pe lângă semnificaţiile calendaristice, răsărituri şi apusuri de Soare în zilele solstiţiilor de vară şi de iarnă (**solstiţiu** - derivă din latinescul oprirea soarelui şi este folosit pentru momentele la care Soarele se situează în cele mai depărtate puncte de pe ecuatorul ceresc; solstiţiul de vară este considerat pentru cea mai lungă zi şi noaptea cea mai scurtă în timp ce la solstiţiul de iarnă este considerată cea mai scurtă zi şi noaptea cea mai lungă), prezicerea **echinocţiilor** (cele două puncte în care se intersectează ecuatorul şi **ecliptica** (planul orbitei Soarelui)), răsărituri şi apusuri de Lună la impasurile minore şi majore şi prezicerea eclipselor. Aliniamentele întrebuinţate pentru Soare puteau prevedea începutul sau finalul anului neolitic.
- Reconstruirea ansamblului de – a lungul timpului a implicat noi semnificaţii şi întrebuinţări, un exemplu în acest sens fiind pietrele station; alinierea diagonalelor unghiurilor drepte a acestor pietre, 93 - 91 şi 94 – 92 indica răsăriturile şi apusurile de Soare în 4 zile ale anului aflate aproximativ la jumătatea perioadei dintre solstiţii şi echinocţii: 5 februarie, 6 mai, 8 august şi 2 noiembrie. Prin adăugarea pietrelor sarsen la ansamblu, pietrele station şi – au pierdut semnificaţia şi utilitatea pentru observarea Lunii, a Soarelui şi a celorlalte obiecte astronomice.
- Rolul ansamblul de la Stonehenge s-a considerat a fi cel pentru studii astronomice, de prevestire a producerii eclipselor şi de calculare a mareelor din Marea Nordului în vederea unei bune navigări.

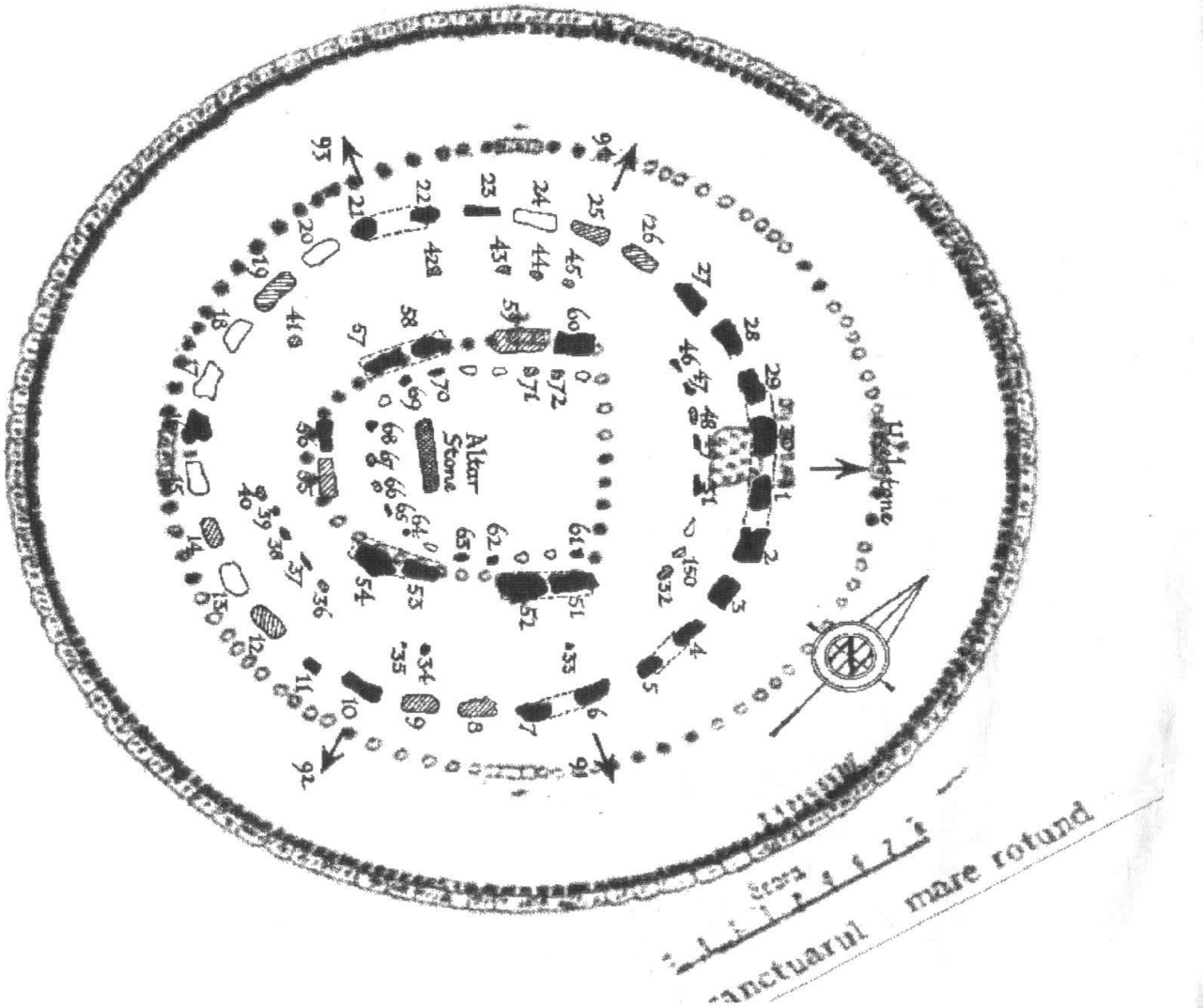
Stonehenge - Anglia



Stonehenge - Anglia

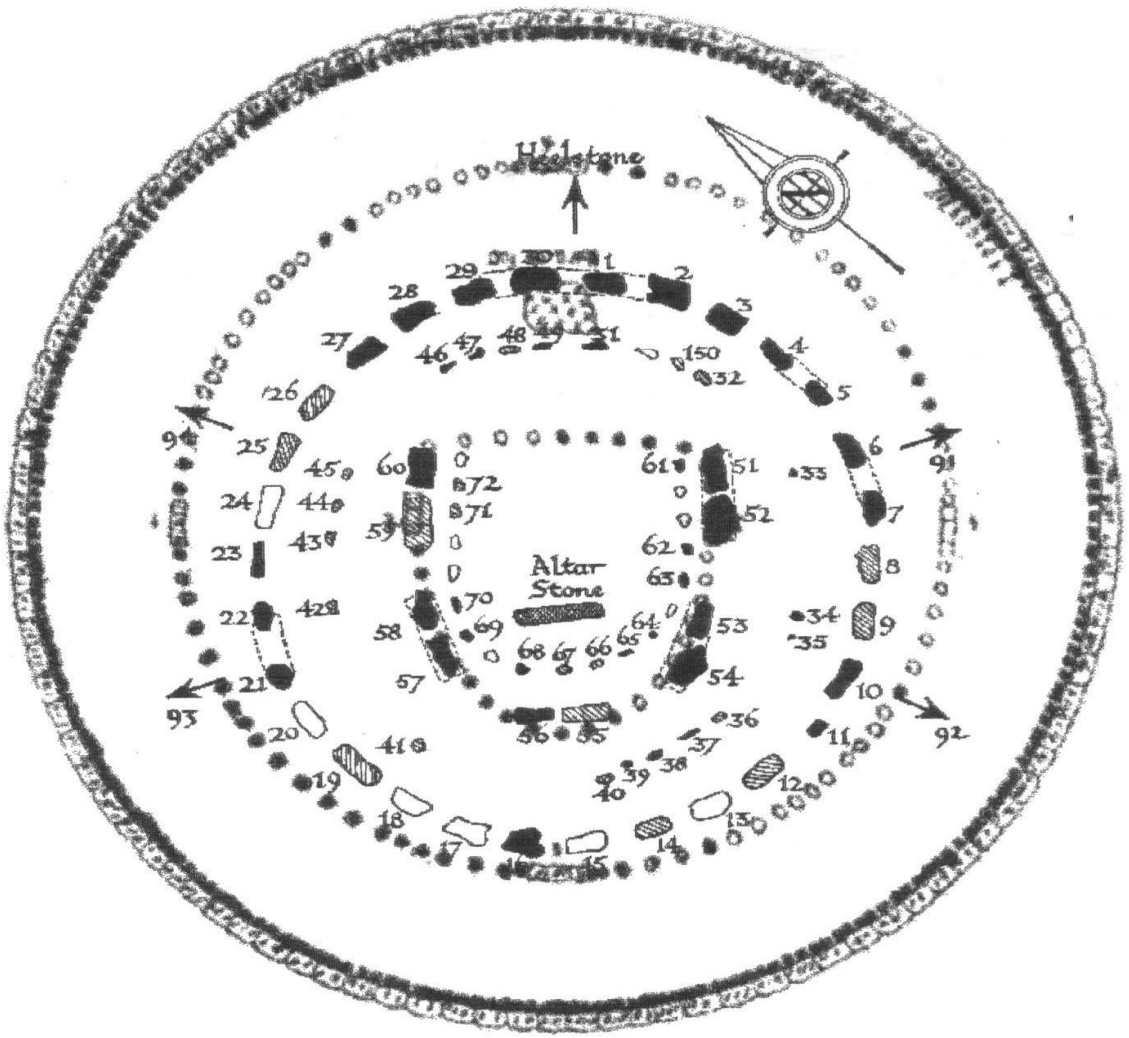


Suprapunere



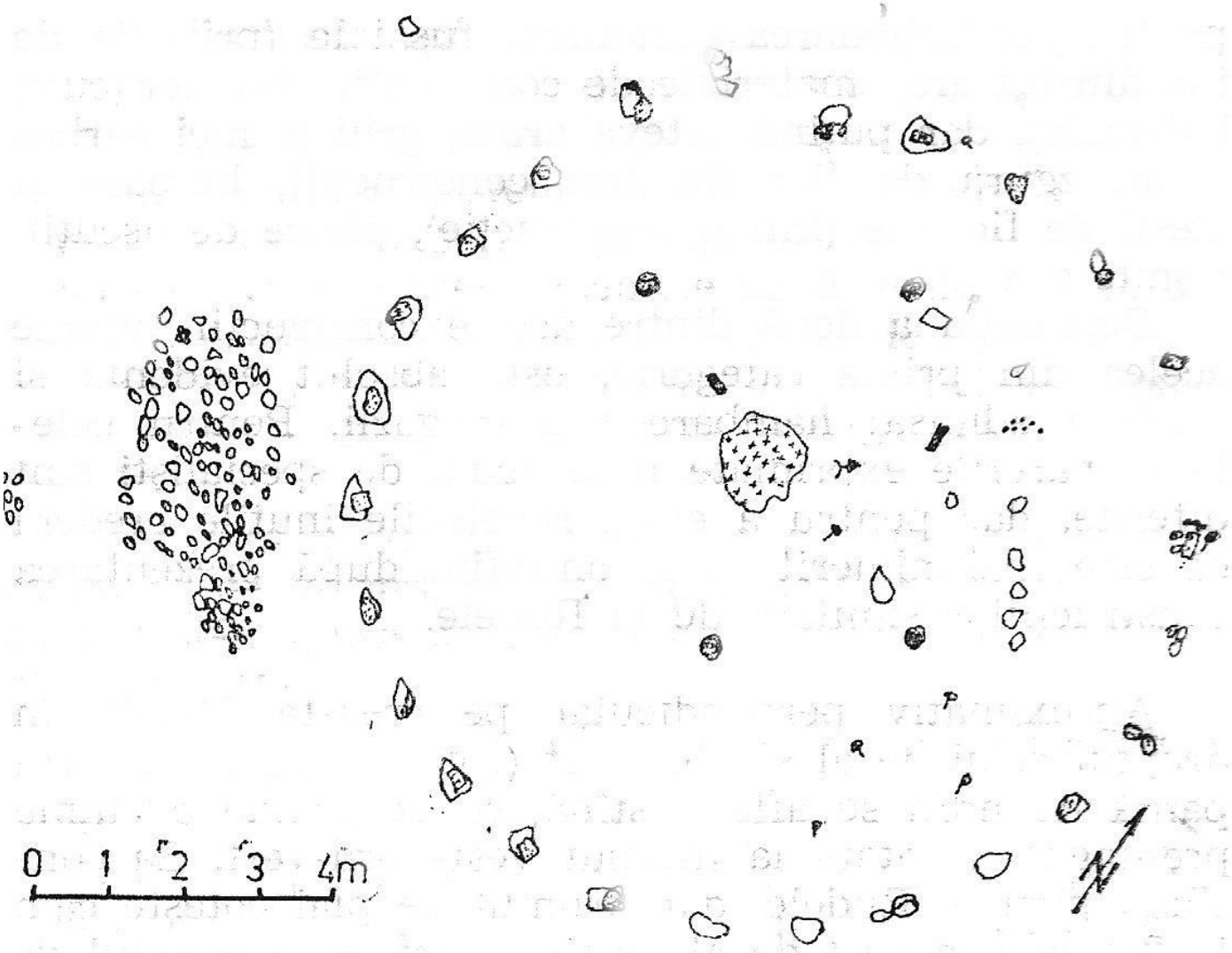
- Între ansamblul dacic şi cel de la Stonehenge există diferite concordanţe neinfluenţate de diferenţa de timp la care au fost create, prin configuraţia centrală sub formă de potcoavă, cercul înconjurător format din 30 de elemente şi marele sanctuar circular ce comunică cu micul sanctuar, respectiv cu piatra călcâi sau prin dreapta ce uneşte centrele lor, aleasă în funcţie de orientarea geografică.
- Ansamblul dacic ne dezvăluie un sistem calendaristic de calcul luni-solar al principalelor funcţii astronomice (**un calendar luni-solar** are ca scop menţinerea lunilor în sincronicitate cu Luna şi anii în sincronicitate cu Soarele), dintre care au fost amintite funcţia de numărare a zilelor şi a lunilor prin utilizarea marelui cerc, funcţia de corectare a perioadelor sinodice prin structura potcoavei şi funcţia de corectare a anului tropic prin cercul intermediar.

Suprapunere



- În Romania, s-au păstrat vestigii astronomice ale civilizaţiei dacice care sunt mărturii ale cunoştinţelor lor astronomice, pe teritoriul vechii Dacii la ruinele cetăţii Sarmizegetusa, la Feţele Albe, Piatra Craivii, Piatra Roşie, Bâtca Doamnei, Costeşti, Băniţa, Blidarul, Barboşi, Popeşti, Pecica sau Melaia.
- S–au studiat aceste centre ce utilizau sistemul calendaristic dacic şi s-a observat similitudinea construcţiilor sanctuarelor astronomice.

Meleia – valea Streiului



X-ray analysis of an archaic syrian-phoenician style statuette uncovered in the sacred zone of Histria

Alexandru Curutiu, FFB, an III,
Mircea V. Rusu, FFB,
Albert Baltres, Institutul Geologic Bucuresti

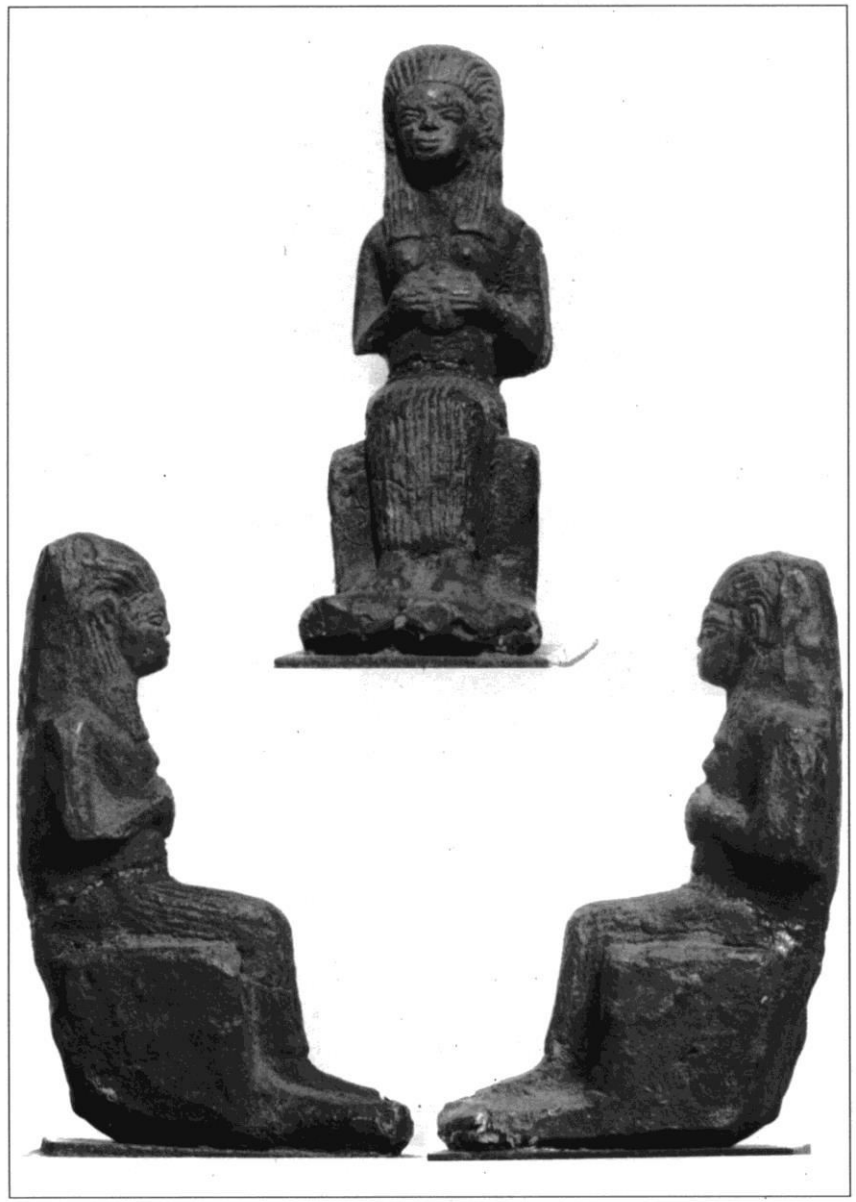
The scope of this report is to present the results of laboratory analysis of an archaic syrian-phoenician style statuette. It was uncovered in the sacred zone of Histria and dates about 6th century BC. The two pieces of the statuette were found in the same location, having also in common the same constitutive material, that is not a clay but nearly pure *melilite*. This suggests the casting material had a special provenance, providing some insight regarding the type of parent rock. We made a sorrow analysis of the materials and the inclusions and we report the results.



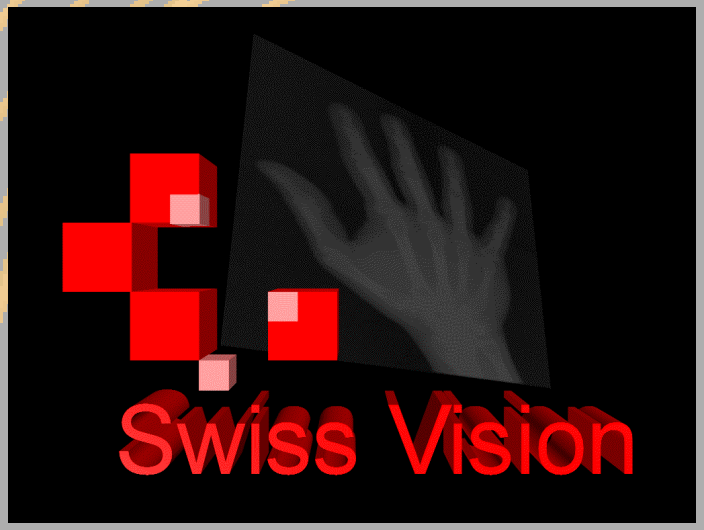








Statuette en terre-cuite appartenant à la collection Ion Minulescu



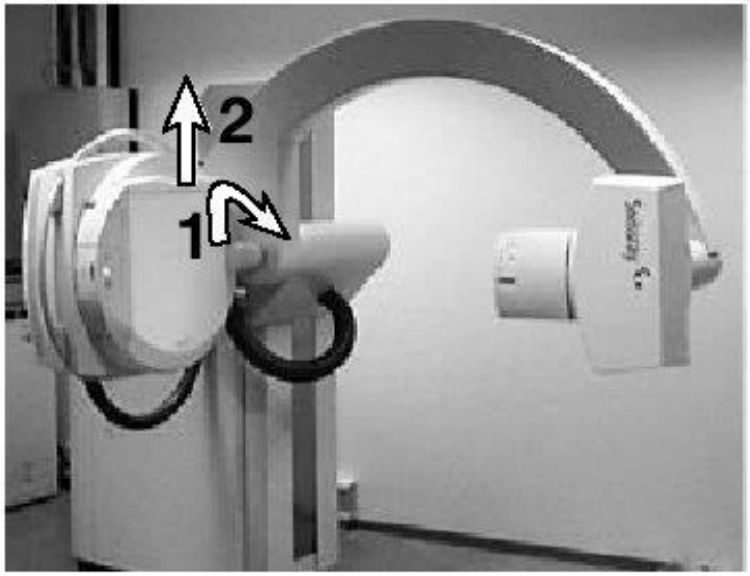


Fig. 3.8

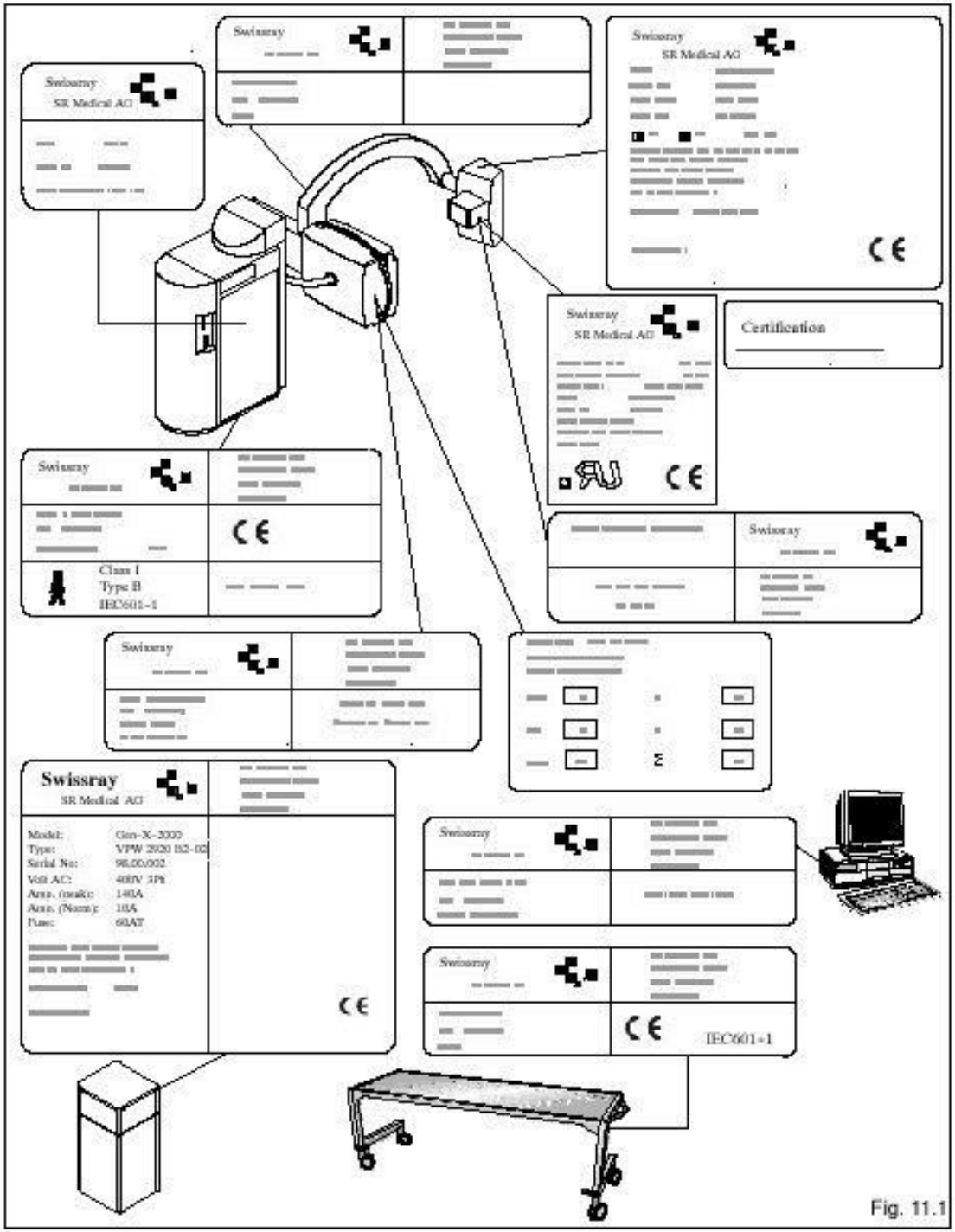
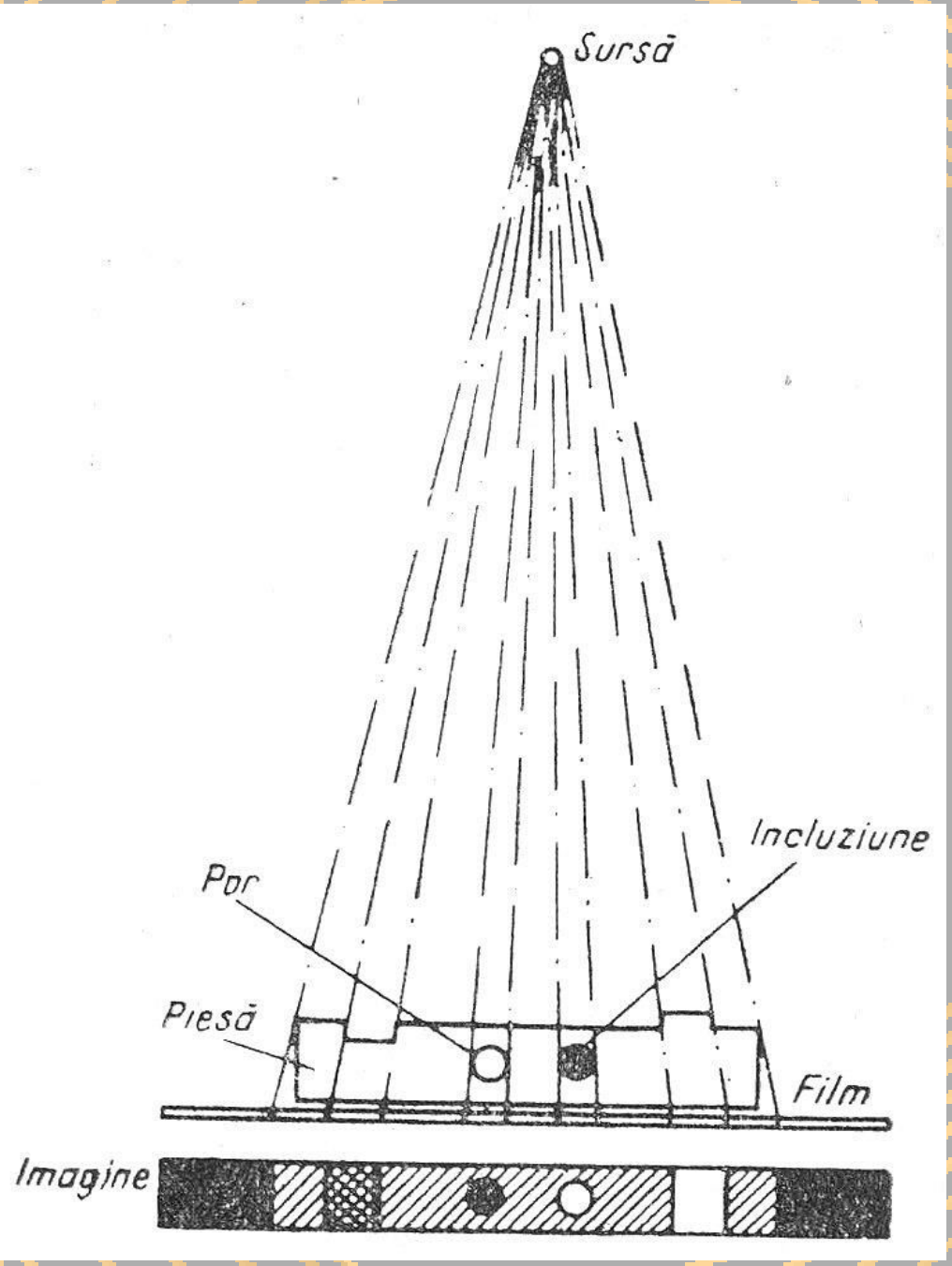
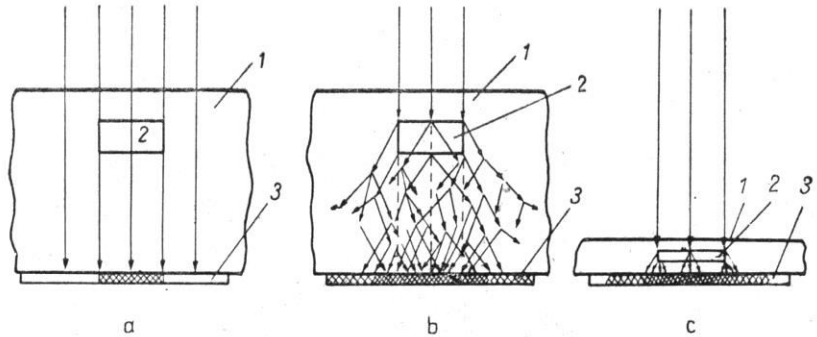
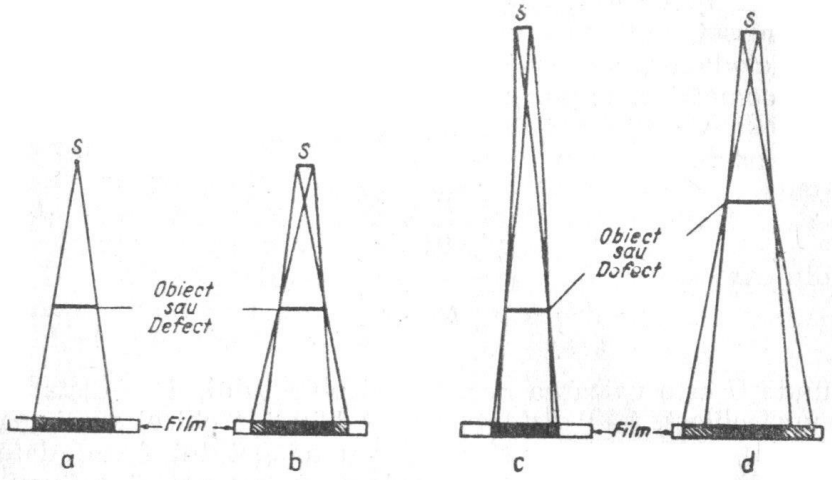


Fig. 11.1





Influența radiației împrăștiate asupra reproducerii pe clișeu:
a — imaginea în cazul radiației neîmprăștiate; *b* — imaginea în cazul radiației împrăștiate; *c* — imaginea în cazul radiației împrăștiate în piese subțiri este mai bună. *1* — piesă; *2* — defect; *3* — film.



Variația neclarității cu distanța sursă-film și sursă-obiect.

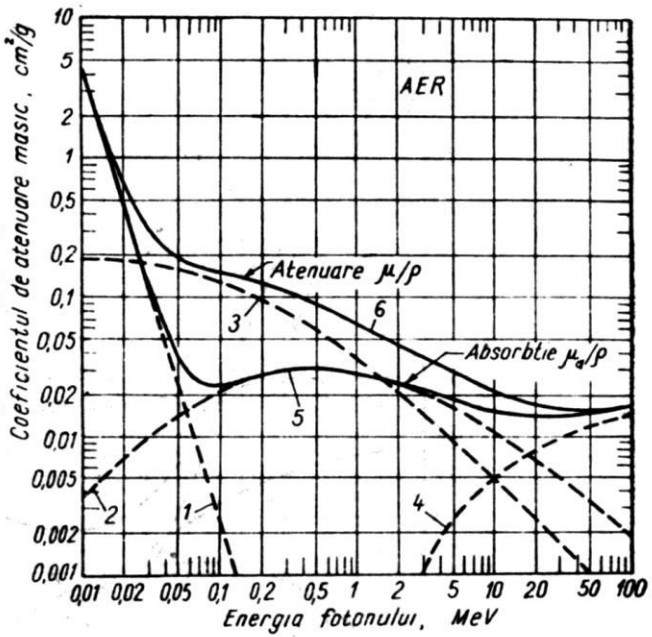


Fig. III.4. Coeficienții de atenuare, de absorbție și de împrăștiere, masici, pentru aer în funcție de energia fotonilor:
1 — absorbție fotoelectrică; *2* — absorbție Compton; *3* — împrăștiere Compton; *4* — absorbție formare de perechi; *5* — absorbție totală; *6* — atenuare.

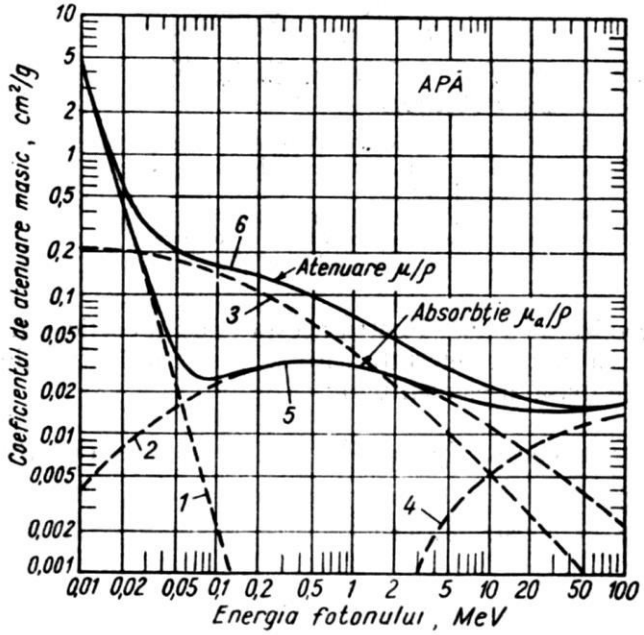


Fig. III.5. Coeficienții de atenuare, de absorbție și de împrăștiere masici, pentru apă, în funcție de energia fotonilor:
1 — absorbție fotoelectrică; *2* — absorbție Compton; *3* — împrăștiere Compton; *4* — absorbția formare de perechi; *5* — absorbție totală; *6* — atenuare.

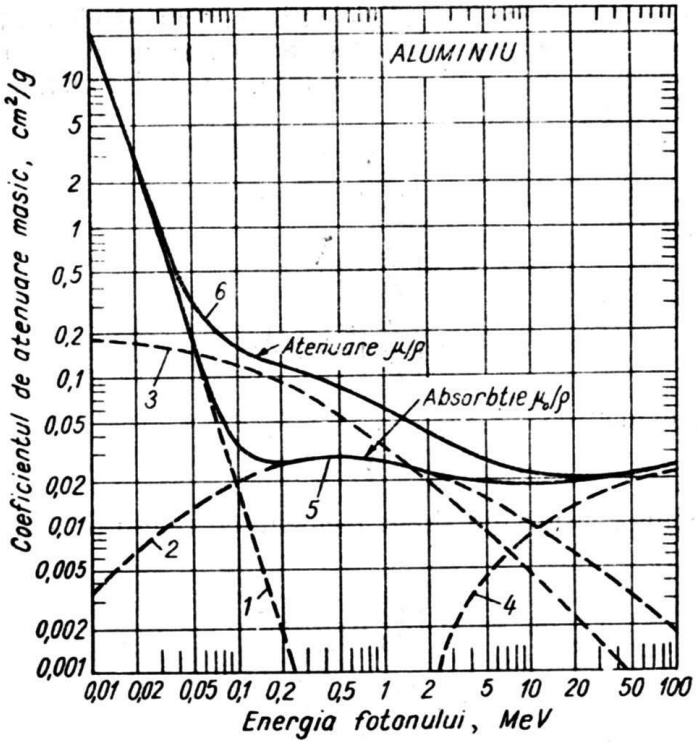


Fig. III.7. Coeficienții de atenuare, de absorbție și de împrăștiere, masici, pentru aluminiu, în funcție de energia fotonilor:
1 — absorbție fotoelectrică; *2* — absorbție Compton; *3* — împrăștiere Compton; *4* — absorbție formare de perechi; *5* — absorbție totală; *6* — atenuare.

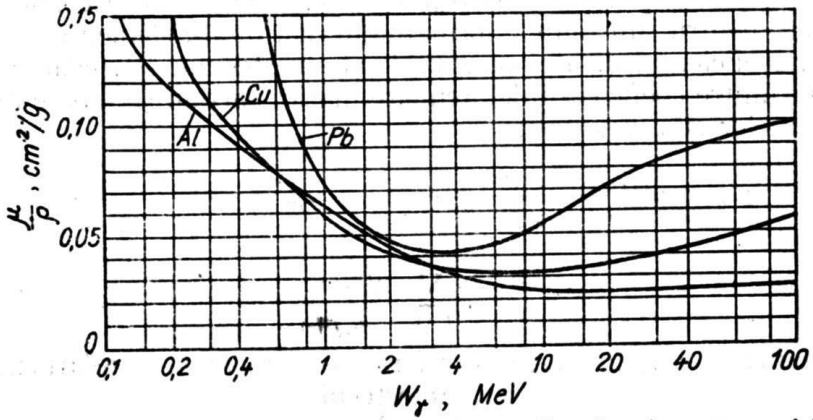
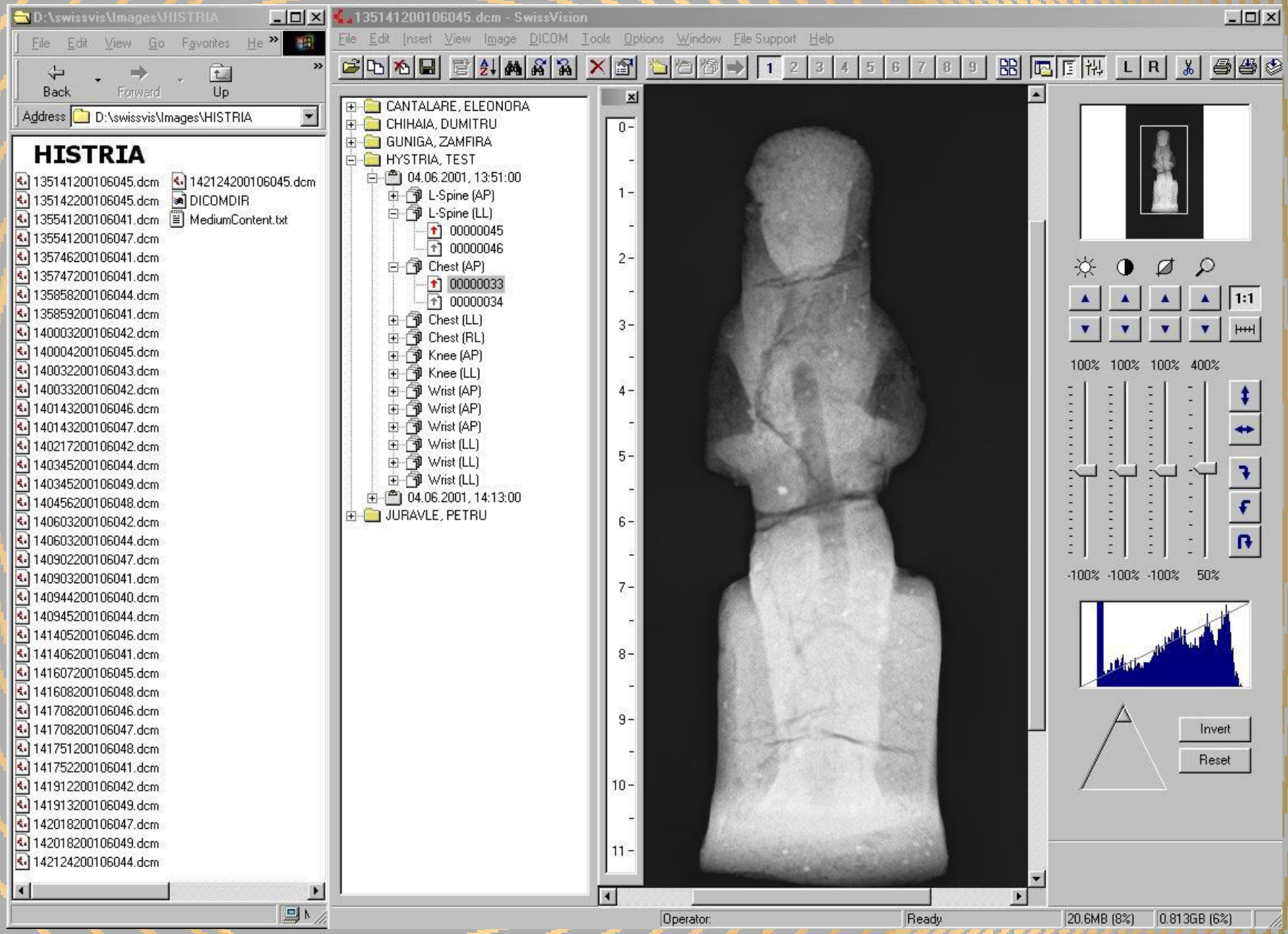
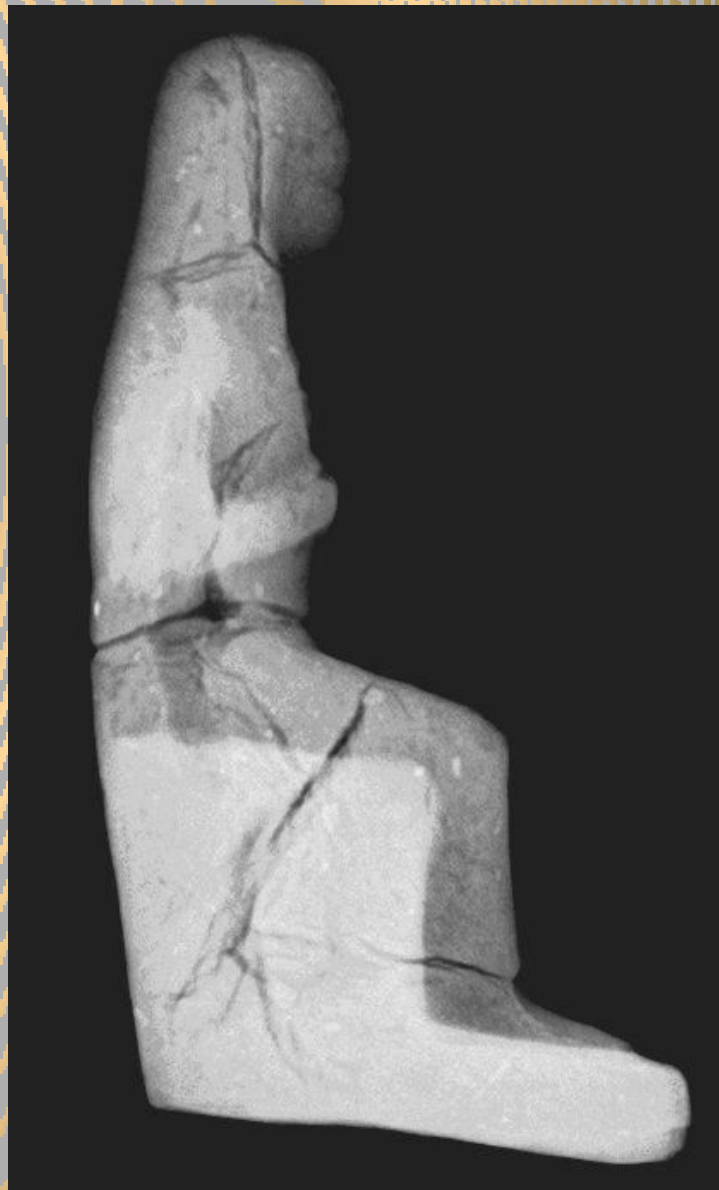


Fig. III.8. Modul de variație al coeficienților de atenuare masici în aluminiu, cupru și plumb pentru radiațiile gama.


D:\swissvis\Images\HISTRIA
File Edit View Go Favorites He
Back Forward Up
Address D:\swissvis\Images\HISTRIA
HISTRIA
135141200106045.dcm
135142200106045.dcm
135541200106041.dcm
135541200106047.dcm
135746200106041.dcm
135747200106041.dcm
135858200106044.dcm
135859200106041.dcm
140003200106042.dcm
140004200106045.dcm
140032200106043.dcm
140033200106042.dcm
140143200106046.dcm
140143200106047.dcm
140217200106042.dcm
140345200106044.dcm
140345200106049.dcm
140456200106048.dcm
140603200106042.dcm
140603200106044.dcm
140902200106047.dcm
140903200106041.dcm
140944200106040.dcm
140945200106044.dcm
141405200106046.dcm
141406200106041.dcm
141607200106045.dcm
141608200106048.dcm
141708200106046.dcm
141708200106047.dcm
141751200106048.dcm
141752200106041.dcm
141912200106042.dcm
141913200106049.dcm
142018200106047.dcm
142018200106049.dcm
142124200106044.dcm
142124200106045.dcm
DICOMDIR
MediumContent.txt
135141200106045.dcm - SwissVision
File Edit Insert View Image DICOM Tools Options Window File Support Help
CANTALARE, ELEONORA
CHIHAIA, DUMITRU
GUNIGA, ZAMFIRA
HYSTRIA, TEST
04.06.2001, 13:51:00
L-Spine (AP)
L-Spine (LL)
00000045
00000046
Chest (AP)
00000033
00000034
Chest (LL)
Chest (RL)
Knee (AP)
Knee (LL)
Wrist (AP)
Wrist (AP)
Wrist (AP)
Wrist (LL)
Wrist (LL)
Wrist (LL)
04.06.2001, 14:13:00
JURAVLE, PETRU
1:1
100% 100% 100% 400%
-100% -100% -100% 50%
Invert
Reset
Operator:
Ready
20.6MB (8%)
0.813GB (6%)





$$\mu/\rho = \sum_i w_i (\mu/\rho)_i$$

NIST Standard Reference Database 7

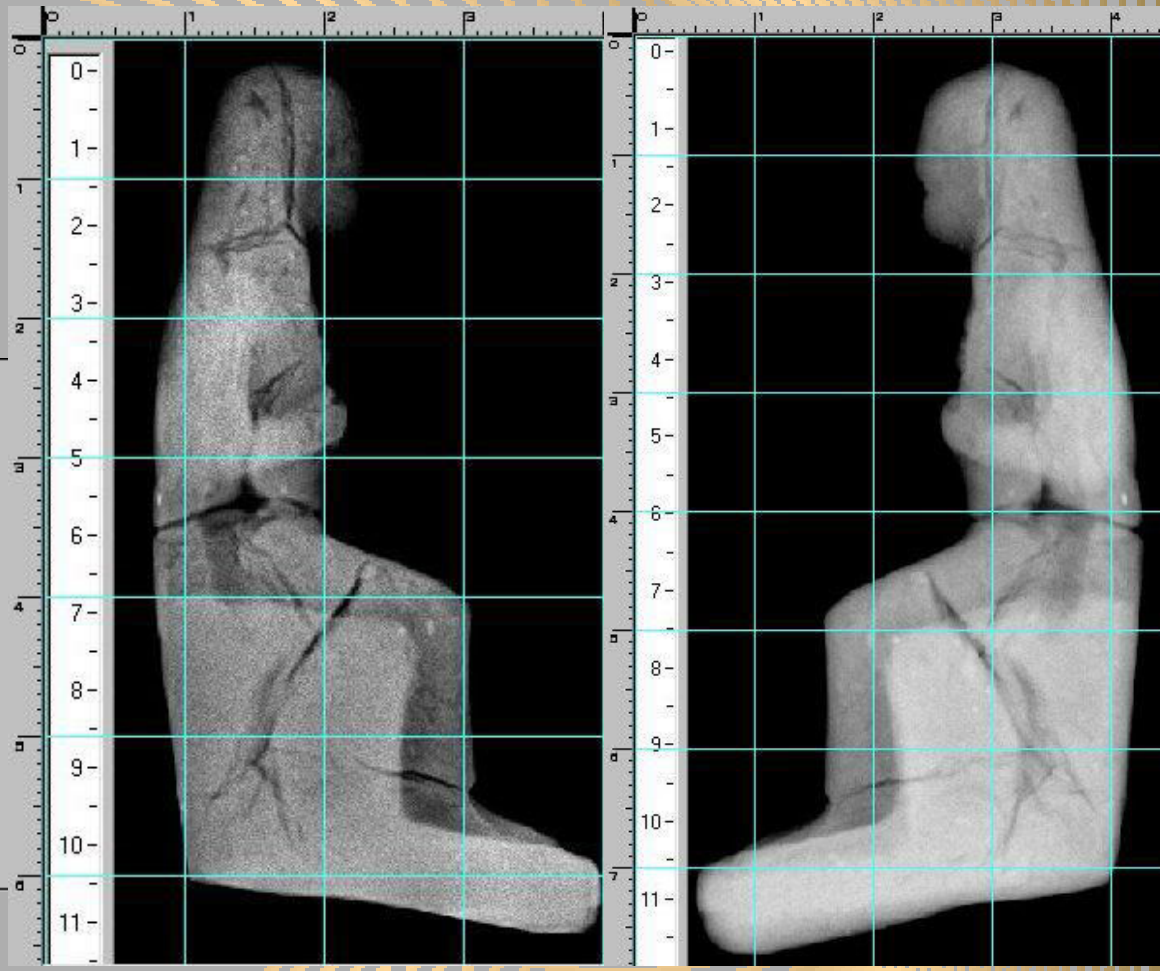
NIST ELECTRON AND POSITRON STOPPING POWERS AND RANGES
DATABASE
Version 2.0

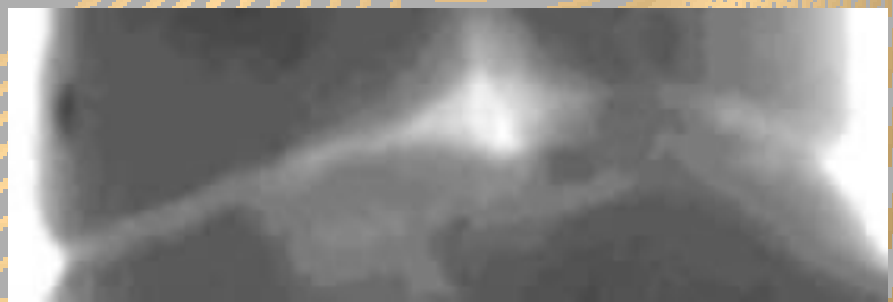
Written by
STEPHEN M. SELTZER
Center for Radiation Research
National Institute of Standards and Technology
Gaithersburg, MD 20899

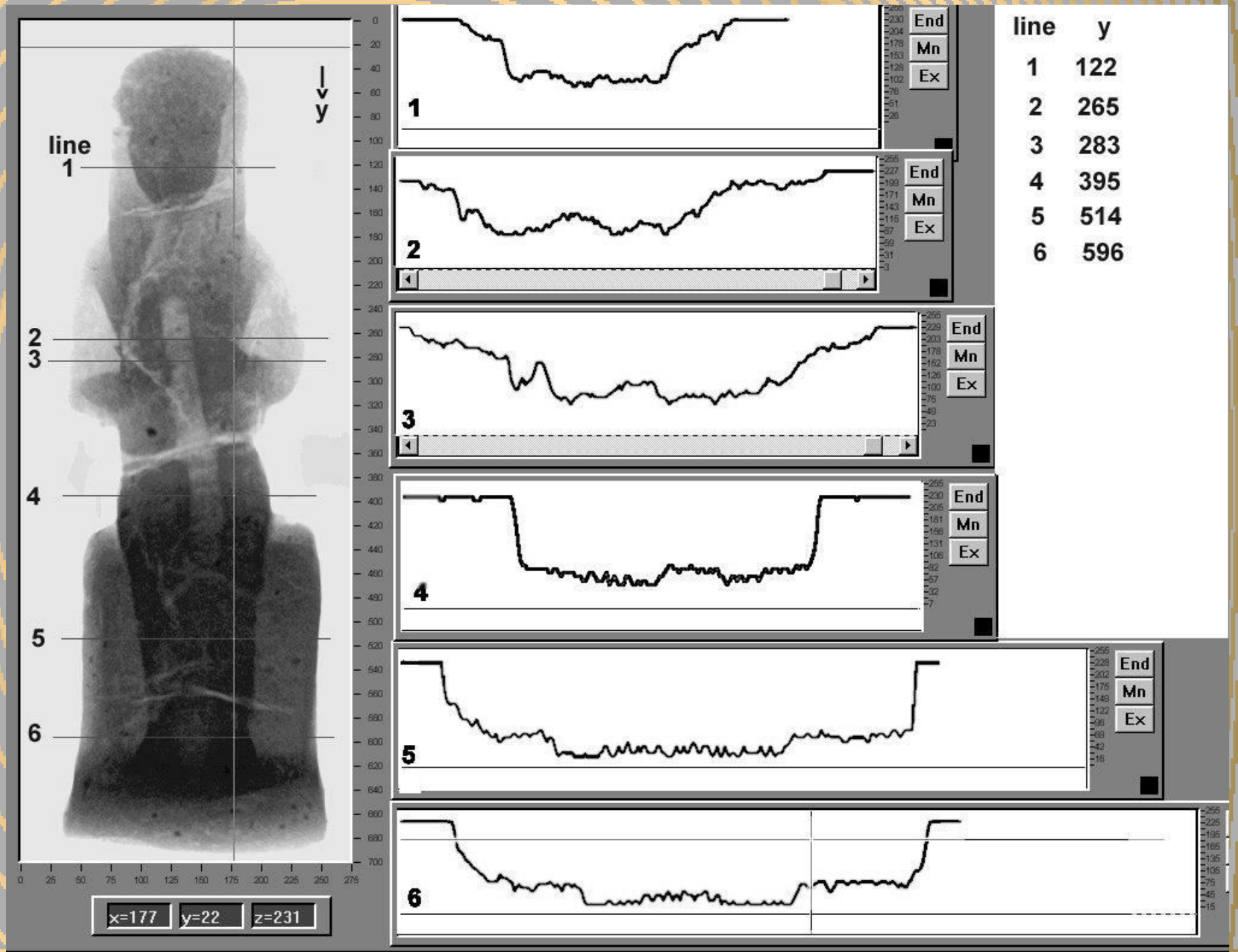
Distributed by
Standard Reference Data
National Institute of Standards and Technology
Gaithersburg, MD 20899

Copyright 1989 by
U.S. Secretary of Commerce
on behalf of the United States Government

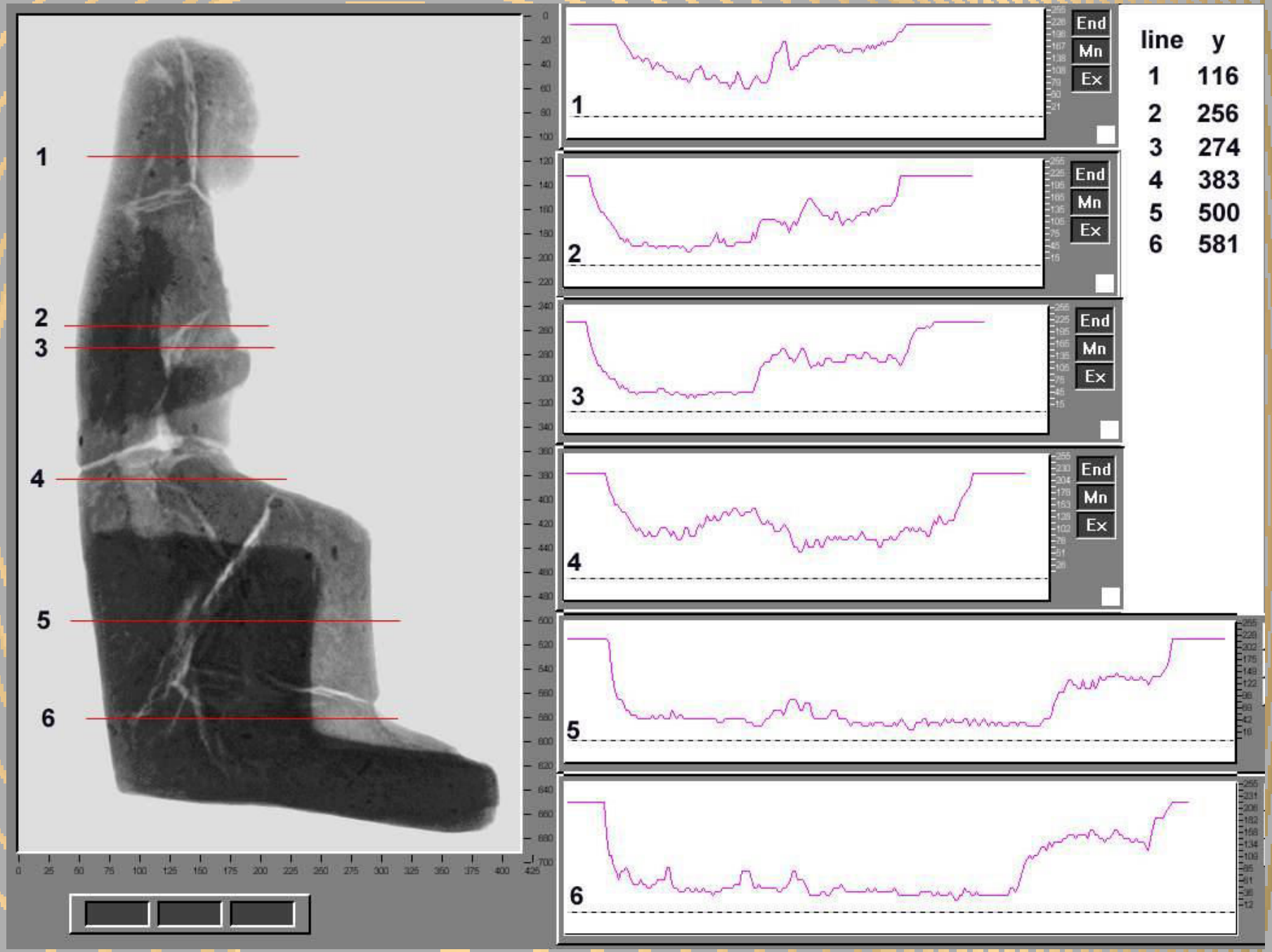
Help (Y/N)? N

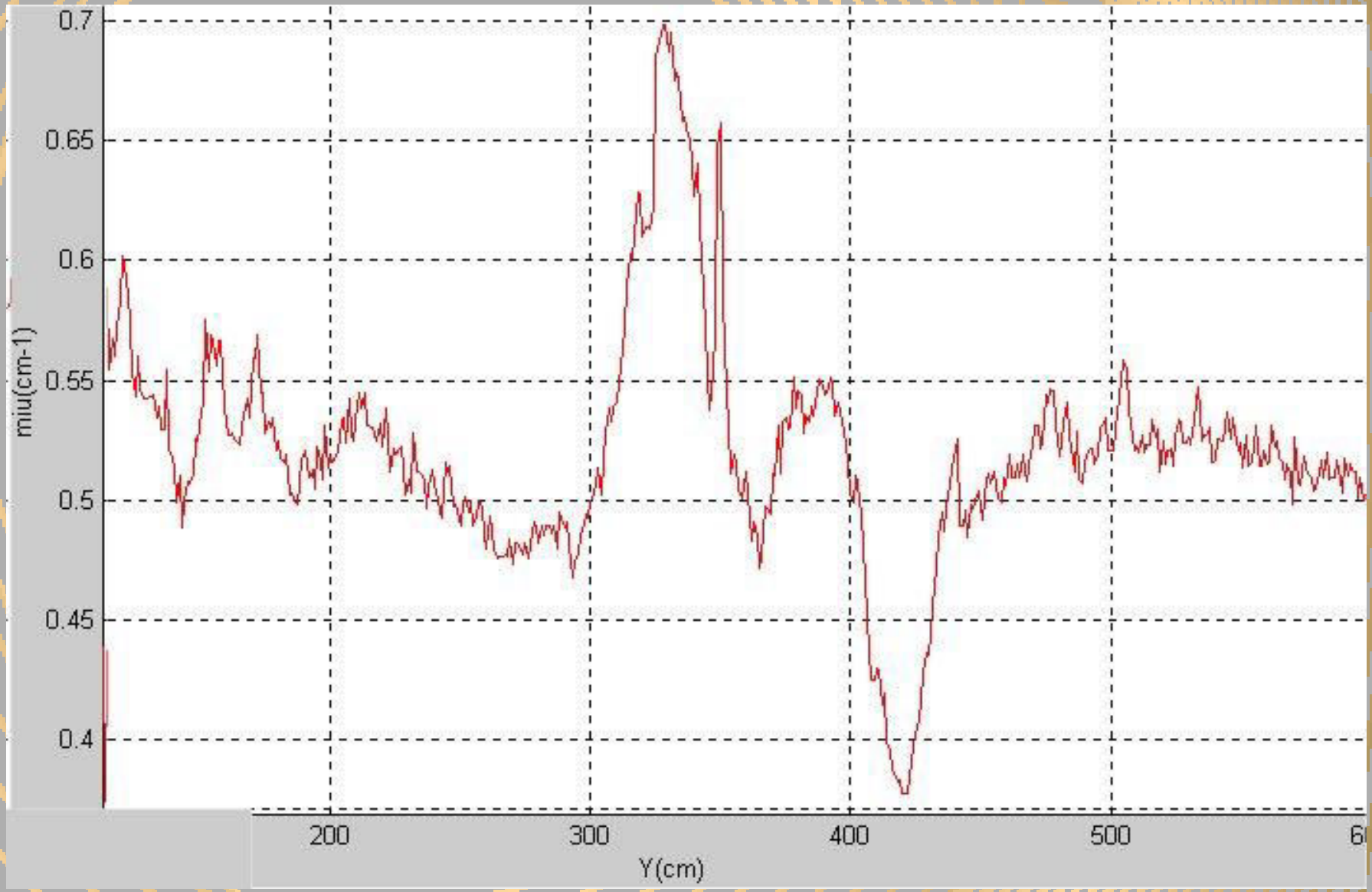






line	y
1	122
2	265
3	283
4	395
5	514
6	596


1
2
3
4
5
6
End
Mn
Ex
line y
1 116
2 256
3 274
4 383
5 500
6 581


0.7
0.65
0.6
0.55
0.5
0.45
0.4
miu(cm-1)
200
300
400
500
Y(cm)

Compoziția chimică medie a tipurilor principale de roce eruptive.
după D a l y, 1933
(în paranteză, numărul analizelor din care s'au calculat mediile)

	Roce calcoalcaline											Roce alcaline		
	Granit (546)	Riolit (126)	Granodiorit (40)	Dacit (90)	Sienit (50)	Trachit (48)	Diorit (70)	Andezit (87)	Gabbro (41)	Bazalt (198)	Peridotit (31)	Picrit*) (14)	Sienit alcalin (32)	Sienit nefelinic (43)	Fonolit (25)
SiO_2	70,18	72,80	65,01	65,68	60,19	60,68	56,77	59,59	48,24	49,06	41,09	41,30	62,00	54,63	57,45
TiO_2	0,39	0,33	0,57	0,57	0,67	0,38	0,84	0,77	0,97	1,36	1,16	0,81	0,57	0,86	0,41
Al_2O_3	14,47	13,49	15,94	16,25	16,28	17,74	16,67	17,31	17,88	15,70	4,80	9,43	17,44	19,89	20,60
Fe_2O_3	1,57	1,45	1,74	2,38	2,74	2,64	3,16	3,33	3,16	5,38	3,96	5,30	2,06	3,37	2,35
FeO	1,78	0,88	2,65	1,90	3,28	2,62	4,40	3,13	5,95	6,37	7,12	8,86	2,68	2,20	1,03
MnO	0,12	0,08	0,07	0,06	0,14	0,06	0,13	0,18	0,13	0,31	0,10	0,29	0,12	0,35	0,13
MgO	0,88	0,38	1,91	1,41	2,49	1,12	4,17	2,75	7,51	6,17	32,25	19,94	0,91	0,87	0,30
CaO	1,99	1,20	4,42	3,46	4,30	3,09	6,74	5,80	10,99	8,95	4,42	8,01	2,26	2,51	1,50
Na_2O	3,48	3,38	3,70	3,97	3,98	4,43	3,36	3,58	2,55	3,11	0,49	1,20	5,86	8,26	8,84
K_2O	4,11	4,46	2,75	2,67	4,49	5,74	2,12	2,04	0,89	1,52	0,96	0,39	5,17	5,46	5,23
H_2O	0,84	1,47	1,04	1,50	1,16	1,26	1,36	1,26	1,45	1,62	3,53	4,27	0,76	1,35	2,04
P_2O_5	0,19	0,08	0,20	0,15	0,28	0,24	0,25	0,26	0,28	0,45	0,12	0,20	0,17	0,25	0,12

*) După Daly 1914

3 2 2 1

— 1266 —

	Roce alcaline						Roce filoniene								
	Gabbro alcalin Essexit (20)	Bazalt nefelinic (26)	Bazalt leucitic (12)	Foidit nefelinic (ijolit) (6)	Nefelinit (9)	Leucitit (9)	Aplit granitic (15)	Minette (10)	Kersantit (20)	Vogesit (1)	Spessartit (10)	Camptonit (15)	Monchiquit (16)	Alnöit (6)	Roce eruptive (media) (5159)	Litosfera
SiO_2	48,64	39,87	46,18	42,81	41,17	46,90	75,00	49,45	50,79	52,62	53,52	40,70	45,17	32,31	59,12	59,07
TiO_2	1,86	1,50	2,13	1,56	1,35	1,22	0,30	1,23	1,02	0,54	1,24	3,86	1,90	1,41	1,05	1,03
Al_2O_3	17,96	13,58	12,74	18,95	16,83	16,33	13,14	14,41	15,26	14,86	14,57	16,02	14,78	9,50	15,34	15,22
Fe_2O_3	4,31	6,71	5,27	3,86	7,61	4,22	0,58	3,39	3,29	3,60	3,52	5,43	5,10	5,42	3,08	3,10
FeO	5,58	6,43	5,06	4,84	6,64	4,14	0,40	5,01	5,54	4,18	5,29	7,84	5,05	6,34	3,80	3,71
MnO	0,19	0,21	0,19	0,19	0,16	0,11	0,07	0,13	0,07	0,84	0,38	0,16	0,35	0,01	0,12	0,12
MgO	4,00	10,46	8,36	3,16	3,72	5,03	0,30	8,26	6,33	8,55	6,60	5,43	6,24	17,43	3,49	3,45
CaO	8,89	12,36	8,16	10,47	10,12	9,72	1,13	6,73	5,73	5,86	7,03	9,36	11,06	13,58	5,08	5,10
Na_2O	4,30	3,85	2,36	9,63	6,45	2,75	3,54	2,54	3,12	3,21	3,48	3,23	3,69	1,42	3,84	3,71
K_2O	2,28	1,87	6,18	2,26	2,49	7,58	4,80	4,69	2,79	2,83	2,28	1,76	2,73	2,70	3,13	3,11
H_2O	1,34	2,22	2,60	0,85	2,42	1,50	0,71	3,04	5,71	2,70	1,75	5,59	3,40	7,50	1,15	1,30
P_2O_5	0,65	0,94	0,77	1,42	1,09	0,50	0,03	1,12	0,35	0,21	0,34	0,62	0,51	2,38	0,30	0,30
CO_2															0,10	0,35

In coloana „roce eruptive" este redată media a 5159 analize de roce eruptive
In coloana „litosfera" este dată compoziția scoarței până la 16 km adâncime } (Clarke și Washington)

— 1267 —

Datele **analizei materialului** din care este facuta **statueta**.

Analiza s-a facut cu ajutorul unui Microscop electronic cu baleiaj in regim de analiza de fluorescenta (Microsonda electronica)
Proba analizata pe o regiune de 30 x 20 μm;

Materialul utilizat pentru producerea statuetei este Melilitul:

Element	concentratie in % atomice	nr. de ioni
Magneziu	0.16	0.08
Aluminiu	5.21	2.70
Siliciu	1.17	7.87
Clor	5.44	2.82
Potasiu	0.44	0.23
Calciu	14.01	7.27
Titan	0.45	0.23
Fier	2.59	1.35
Cupru	0.11	0.06
Zinc	0.12	0.06
Oxigen	56.29	29.18

suma cationi **19.84**

anioni **32 anioni per formula**

varietatea analizata este deci usor feriera

Formula chimica pentru Melilit:

formula chimica:	**densitate:**
$Ca_2Al_2Si_2O_7$	**3.04 g/cm3**
$Ca_2Fe_2Si_2O_7$	**3.20 g/cm3 sau**
$Ca_2Al_{2-x}Fe_xSi_2O_7$	**3.04 - 3.20**

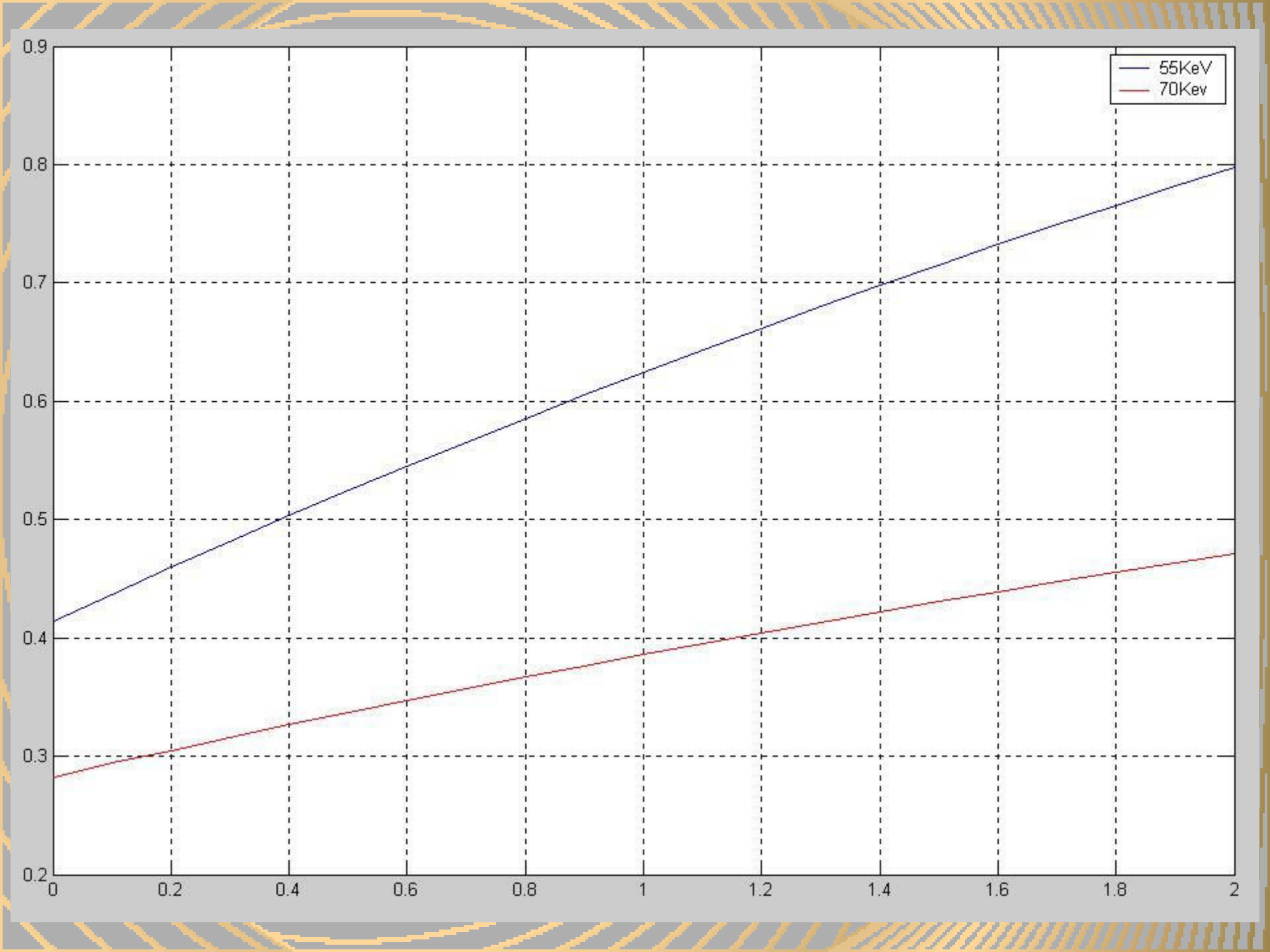
Image data computed at different heights
(image files: 40 and 41, at 70 keV)

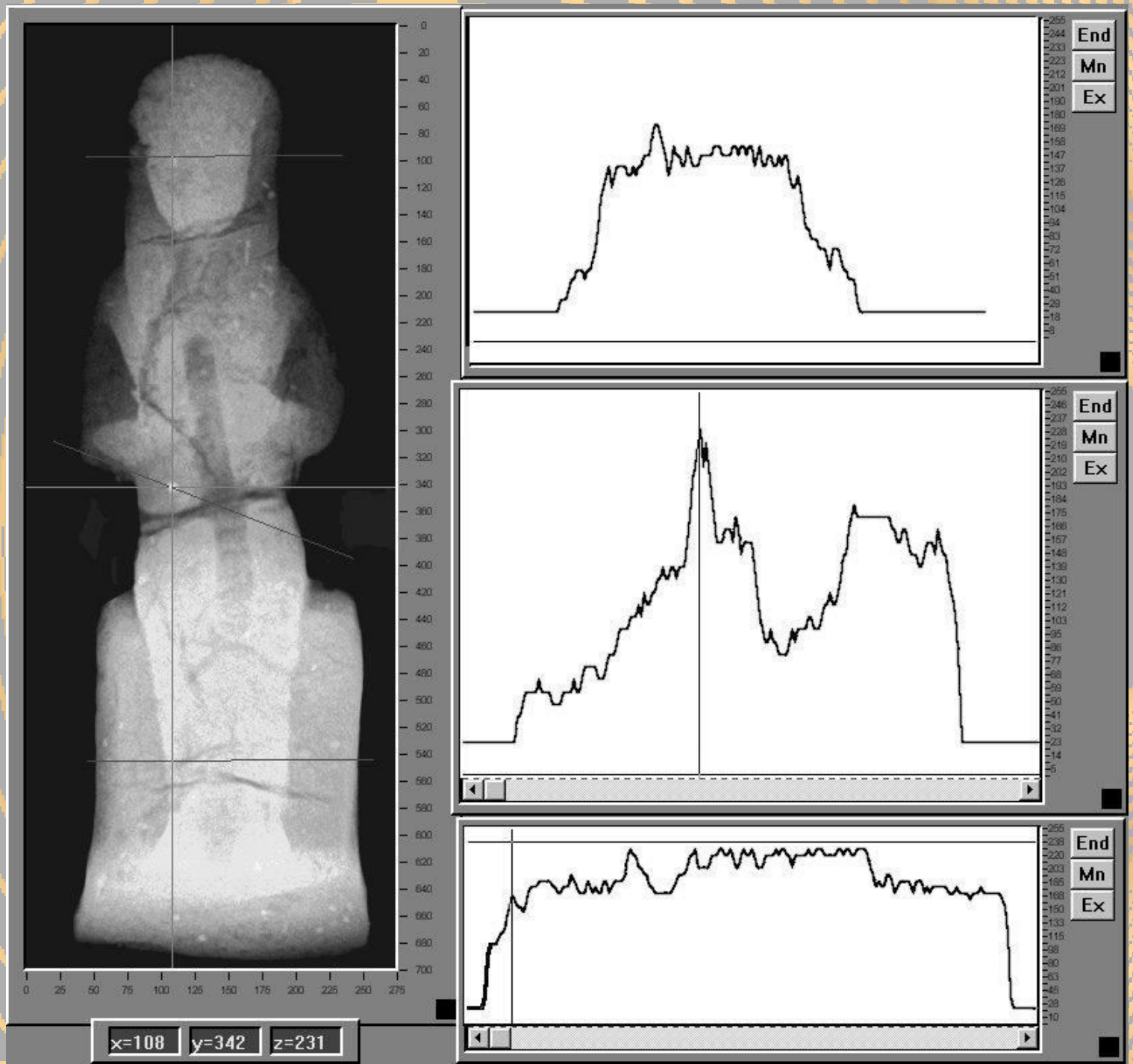
Line profile	Intensity (relative scale)	μ (1/cm)	μ/ρ (cm^2/g) mean density 3.1 g/cm^3
1	1500	0.608	0.196
2	1250	0.724	0.233
3	1525	0.662	0.214
4	540	0.611	0.197
mean value		0.651 ± 0.03 cm^{-1}	0.210 ± 0.02 cm^2/g

Image data computed at different heights
(image files: 48 and 54, at 55 keV)

Line profile	Intensity (relative scale)	μ (1/cm)	μ/ρ (cm^2/g)
1	400	1.084	0.350
2	355	1.096	0.353
3	435	1.115	0.359
mean value		1.098 ± 0.03 cm^{-1}	0.354 ± 0.02 cm^2/g

Computed value at this energy [mean density 3.1 g/cm^3]
Gehlenit: 0.3283 cm^2/g
and the iron concentartion is x = 0.85


55KeV
70Kev
0.9
0.8
0.7
0.6
0.5
0.4
0.3
0.2
0
0.2
0.4
0.6
0.8
1
1.2
1.4
1.6
1.8
2

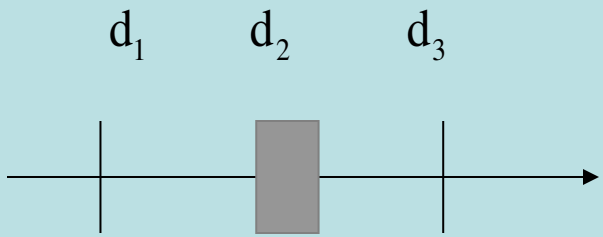

End
Mn
Ex
End
Mn
Ex
End
Mn
Ex
x=108
y=342
z=231

Intensitatea unui fascicul trasmis printr-un esantion este data de:

$$I = I_0 \cdot e^{-\rho \cdot \mu_m \cdot x}$$

Relatiile de mai sus pot fi folosite pentru determinarea coeficientului de atenuare:

$$\mu = \frac{1}{d} \ln \frac{I_0}{I}$$



Pentru un element de incuziune avem :

Fie:

$$d = d_1 + d_2 + d_3$$

Obtinem expresia pentru coeficientul de atenuare a incluziunii:

$$\mu_2 = \frac{1}{d_2}\left[\ln \frac{I_0}{I_3} - \mu_1 (d - d_2)\right]$$

Nume	Formula	Densitate	ρ g/cm^3	μ/ρ (cm^2/g), dedus din datele experimentale
	Masuratoare la energia = >		55 keV	70 keV
Cuartz	SiO_2	2.65	0.975	0.787
Hematit	α-Fe_2O_3	5.4	0.480	0.401
Magnetit	Fe_3O_4	5.2	0.499	0.401
Goethit	α-FeOOH	4.3	0.603	0.485
Coeficientul de atenuare liniar al inculziunii dedus experimental			2.593	2.086

Concluzia este aceea ca cel mai probil compus al incluziunii vizibile prin absorbtie X este Goethitul, dar cu o mare imprecizie numerica.

8) Learning activities

- **8.1 Preparing future researchers beginning from the school, university and PhD activities:**
- - Science popularization
- - Helping teaching science in school: math, physics, astronomy
- - Involvement in school contests, national and international Olympiads in physics and astronomy
- - Involvement in in-service teacher training
- **8.2 Universities**
- - Physics and chemistry
- - Astrophysics
- - Nonlinear dynamics
- - Complexity
- - PhD – in astrophysics

1. Experiments

- A *very high intensity laser*, where the beams from two 10 PW lasers are coherently added to the high intensity of 10^{23} - 10^{24} W/cm^2 or electrical fields of 10^{15} V/m.

1.1- Changing radioactive time decay of some nuclei by modifying coulomb barrier height

1.2- Compressing deuterium gas – changing the rate of D-D fusion reaction

1.3- Coulomb excitation and Mössbauer experiments with non-Mössbauer nuclei (32Ge-71; 11.26d)

1.4- Checking symmetry of electromagnetic interactions: equality of electromagnetic force constant for interactions between particles with the same charge sign and opposite charge sign (high field QED)

1. Experiments

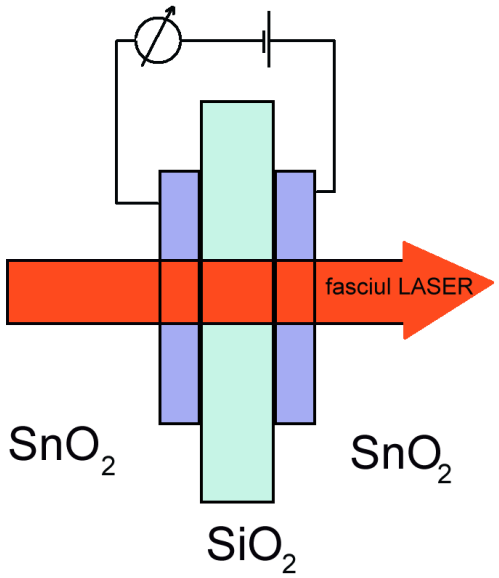
1.5- *Small-angle neutron scattering* allows one to study nanoscaled materials, taking advantage of the sensitivity of neutrons towards isotopes and spin direction and *diffraction image* of a nanostructure sample :

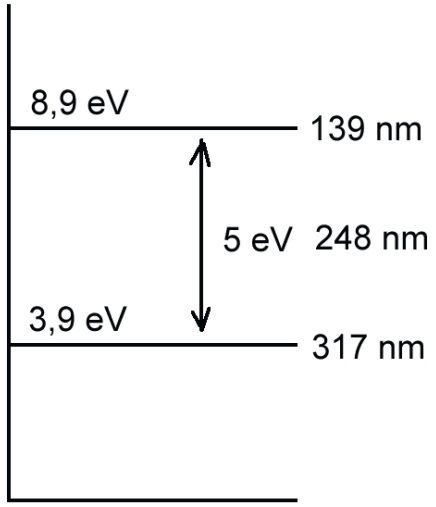
- Study the order for disordered materials: Ge-a si Si-a (ordinea in apropiere):
  - disordered polyhedron ?
  - Voronoy polyhedron ?
  - “amorfon” ?

2. Detectors

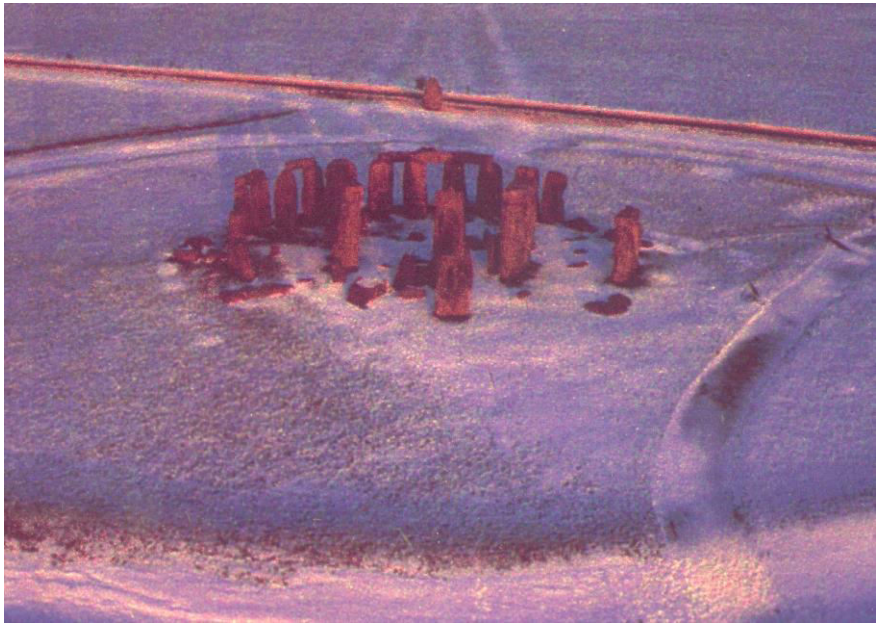
- A *very high intensity laser*, where the beams from two 10 PW lasers are coherently added to the high intensity of 10^{23} - 10^{24} W/cm^2 or electrical fields of 10^{15} V/m.

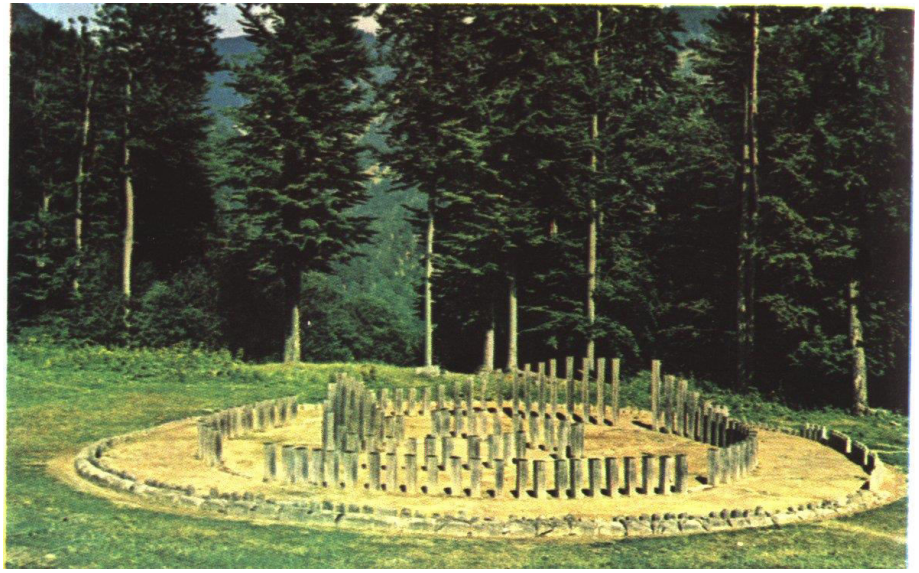
2.1- Laser beam power monitor – solid state detector







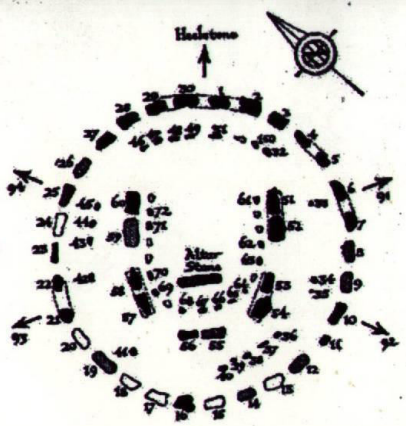


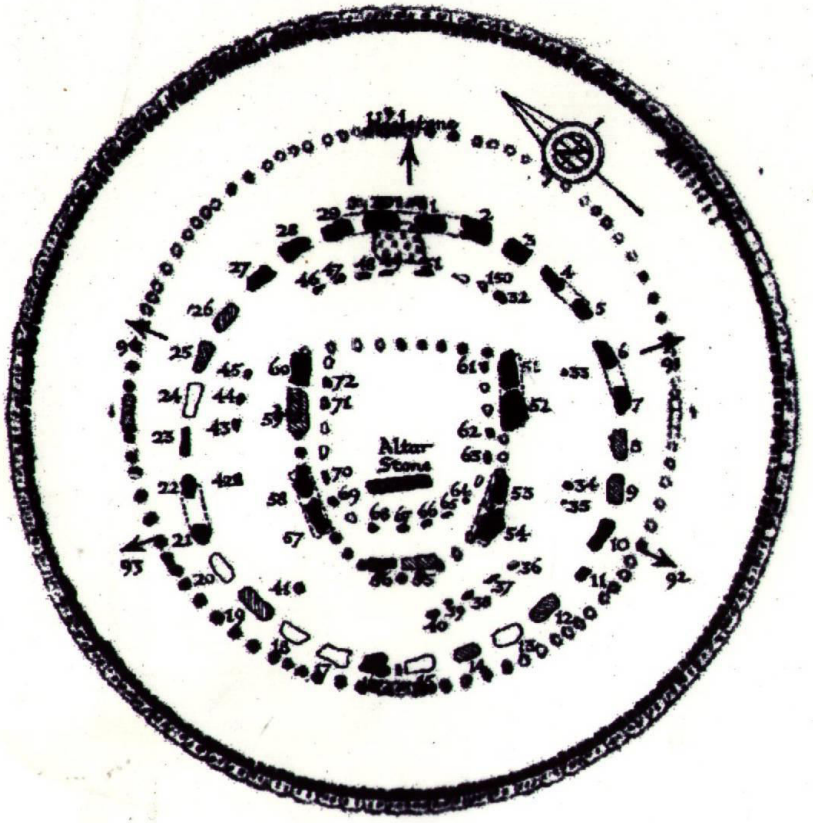


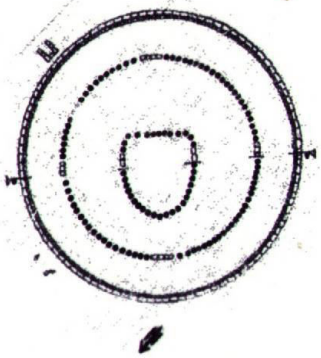


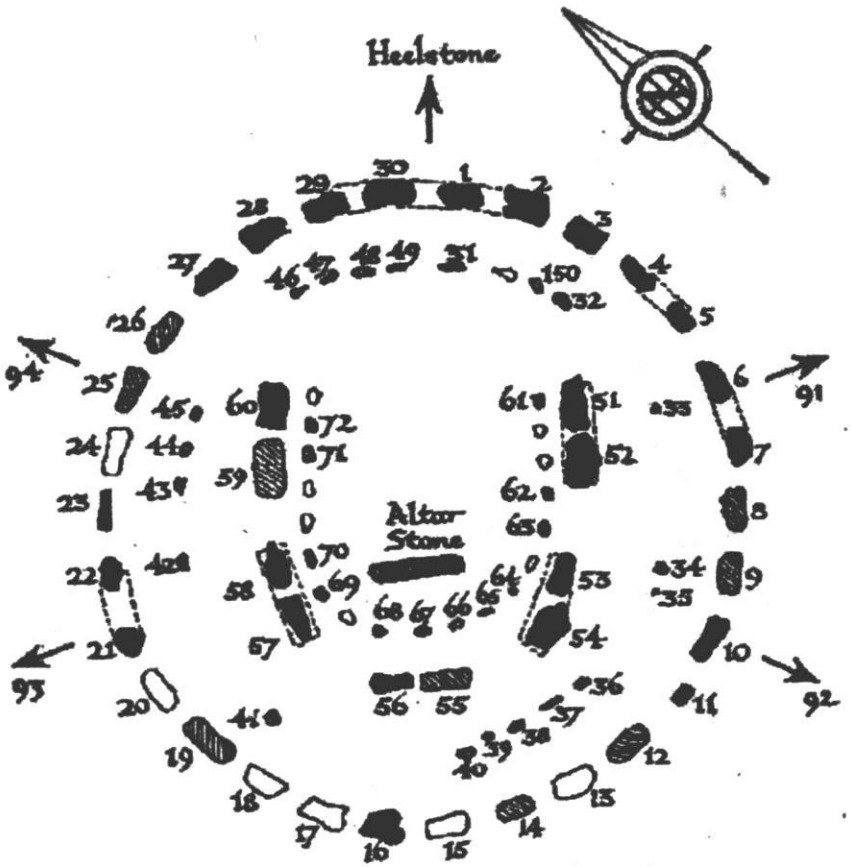
Superposition

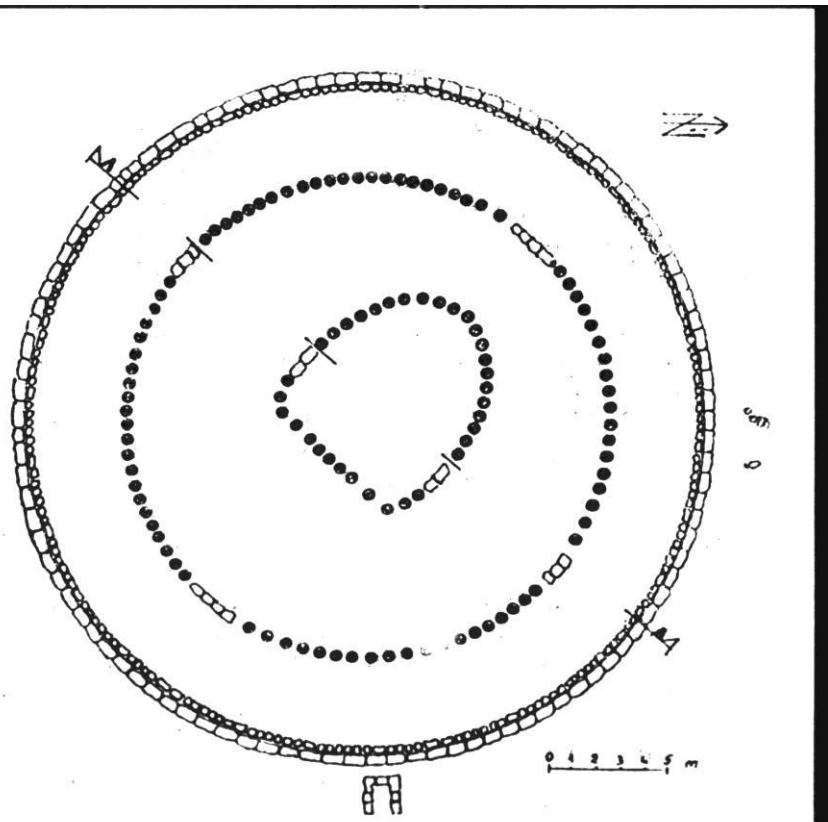
scaling and rotation








Heelstone
Altar Stone



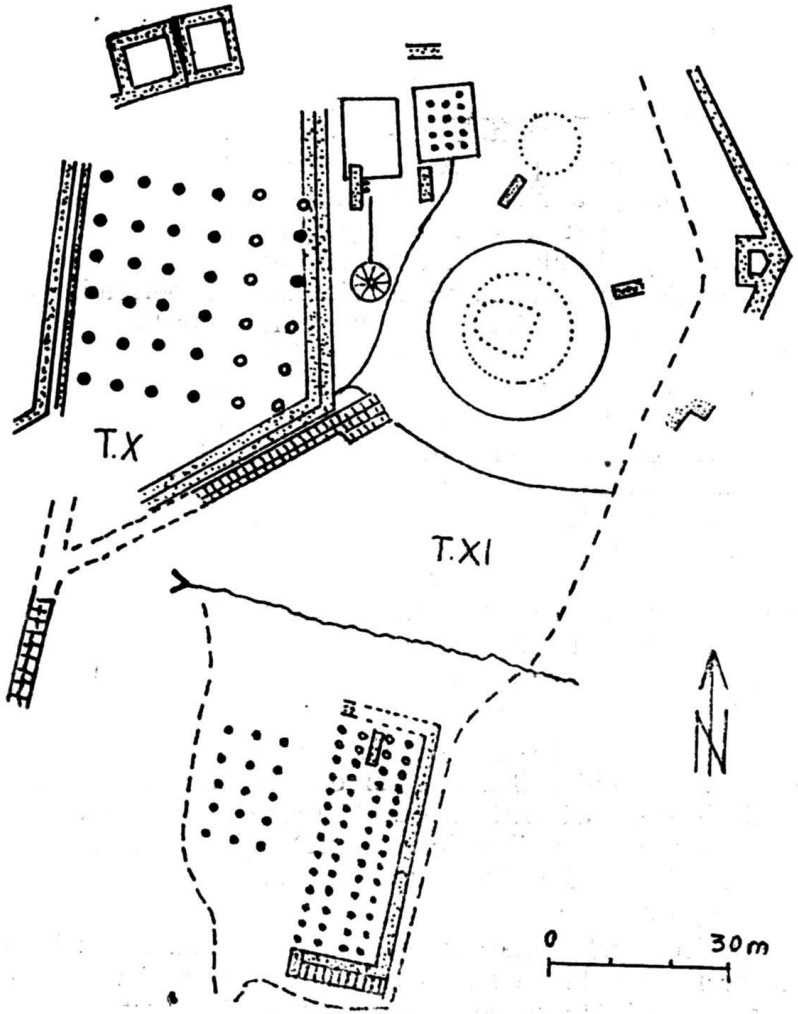


Fig. 11. Planul general al zonei sacre de la Sarmizegetusa.

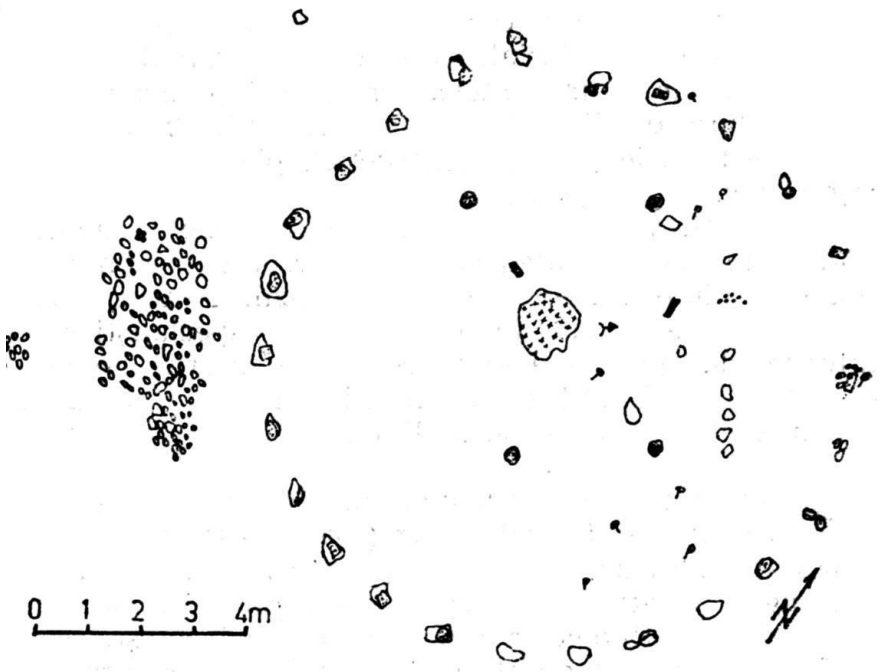
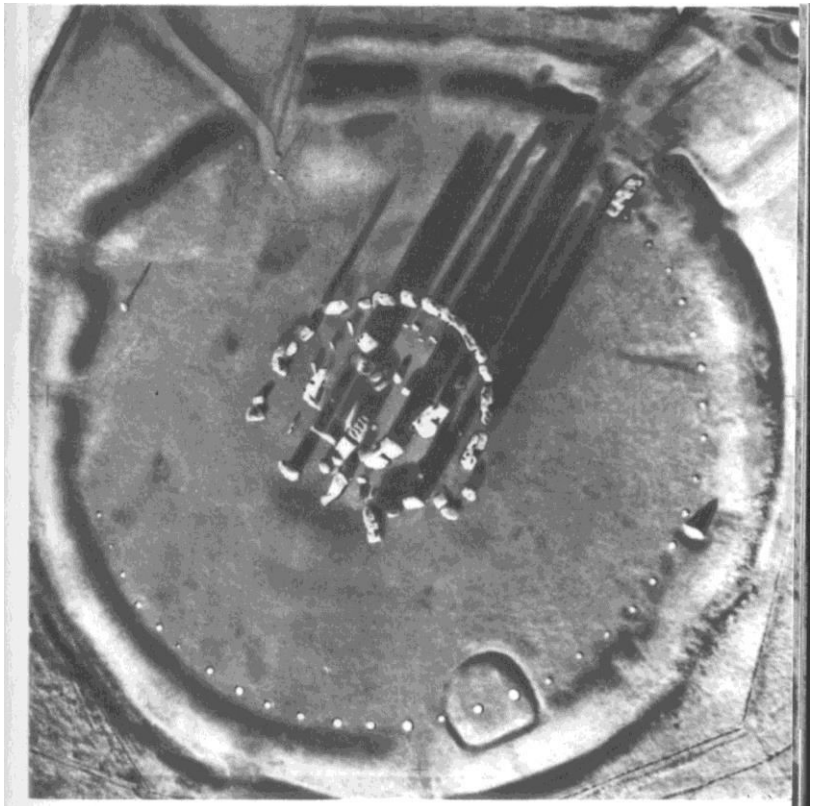


Fig. 32. Planul construcției cu lespezi de micașist și blocuri de calcar de la Meleia.



I. Плановый аэрофотоснимок Стоунхенджа.

Fcto 43. Sarmizegetusa Regia, machetă







3. Astrophysics

- 3.1- Element synthesis in astrophysics (in Sun) and instabilities of stars
- - fundamental problems of astrophysics
- - rate generation of energy in Sun's core
- - modeling periodicity of Sun's activity
- - modeling supernova explosion
- - simulating nucleosynthesis in stars

4. Learning activities

Preparing future researchers beginning from the school, university and PhD activities:

- - science popularization
- - helping teaching science in school: math, physics, astronomy
- - involvement in school contests, national and international Olympiads in physics and astronomy
- - involvement in in-service teacher training

Universities

- - Physics
- - Astrophysics
- - Nonlinear dynamics
- - Complexity
- - PhD – in astrophysics